Journal of the European Ceramic Society 42 (2022) 3049–3088

Contents lists available at ScienceDirect

Journal of the European Ceramic Society

journal homepage: www.elsevier.com/locate/jeurceramsoc

Feature article

Additive manufacturing of ceramic materials for energy applications: Road map and opportunities

Corson L. Cramer [a,*,1], Emanuel Ionescu [b,m,2], Magdalena Graczyk-Zajac [c,3], Andrew T. Nelson [d,4], Yutai Katoh [e,5], Jeffery J. Haslam [f], Lothar Wondraczek [g,h,6], Trevor G. Aguirre [a,e,7], Saniya LeBlanc [i,8], Hsin Wang [e,9], Mansour Masoudi [j], Ed Tegeler [j], Ralf Riedel [b,10], Paolo Colombo [k,l], Majid Minary-Jolandan [n,*,11]

[a] Manufacturing Science Division, Oak Ridge National Laboratory, Oak Ridge, TN 37831, USA
[b] TU Darmstadt, Institute for Materials Science, Darmstadt D-64287, Germany
[c] EnBW Energie Baden-Württemberg AG, Karlsruhe D-76131, Germany
[d] Nuclear Energy and Fuel Cycle Division, Oak Ridge National Laboratory, Oak Ridge, TN 37831, USA
[e] Materials Science and Technology Division, Oak Ridge National Laboratory, Oak Ridge, TN 37831, USA
[f] Materials Engineering Division, Lawrence Livermore National Laboratory, Livermore, CA 94550, USA
[g] Otto Schott Institute of Materials Research, University of Jena, 07743 Jena, Germany
[h] Center for Energy and Environmental Chemistry (CEEC Jena), University of Jena, 07743 Jena, Germany
[i] The George Washington University, Department of Mechanical & Aerospace Engineering, Washington DC, USA
[j] Emissiol, LLC, Mill Creek, WA, USA
[k] University of Padova, Department of Industrial Engineering, Padova, Italy
[l] Department of Materials Science and Engineering, The Pennsylvania State University, University Park, PA 16802, USA
[m] Fraunhofer Institution for Materials Recycling and Resource Strategies IWKS, Brentanostr. 2a, D-63755 Alzenau, Germany
[n] Mechanical and Aerospace Engineering, School for Engineering of Matter, Transport and Energy, Arizona State University, Tempe, AZ 85287, USA

ARTICLE INFO

Keywords:
Ceramics
Additive manufacturing (AM)
Energy and environment
Processing
Materials selection
Advanced manufacturing

ABSTRACT

Among engineering materials, ceramics are indispensable in energy applications such as batteries, capacitors, solar cells, smart glass, fuel cells and electrolyzers, nuclear power plants, thermoelectrics, thermoionics, carbon capture and storage, control of harmful emission from combustion engines, piezoelectrics, turbines and heat exchangers, among others. Advances in additive manufacturing (AM) offer new opportunities to fabricate these devices in geometries unachievable previously and may provide higher efficiencies and performance, all at lower costs. This article reviews the state of the art in ceramic materials for various energy applications. The focus of the review is on material selections, processing, and opportunities for AM technologies in energy related ceramic materials manufacturing. The aim of the article is to provide a roadmap for stakeholders such as industry,

* Corresponding authors.
E-mail addresses: cramercl@ornl.gov (C.L. Cramer), emanuel.ionescu@tu-darmstadt.de (E. Ionescu), m.graczyk-zajac@enbw.com (M. Graczyk-Zajac), nelsonat@ornl.gov (A.T. Nelson), katohy@ornl.gov (Y. Katoh), haslam2@llnl.gov (J.J. Haslam), lothar.wondraczek@uni-jena.de (L. Wondraczek), aguirretg@ornl.gov (T.G. Aguirre), sleblanc@gwu.edu (S. LeBlanc), wangh2@ornl.gov (H. Wang), mansour.masoudi@emissol.com (M. Masoudi), ed.tegeler@emissol.com (E. Tegeler), ralf.riedel@tu-darmstadt.de (R. Riedel), paolo.colombo@unipd.it (P. Colombo), majid.minary@asu.edu (M. Minary-Jolandan).
[1] 0000-0002-0179-088X
[2] 0000-0002-3226-3031
[3] 0000-0002-4283-6549
[4] 0000-0002-4071-3502
[5] 0000-0001-9494-5862
[6] 0000-0002-0747-3076
[7] 0000-0002-8146-9630
[8] 0000-0002-6975-6776
[9] 0000-0003-2426-9867
[10] 0000-0001-6888-720
[11] 0000-0003-2472-302X

https://doi.org/10.1016/j.jeurceramsoc.2022.01.058
Received 12 October 2021; Received in revised form 23 January 2022; Accepted 26 January 2022
Available online 7 February 2022

academia and funding agencies on research and development in additive manufacturing of ceramic materials toward more efficient, cost-effective, and reliable energy systems.

1. Introduction

Among engineering materials, ceramics are indispensable in energy applications such as batteries, capacitors, solar cells, smart glass, fuel cells and electrolyzers, nuclear power plants, thermoelectrics, thermionics, carbon capture and storage, piezoelectrics, turbines and heat exchangers, among others. They are of particular interest because of their inherent high temperature capabilities and corrosion resistance, but they possess many other useful properties at ambient and elevated temperatures and pressures. Fig. 1 shows the US advanced ceramic market size, it was valued at USD 97.0 billion in 2019 and is expected to grow at a compound annual growth rate (CAGR) of 3.7% by 2027 [1]. Rising demand from industry, including renewable energy and medical sectors, are expected to propel market growth over the forecast period. Rising product demand from the clean technology industry will also support market growth. Many of these applications are directly for energy usage and storage and rely on the advancements of ceramic processing and materials technology.

1.1. Ceramics in energy applications

Ceramics are used in many energy applications, and some of them are specifically introduced in section. Ceramics are used in emission reduction, for example through control of emissions from combustion engines, and CO_2 (or carbon) capture. For emission control in combustion engines, ceramic honeycombs (more than 90% of honeycombs currently used worldwide in combustion engines) function as a filtering device and building foundation hosting the catalytic coating. For these applications, the ceramic of choice is often cordierite, an extremely low-cost refractory oxide ceramic capable of withstanding substantial temperature variations downstream of an engine.

Significant advances in battery energy storage technologies have occurred over the past decade with solid state batteries; in these systems, the materials used for the electrolyte and cathode are monolithic ceramic oxides. Much of this work has led to battery pack price decreases of over 90% since 2010, with the lowest reported price under $100/kWh in 2020 [2]. Li-ion battery performance has increased, and the cost has decreased, which is especially good for the current high demand for Li-ion batteries for electric vehicles (EVs). The annual deployment of Li-ion batteries is projected to increase roughly eightfold over the next 10 years, reaching nearly 2 TWh of capacity globally [3]. However, there is a strong demand for increased performance, system safety, lower manufacturing costs and lower environmental footprint. For example, transportation applications will require additional advances including cost reductions below $60/kWh of usable energy at the pack level, fast charging capabilities of less than 15 min, and energy densities that will allow increased EV range between charges [4].

Nuclear reactors of both the fission and fusion types impose high temperatures, aggressive corrosion requirements, and high radiation fluxes on materials. Silicon carbide (SiC) fiber reinforced SiC matrix composite (SiC_f/SiC), among other ceramics, have seen significant worldwide interest in the development of cladding materials that are more resilient to high temperature steam oxidation as would be experienced in many design-basis and beyond design-basis nuclear accidents. Specifically in nuclear applications, SiC has resistance to swelling with high dose of neutron fluences of up to 100 displacements per atom (dpa) [5]. Because of their high temperature severe environment capabilities and the unique functionality, ceramic materials, in monolithic or composite forms, are essential for enabling fusion energy, in components such as the flow channel inserts in liquid metal blankets, tritium breeders, the radio frequency plasma heating window, diagnostic mirrors, the blanket and first wall structures. Additionally, ceramics with high thermal conductivity (to transfer heat effectively) and high strength (to afford thin tubular shapes or channels) are considered the best materials for high temperature heat exchangers. These materials include metal oxides, nitrides, and carbides such as WC, SiC, Si_3N_4, and Al_2O_3.

Nanocomposite materials based on electrically conducting percolative networks, particularly those consisting of carbon-based secondary phases dispersed within a ceramic matrix (as in polymer-derived ceramics) possess high piezoresistive response and are attractive for applications operating in harsh conditions, e.g., high temperatures, corrosive environments, etc., because of the intrinsic robustness of the ceramic matrix materials. Piezoelectric ceramics such as lead zirconate titanate, barium titanate, lead titanate, and potassium sodium niobate are excellent candidates for sensors and energy harvesting devices, such as in wind energy harvesters.

Yttria-stabilized zirconia (YSZ) for the electrolyte and YSZ-based composites (for example Ni-YSZ cermet) as the fuel electrode are the state-of-the materials for solid oxide fuel cells (SOFCs) and solid oxide electrolysis cells (SOECs). In these devices, the electrolyte must be sufficiently densified to avoid leakage of the fuel/oxidant gases through the

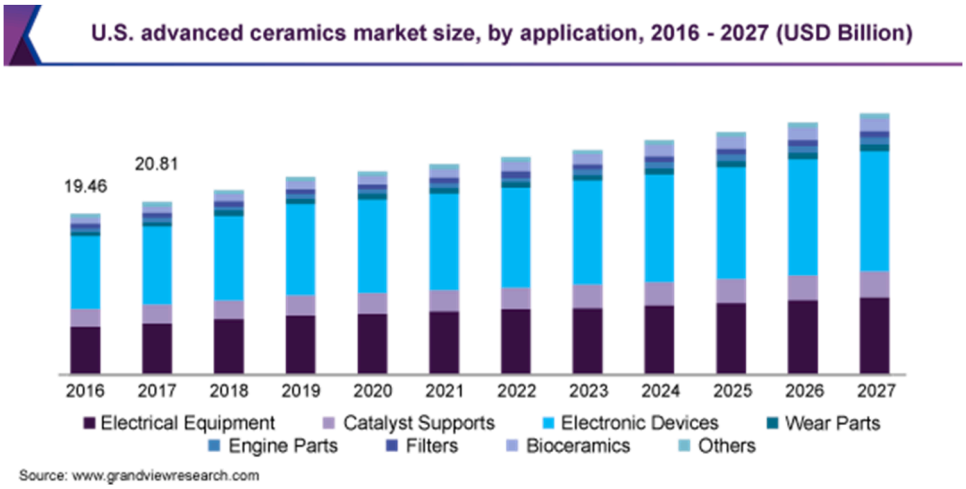

Fig. 1. The US advanced ceramics market size and projection [1].

electrolyte to the electrodes, while both cathode and anode are required to be porous, electrically conductive and should possess high activities for fuel oxidation and oxygen reduction.

Semiconductor materials alloyed to provide high ZT values are used in thermoelectric solid-state energy conversion devices that convert heat to electricity and vice versa. For conversion of very high temperature heat (from sources such as hydrocarbon combustion, concentrated sunlight, or nuclear generation processes) directly into electricity, ceramic materials with high power density outputs are needed for heat-to-electricity conversion efficiencies of interest in thermionic energy converters (TECs).

Ceramic turbine blades and vanes are needed to further improve turbine efficiency owing to the refractive ceramic properties including higher melting temperature, potentially high creep resistance, potential for high corrosion resistance at elevated temperatures, and low density. Ceramic cores and molds are also essential to the casting of the highest performance conventional, superalloy turbine components. High precision and careful control of thermal and mechanical properties of the ceramic cores and molds during superalloy casting is critical to obtain the complex, internal cooling passageways needed in high performance turbine components.

Smart glass and smart glass devices are glass-based materials or devices utilizing constructions for active or adaptive response to environmental or interventional stimulation to tailor functional properties. Most prominently, these can be smart windows or other components of a building with adaptive energy (photovoltaic or heat) harvesting ability, cooling functions or emissivity control and shading techniques.

1.2. Traditional ceramics processing

Ceramics have inherently high melting temperatures, and this makes them difficult to process by melting. Oxide ceramics have some degree of ionic bonding, which allows for self-diffusion, so they can be sintered in powder form. Because of high degree of covalent bonding in carbide, nitride, and boride ceramics, their sintering is very difficult. Traditionally, casting and molding, sintering, and machining is carried out to reach high precision monolithic ceramic parts. Additionally, for many carbides and ultra-high temperature ceramics, hot pressing and spark plasma sintering with subsequent machining is done. These methods achieve highly dense material with good properties and microstructure, but the geometries formed by these methods are simple and axis symmetrical, as shown in Fig. 2A and B. Also, these methods require tooling to shape the preform (as in injection molding) or tooling to keep the powder compact under constant mechanical load during heating and sintering (as in hot pressing). After densifying into objects with simple shapes, they may need to be machined into complex shapes, which requires machining with expensive tooling.

Several methods have been developed to form SiC preforms with more complex geometries such as die extrusion, slip casting, tape casting, gel casting, and injection molding [6–8]. These methods utilize solvent-based slurries with dispersed powders to shape parts, typically with dies. These methods can achieve high solids loadings, which translates to high green density and less shrinkage during sintering. These methods also provide high volume production. In die extrusion, axisymmetric dies are used in extrusion producing geometries like the ones in Fig. 2B. The geometries achievable with the other slurry-based casting methods are shown in Fig. 2C. Although the forming provides more freedom compared to compacts and pressure-assisted methods with dies (not including hot isostatic pressing (HIP)), there are still certain designs such as ones with internal features that are not achievable. Additionally, there is a cost associated with die tooling, so there is motivation to use methods without the associated dies.

Methods for reinforced ceramics also have more specialized processing and are of large interest in energy applications. As such, ceramic matrix composites (CMCs) are processed by different methods because they rely on continuous fiber reinforcement, interface coating, and a matrix material that can bear and transfer mechanical load giving the CMC damage tolerance through interfacial debonding, crack deflection and propagation along the interface leading to fiber sliding and pullout [10]. To process CMCs, the fibers must be spun into tows, pyrolyzed, and sintered or slightly crystallized. Next, fiber tows are woven into 2-D plies or fabrics and coated with an interface coating. Then, the cloths are prepregged with slurries to help hold the fabrics together and improve the fiber packing and density and laid up onto tools where they are subjected to some pressing with or without heating. Before deciding on a densification method, the pre-impregnated preform is pyrolyzed. Preforms are infiltrated with methods such as reactive melt infiltration (RMI), chemical vapor infiltration (CVI), or polymer impregnation and pyrolysis (PIP).

1.3. Additive manufacturing of ceramics

The market for ceramics made via additive manufacturing is also growing, as many industries realize the benefits provided by advanced techniques for design, cost savings and, in some cases, time saving. A recent report analyzed pros and cons and generated revenues of the dominant AM technologies for processing ceramics, both technical (advanced) and traditional (clay-like) [11]. Trends can be seen in Fig. 3. The advanced methods in the study included material extrusion, photopolymerization and binder jetting 3D printing technologies. As the aggressive design demands call for low-cost, high temperature ceramics in complex shapes, the need for improved solutions is significant. Compared to traditional ceramic processing techniques and even casting techniques, solid free-form fabrication (SFF), additive manufacturing (AM), or 3D printing will be used in energy industries where it is necessary and makes sense for the design, properties, and cost. In this article, the three terms will be called AM to limit confusion. For ceramics AM, there are several leading technologies for shaping preforms [12,

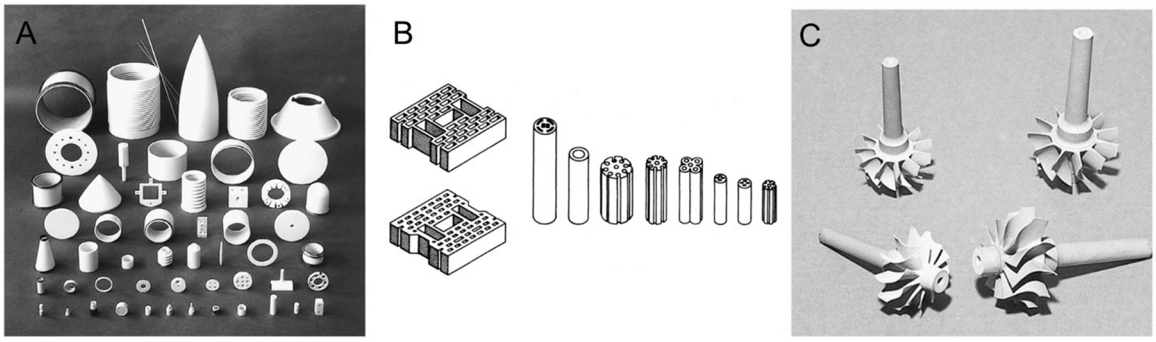

Fig. 2. (A) Preforms of ceramic green parts formed by uniaxial and isostatic pressing (some with green machining), (B) examples of the types of shapes that are commonly extruded, and (C) sintered silicon nitride turbocharger rotors fabricated by injection molding [9].

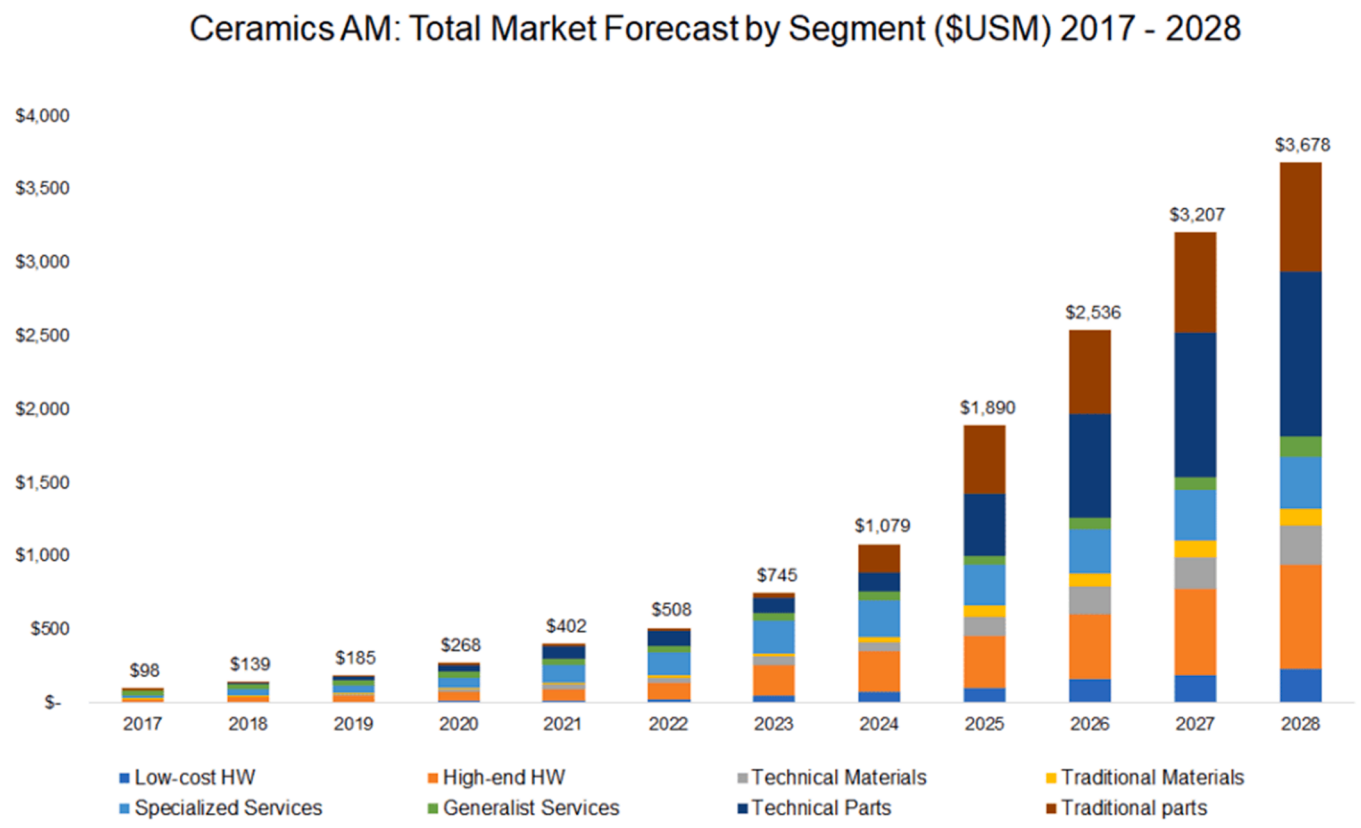

Fig. 3. Market for ceramics AM [11].

13]. One method is called Vat photopolymerization, where a laser (traditionally called stereolithography) or light projection (digital light processing (DLP) with LEDs or LCD screens) is used to cure the resin. Another Vat photopolymerization method is called Lithography-based Ceramic Manufacturing (LCM) and can use a laser, LED, or LCD system. Some newer light-based curing techniques use machines without vats but rather use reservoirs of slurry or paste that is spread onto build platforms and subsequently cured with a light source (such as companies Admatec and 3DCeram). Another method is nozzle extrusion and is called direct ink write or robocasting if a liquid material (gel/slurry/-paste/thermosets) is used and FDM if a solid, thermoplastic material is used. A method of forming dry powder bed with liquid binder is typically called binder jet 3D printing (BJ3DP). A dry powder bed method with laser source to sinter layers is called selective laser sintering or melting (SLS/SLM). Low viscosity slurry forming is called material jetting/inkjet printing.

Vat photopolymerization techniques such as stereolithography (SLA) and digital light processing (DLP) cure 2D layers of photosensitive monomer resins loaded with powder or preceramic polymers by curing with light. High resolution and low surface roughness are achievable with lithography, and it is a proven technology for powders with low light absorbance such as oxide ceramics. It is also a proven technique for preceramic polymer forming. The drawbacks of lithography are the material limitation and use of support material. As pointed out in [14], debinding of printed parts is achieved when the crosslinked resin decomposes, so pyrolysis must be done. High solids loading is difficult in resins, and limitation on solids loading in relation to viscosity and spreading must be monitored. Between crosslinked binder and more resin present in the green bodies, debinding can be difficult and lead to more defects like the ones seen in [15,16]. Generally, across all 3D printing methods, there are more defects and deviations in porosity and microstructure at layer interfaces.

Extrusion printing methods utilize solvent, gel, paste, thermoplastic, or thermoset slurries that are extruded through a nozzle onto a build platform. Extrusion methods can print particulate with orientation as well as many different materials, but their drawbacks are resolution, speed, throughput, and filament adherence. One other drawback is that viscosity must also be monitored in order to get enough shear and flow through the nozzle. BJ3DP utilizes a dry powder bed where a solvent and polymer mix is sprayed onto the powder bed in 2D layers [17,18]. BJ3DP can achieve high throughput and high resolution of parts because of the printing nozzles and accuracy of the jets. The drawbacks of printing with BJ3DP are the large particle sizes needed, random orientation of printed fibers and particulate, depowdering difficulty and time, and low green (and final) density. Material jetting is the expulsion of a low viscosity slurry onto a platform with subsequent drying of the layers. This method provides a thin layer of material, but the solids loading is typically low and drying effects can cause cracking.

Selective laser sintering or melting utilizes a dry powder bed and a laser to sinter or melt patterns into 2D layers. It can achieve some solid-state or liquid-phase sintering of ceramics, but it is not as commonly used for ceramics because of cracking of parts due to large thermal gradient during the process. It should be noted that SLS is the only method that can provide some direct consolidation of the ceramic powder during printing because of the heat applied. For all the other ceramic AM techniques, post processing steps such as solid-state sintering, liquid-phase sintering, reaction synthesis sintering, reactive melt infiltration (RMI), chemical vapor infiltration (CVI), or polymer impregnation and pyrolysis (PIP) are needed to consolidate the printed preforms into dense, usable parts. A schematic of these AM methods with images of the processes used for ceramics is shown in Fig. 4.

Multi-material ceramic AM is still a considerable challenge both in terms of the actual printing as well as the subsequent processing (debinding and sintering), although some recent advancements have occurred, with the development of multi-vat lithographic printers and multi-nozzle extrusion and in-line mixing devices [19].

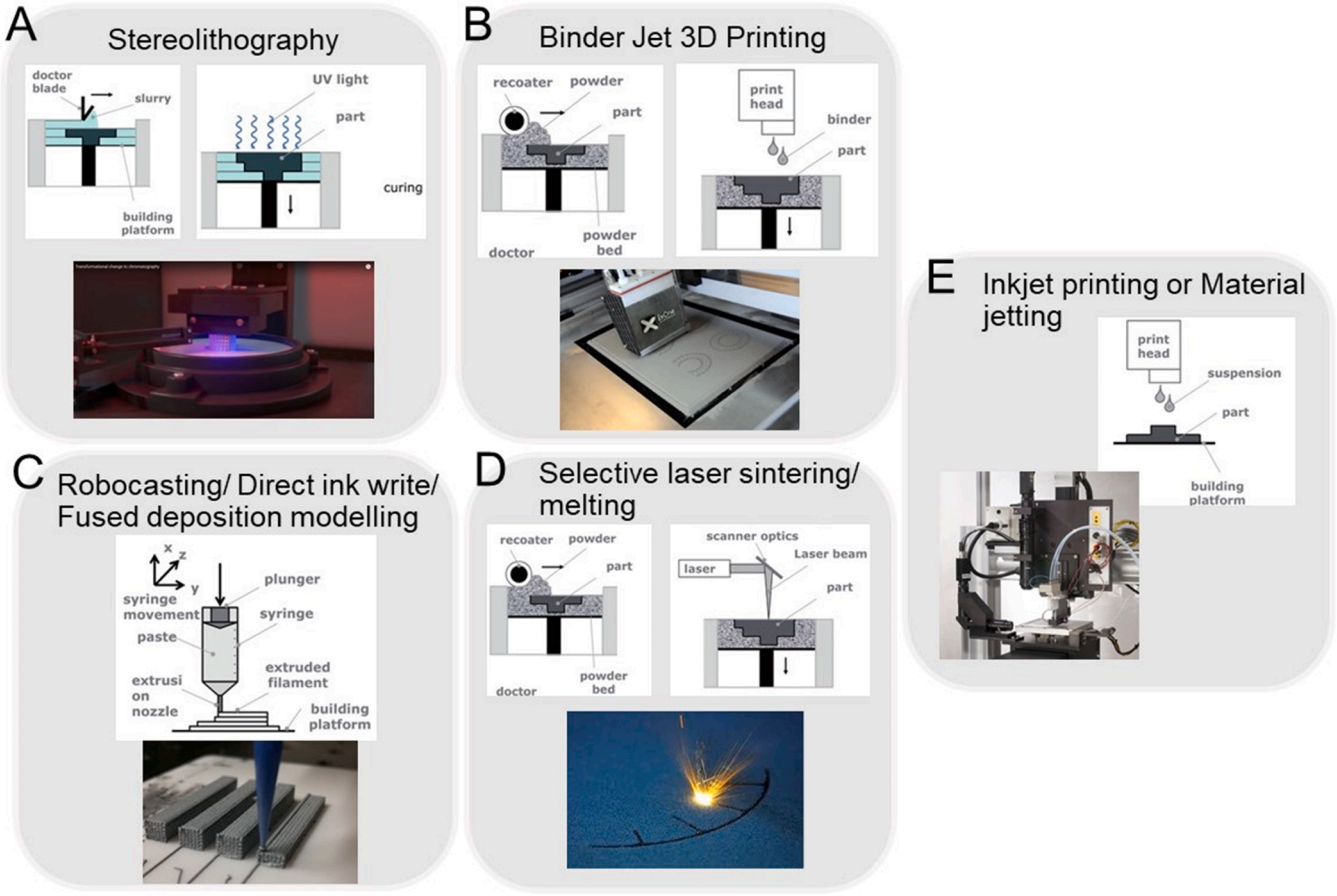

Fig. 4. . Schematics and example images of the most common ceramic AM methods by category. (a) Reproduced from ref. (b) [12] with permission from the John Wiley and Sons.

1.4. Designing and improving ceramics for energy applications

Additive manufacturing opens the design space and allows for improved design in terms of material placement, architecture, microstructures, and properties. Designs that were not thought possible have become a reality. As an example, there are many architectures to consider when manufacturing a battery, and Fig. 5 presents a variety of 3D printing techniques suitable for electrode fabrication and the pattern and its mechanism for the optimization of electrodes. These architectures are achievable with various AM methods, so these materials and architectures can be made and have a large impact on the performance and properties of batteries. Another example is small channels and tortuosity that can be achieved with AM of SiC and other materials for high temperature heat exchangers. It is the same parallel for many other ceramic materials used in energy.

Each energy application in Fig. 6 has certain design criteria for success and improvements that are dictated by the properties. Based on the properties outlined, the most appropriate material can be selected. For given materials, the manufacturing process can be selected to provide the best selected material with the best properties to meet the application design needs. This process and idea are outlined in Fig. 6. These factors may result in several potential AM technologies to be appropriate for each application. More specifically, energy applications outlined above may require high fracture toughness and high strength, high thermal conductivity, high corrosion resistance, high temperature stability, radiation resistance, high electromechanical coupling coefficients, ion conductivity, high ZT values, high power density outputs, among others. Added to these properties may be the requirement for low-cost and availability (in the cases of high-volume productions). In certain applications, two or more properties may be required. As an example, high temperature and high-pressure heat exchangers require high thermal conductivity (as usual), with the added requirement for high fracture toughness to withstand high pressures. In these scenarios, a good approach is using multi-physics topology optimization (TO) to obtain the optimal designs. The next step would be identifying AM technologies that are able to process and manufacture those certain ceramics in identified geometries from TO results. In the latter process, the design for additive manufacturing (DFAM) principle should be considered.

This review article is divided into sections focused on specific energy applications. For each application, its requirements are discussed, followed by why ceramic materials are the best choice for that application. Traditional fabrication and manufacturing processes for each application is outlined, and the case is made for potential improvements AM technologies may offer for each application. There are several reports in the literature on covering various AM processes for specific applications [22–32]. The focus on this article is on ceramic materials and processing, and hence the readers are referred to those reports for in depth discussion on various AM processes.

2. Energy applications utilizing ceramics and potential for additive manufacturing

There are several energy applications that require high temperatures, low thermal expansion, high strength, and corrosions resistance. To engineer many energy materials and devices, ceramics must be used, and ceramics are exploited for the above properties, but ceramics can also provide the functional properties needed as well as mechanical or

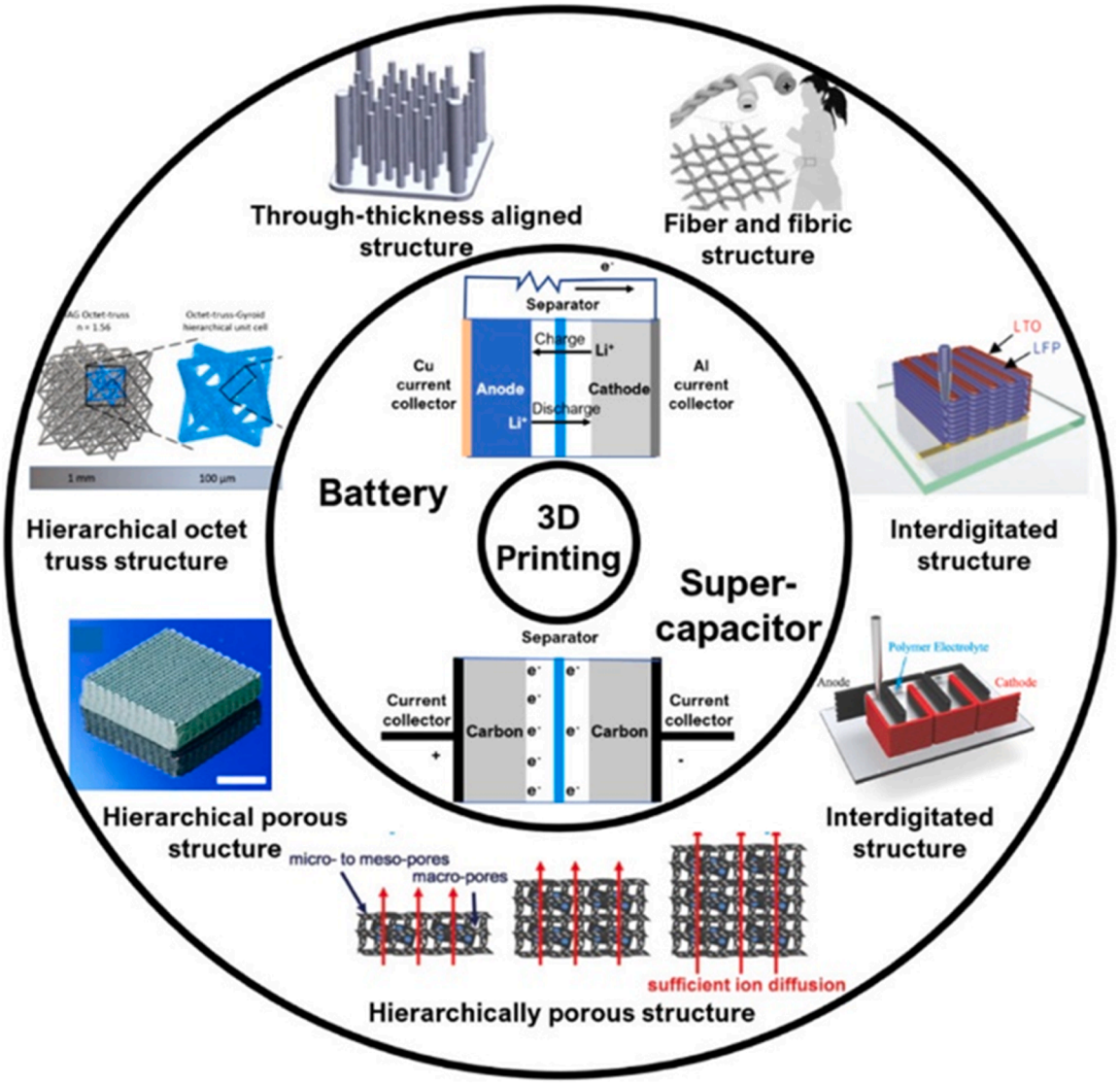

Fig. 5. . Overview of three-dimensional (3D) printing for emerging advanced electrode architectures. Reproduced from ref. [20] with permission.

structural properties. In that regard, the first few applications utilize ceramics that are used for functional properties such as electrical conductivity and magnetic properties, which mostly come from the ionic behavior of oxide ceramics. In many cases, the functional ceramics are oxides, silicates, perovskites, Spinel, and others for the functional (electrical, magnetic, optical, etc.) properties. Several applications where thermal transport as well as functional properties are discussed (as in thermoelectrics and thermionics), and the last several applications are ones that deal with thermal transport and structural properties, which naturally leans toward carbide, borides, silicide, and other ceramics with high strength and thermal conductivity. In many advanced energy applications, there could be a need for structural and functional ceramics, so careful selection of materials must be considered for those engineering designs and would not be limited to hybrids and composites. These sections focus on the primary monolithic ceramic material for the most prominent energy applications.

2.1. Batteries

An efficient electrochemical energy storage for portable and stationary applications is one of the greatest technological challenges of today. Devices such as batteries or supercapacitors play an important role in modern society and the main objective of energy storage device (ESD) development is to reach the requirement of high energy density and high power density while maintaining a long cycling lifetime during practical service, and in parallel fulfilling the safety requirements [33]. Although existing ESDs that are prepared by traditional technologies meet the demands of numerous applications, their use in various special scenarios such as flexible devices and structural devices still cannot be implemented [34–36]. The emerging additive manufacturing techniques generated a great revolution in the fabrication process of devices for electrochemical energy storage and their components. Additive manufacturing also allows to promote the performance of energy storage devices through advanced electrode architecture designs. Moreover, 3D printing technologies have some advantages over traditional methods used to fabricate common electrode/ESDs, as pointed out in [25,37,38]. Fast and repeatable production of the entire device (electrode/electrolyte/current collectors/packaging) is realized using the same printing machine, that significantly simplifies the process, reduces costs and improves the quality of the final product. Further, 3D printing enables the control of the printed shapes and structures via adjustment of printed ink properties such as viscosity, composition, and printing parameters such as speed, flow rate, and tool path. It also allows for a precise control of the electrode loading and microstructure. This

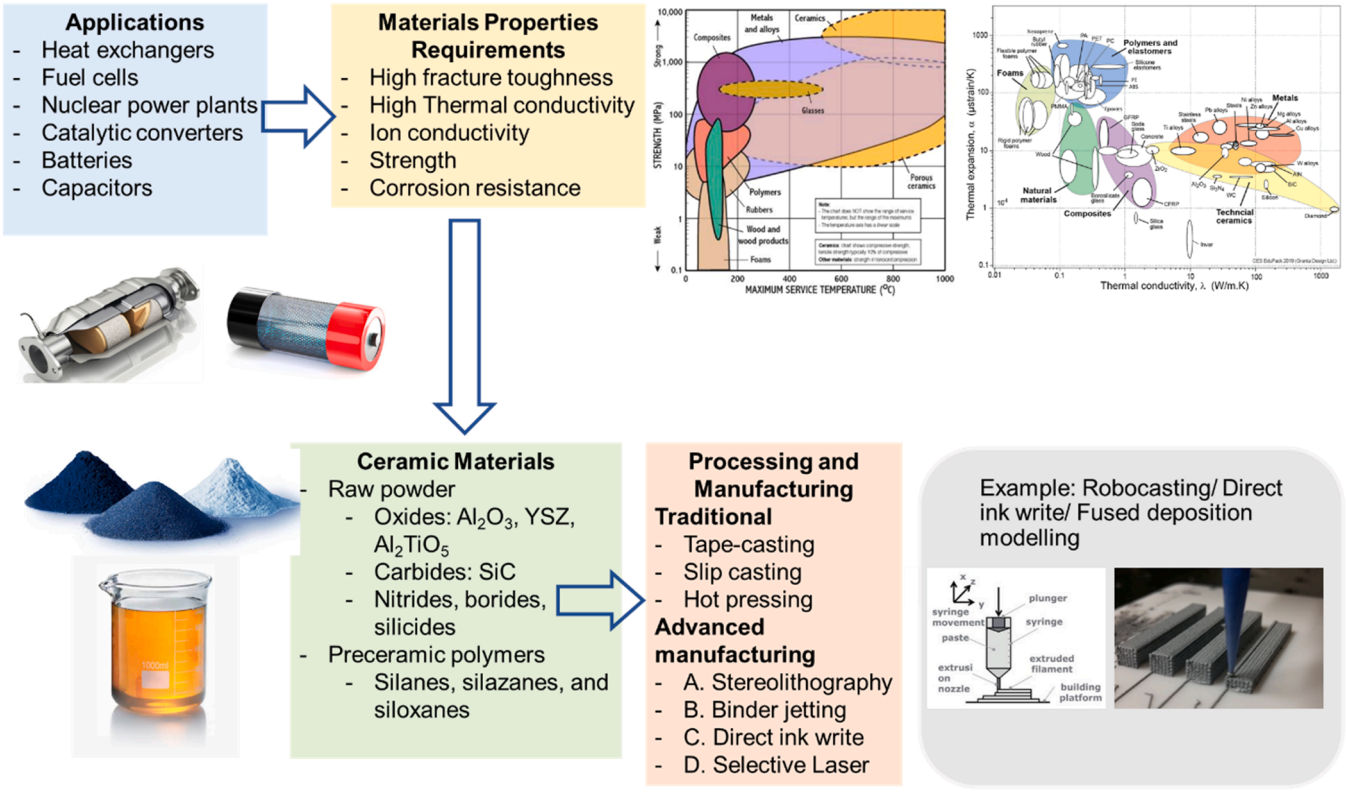

Fig. 6. . Schematic and process flow for determining ceramic processing routes for energy applications [12,21].
(a) Part of the figure is reproduced from ref. (b) [12] with permission from the John Wiley and Sons.

accurate control leads to a significant reduction of the used raw materials and produced wastes [39–41]. Moreover, a more complex design can be easily manufactured in a scalable way [42].

In this section, we highlight the critical role of additive manufacturing techniques in advanced electrode architecture design and fabrication. The current progresses of the 3D printing technologies in the fabrication of structural ESDs (e.g., lithium-ion batteries (LIB), zinc-manganese oxide (Zn-MnO_2), lithium-sulfur batteries (LiS) and supercapacitors are summarized. Only the most prominent examples of entire energy storage devices produced by additive manufacturing processes are addressed here. For technical details and exhaustive number of examples the reader might refer to numerous recent reviews devoted to this topic [20,28,36,42–47].

2.2. *Traditional fabrications of batteries, opportunities for additive manufacturing and outlook*

LIBs have become ubiquitous in our daily lives because of their high specific capacity, high energy density, low price, and environmental friendliness [48,49]. The basic working principle of LIB is as follows: during charging the lithium cations are pulled out from the lithium-rich cathode material, diffuse across the electrolyte, and are inserted into a lithium-poor anode, whereas the electrons are transferred in the same direction via external circuit. When discharged, a reverse process takes place, and electrical energy is released. Commonly, LIBs are made up of a cathode/anode, separator, electrolyte, and packaging material [50]. The overall electrochemical performance of LIBs is affected by each of these components.

Conventional LIBs are mainly manufactured using 2D printing techniques [42,51]. The electrode is prepared by doctor-blading the slurry that is made up of active materials, conducting additives and binders onto current collectors. Lithium cobalt oxide (LCO), lithium nickel manganese oxide (NMC), lithium nickel cobalt aluminum (NCA) and lithium iron phosphate (LFP) are the most prominent examples of cathode active materials whereas graphite, graphite-silicon composites and lithium titanate (LTO) represent the most common anode materials [52]. To improve the capacity of an electrode and to reach optimal energy density, a high thickness of the 2D planar geometry electrode is required. However, a thicker electrode means a longer Li-ion transfer pathway, which subsequently leads to impaired rate performance and durability of the Li-ion battery [20,53]. Additive manufacturing can be utilized to develop diverse architectures of the electrode with a high surface area, higher electrical conductivity, and ion transferability, at the same time, a good structural stability that is required to reach the aim of next generation of LiBs [54]. A fast transfer of ions benefits from a low tortuosity of the electrode materials [55], thus an aligned 3D printed structure of an electrode with a much lower tortuosity leads to shorter ion/electron transfer pathways and enables a faster transfer of charge [36].

There are various 3D architecture designs of Li-ion battery electrodes to achieve high energy density and high-power density batteries. Among those 3D printing methods, direct ink writing (DIW) is one of the most used techniques to print Li-ion batteries given the simple printing mechanism and low-cost fabrication process. Besides, the DIW 3D printing method offers a broad material selection including ceramics, metal alloys, and polymers, which provides it with the ability to print active materials directly with high mass loading [54]. Sun et al. [56] produced a Li-ion battery with a LFP cathode and LTO anode micro-electrode arrays in an interdigitated architecture by DIW method (Fig. 7A and B), which showed a high areal energy density of 9.7 J cm^{-2} at a power density of 2.7 $mWcm^{-2}$ (Fig. 7C).

The stereolithography (SLA) printing method is also used in Li-ion battery manufacturing. Cohen et al. [57] designed 3D-printed micro-batteries by SLA with various shapes and sizes comprised of a tri-layered structure including the LFP cathode, $LiAlO_2$–PEO membrane, and LTO-based anode produced by electrophoretic deposition. When the 3D

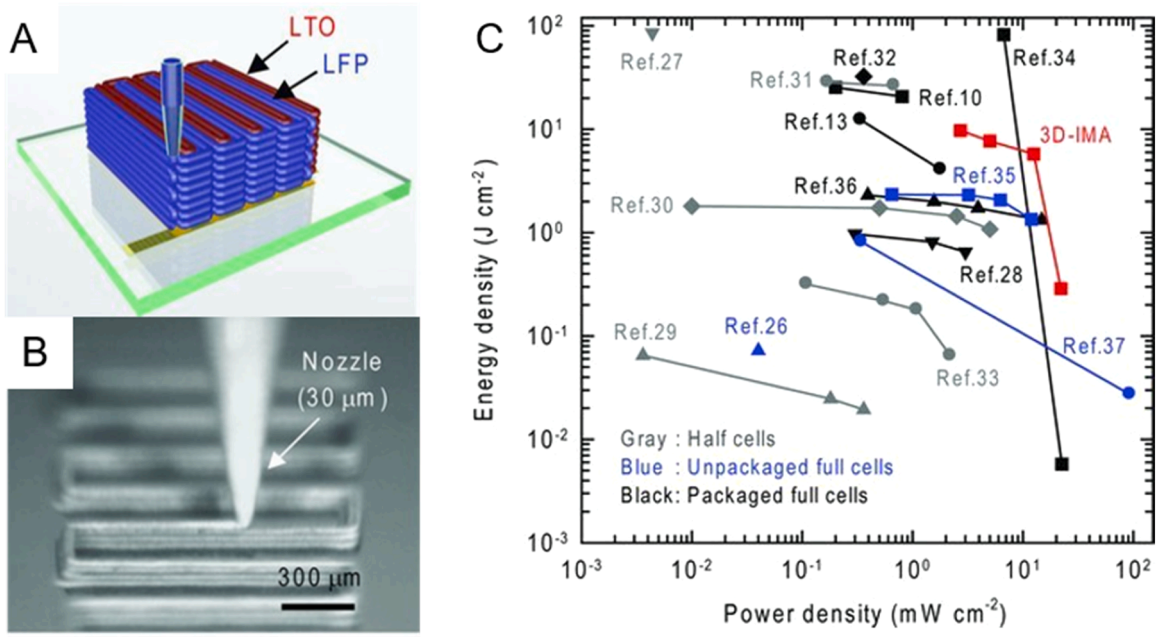

Fig. 7. (A) A schematic illustration of 3D interdigitated microbattery architectures, (B) an optical image of $LiFePO_4$ (LFP) ink (60 wt% solids) deposition through a 30–μm nozzle to yield a multilayer structure. (C) Comparison of the energy and power densities of printed, unpackaged 3D interdigitated microbattery architectures (3D-IMA) to reported literature values.
(a) Reproduced from ref. (b) [56] with permission from the John Wiley and Sons.

LFP electrode was cycled from 0.1 to 10 C, a high areal capacity of 400–500 Ah cm^{-2} was obtained on perforated graphene-filled polymer substrate, and the areal energy density of these full cells was three times higher than that of the commercial planar thin-film battery. With these 3D electrode architecture designs, high energy density Li-ion batteries with close to ideal rate performance can be realized.

A solid electrolyte-based battery has extraordinary advantages in terms of safety and stability, what makes it the most promising high energy density next-generation battery. The solid-state electrolyte is generally a non-flammable material rather than organic carbonate solvents and reactive lithium salts used in conventional Li-ion battery electrolytes. Strong mechanical properties and high electrochemical stability of the solid electrolyte enable to form a battery with lithium metal as the anode, since the electrolyte inhibits the growth of lithium dendrites and chemical deposition at high voltage during cycling. However, the solid-state electrolytes lead to high interface resistance as compared with traditional liquid electrolytes. Poor interfacial contact between the electrolyte and the electrode and the limited ionic conductivity of a thick solid electrolyte are the major cause of high electrical resistance. As for a traditional manufacturing method of solid-state electrolytes, flat pellets are the most common architecture, and a planar interface minimizes the interfacial contact area and increases the battery resistance. However, 3D printing provides a solution to reduce the battery resistance by constructing complex architectures. Multiple ink formulations have been developed for 3D printing and unique solid electrolyte structures with a variety of patterns can be formed after further sintering. For instance, McOwen et al. [58] printed solid electrolyte microstructures by 3D printing with ceramic garnet-type $Li_7La_3Zr_2O_{12}$ (LLZ) as a model solid electrolyte material. The stacked-array pattern provides the electrolyte with higher surface area than traditional planar structures to combine with a lithium metal electrode. As a result, the interfacial resistance of the full cell is reduced. The dramatically decreased full cell resistance induced by improved interfacial contact areas leads to higher energy and power density of a solid electrolyte-based battery [20].

Zn-MnO_2 batteries have been on the market as the non-rechargeable version, but the rechargeable version also exists. Zn-MnO_2 are known as alkaline batteries and are widely used in printable batteries as they are non-lithium based, safe and environmentally friendlier. A printed Zn–MnO_2 battery has been realized with a polyacrylic acid (PAA)-based polymer gel electrolyte (PGE) with discharge capacity of 5.6 $mAhcm^{-2}$ when discharged at 0.5 mA. The discharge capacity of the printed battery has been characterized in bend conditions, and two batteries connected in series and bent to a radius of 0.3 cm managed to power a green light-emitting diode [59]. Another study shows a high energy density Zn–MnO_2 battery with electrodes prepared by using a solution-based embedding process. It has been stated that the battery can be used to power a light-emitting diode display integrated with a strain sensor and microcontroller [60].

A sulphur electrode with a theoretical capacity of 1675 mAh g^{-1} and theoretical energy of 2600 $Whkg^{-1}$ when combined with metallic lithium anodes makes a Li–S battery a highly promising candidate for the next-generation batteries [61]. Nevertheless, the electrically insulating nature of sulphur and lithium sulphide, its poor cycling performance due to the high polysulphides solubility and the large volume (80 %) changes during the redox reaction impede the use of LiS, thus designing highly efficient Li-sulfur system still remains a challenge. Like LIB, the areal capacity determines the total capacity of the electrode and, consequently, the energy density of the full battery. Thus, a thicker sulphur electrode with high active material loading is required for a high energy density Li–S battery. Thicker sulphur electrodes with a fair electrical conductivity can be realized by 3D printing through stacking multilayer active materials during printing. For instance, Shen et al. [62] demonstrated that a thickness of 600–μm S electrode can be printed by stacking six layers, which resulted in a high reversible capacity of 812.8mAh g^{-1}. Moreover, electronic, and ionic conductivity of the S electrode can be optimized by an architectural design. Gao et al.[63] developed a 3D-printed grid architecture sulfur/carbon (S/C) cathode with commercial carbon black as host material for sulphur, which contains abundant micropores. Such hierarchical porous structure is constituted by the macrosized pores (several hundred micrometers) produced by 3D printing and nanosized pores produced by phase inversion of the polymeric binder polyvinylidene fluoride-hexafluoropropylene, which increase the surface area of the electrode for Li^+

transport channels. At high active sulphur loading of 5.5 mg cm^{-2}, high initial discharge specific capacity of 912 $mAhg^{-1}$ and a capacity retention of 85% within 200 cycles at high C-rates of 2 C are achieved. This performance was significantly enhanced compared with S electrodes without such microarchitecture design, which showed a low capacity of 186 $mAhg^{-1}$ and low-capacity retention of 43.4% at C-rate of 0.5 C.

2.3. Supercapacitors

Supercapacitor, as one of the energy storage devices, is a high-capacity capacitor which bridges the gap between electrolytic capacitors and rechargeable batteries. According to charge storage mechanism, supercapacitors are broadly classified into two classes: electric double layer capacitors (EDLCs) and pseudocapacitors. The former mainly relies on the non-faradaic double layer charge stored at the electrode-electrolyte interface and the latter on the redox pseudocapacitance due to redox reactions at the interfaces to store electric energy [64]. In both cases, the high active area of the electrode and the ability of the fast charge transfer is of crucial importance. 3D printing techniques have been widely used to achieve high areal capacitance and long cycling lifetime of supercapacitors by rational control of high surface area 3D-conductive frameworks with precise interior hierarchical nanostructures and low-tortuosity structure reversing traditional high--volume bulk-building electrodes of supercapacitors [47]. Besides, flexible customized electronics fabricated by highly stretchable polymer materials can be easily manufactured with the aid of 3D printing techniques [20].

2.4. Traditional fabrications of supercapacitors, opportunities for additive manufacturing and outlook

An electric double-layer capacitance supercapacitor stores energy through charge absorption on the surface of two electrodes, usually made of highly porous carbonaceous material. The DIW method has received much attention for double layer capacitance supercapacitors due to the ability to print electrodes with high mass loading. Li et al. [65] printed a double-layer capacitance micro supercapacitor with a highly concentrated graphene/DMF dispersion ink. The high viscosity (about 40 cP at 20 °C) and environmentally friendly terpineol was used to concentrate graphene and adjust the ink rheology, and a small amount of polymer (ethylcellulose) was added into the harvested graphene/DMF dispersion to protect graphene from agglomeration. The combination of solvent exchange and polymer stabilization techniques enables the formulation of stable graphene inks with high-concentration and compatible fluidic characteristics for efficient and reliable inkjet printing, and the printed micro-supercapacitors achieve a high specific capacitance of 0.59 mF cm^{-2} and a rapid frequency response time around 13 ms, which deliver a high areal power density of 8.8 $mWcm^{-2}$.

Pseudocapacitance is a Faradaic charge storage mechanism based on fast and highly reversible surface or near-surface redox reactions. Importantly, the electrical response of a pseudocapacitive material is ideally the same as that of an EDLC, i.e., the state of charge changes

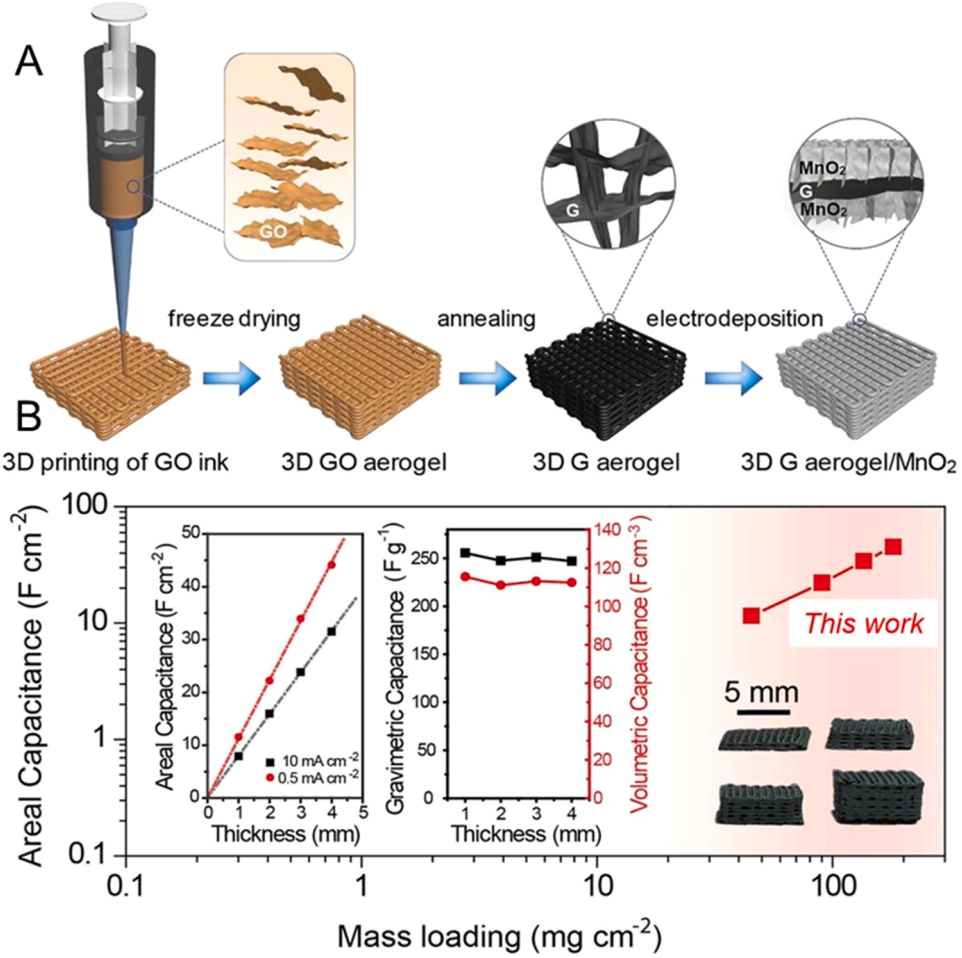

Fig. 8. (A) Schematic representation of the manufacturing strategy developed for G aerogel/MnO_2 pseudocapacitive electrodes. (B) Capacitance versus thickness of thick electrodes at various mass loadings [67].
Reprinted from [67] Copyright (2019), with permission from Elsevier.

continuously with the potential, leading to a proportionality constant that can be formally considered as capacitance. Some materials store a significant charge in a double layer, such as functionalized porous carbons, combining both capacitive and pseudocapacitive storage mechanisms. Different charge storage mechanisms can be distinguished in a pseudocapacitive electrode: underpotential deposition, redox reactions of transition metal oxides, intercalation pseudocapacitance, and reversible electrochemical doping and de-doping in conducting polymers. Materials used for building such electrodes are normally carbons, metal oxides, and conducting polymers [66]. Yao et al. [67] developed a 3D-printed graphene aerogel pseudocapacitive electrode with ultrahigh MnO_2 loading (Fig. 8A) by the DIW method. The pseudocapacitive materials such as manganese oxide (MnO_2) exhibit outstanding gravimetric capacitances, and the grid architecture realized by 3D printing avoids the sluggish ion diffusion in thick electrodes, which achieve a record-high areal capacitance of 44.13 F cm^{-2} with high MnO_2 loading of 182.2 mg cm^{-2} (Fig. 8B). Besides, FDM (fused deposition modelling) and SLA techniques have also been reported in double-layer capacitance supercapacitor fabrication. Yang et al. [68] used the high electronically conductive active material MXene as the building material and printed electrodes with high specific surface area architectures by FDM. The additive-free 2D $Ti_3C_2T_x$ ink-printed current collector-free supercapacitor exhibited a high gravimetric capacitance of 242.5 F g^{-1} at 0.2 A $g^{-1}$with retention of above 90% capacitance for 10,000 cycles.

A solid-state supercapacitor, like a solid-state battery, is a device where all the components are in the solid state. Solid-state supercapacitors have attracted increasing interest because they can provide substantially higher specific/volumetric energy density, compared with conventional liquid supercapacitors, and they are promising as new energy storage devices for flexible and wearable electronics application. Many 3D-printed solid-state supercapacitors with areal energy density have been reported. For example, Shen et al. [69] first developed 3D-printed quasi-solid-state asymmetric micro-supercapacitors with efficient interdigitated patterning electrodes by DIW method. A V2O5-graphene ink was used to construct a cathode, and graphene–vanadium nitride quantum dots were printed as anode, combining with a quasi-solid-state LiCl–PVA gel electrolyte. The asymmetric capacitor design and integrated structure construction exhibit excellent structural integrity, a large areal mass loading of 3.1 mg cm^{-2}, and a wide electrochemical potential window of 1.6 V. Consequently, this 3D-printed asymmetric micro-supercapacitor displays an ultrahigh areal capacitance of 207.9 mF cm^{-2} and areal energy density of 73.9 μWh cm^{-2}, which is superior to that of most reported interdigitated micro-supercapacitors.

3D printing techniques have shown their benefits in the electrochemical performance enhancement such as high power and energy density and mechanical properties improvement by an architectural optimization of electrodes. Among the various 3D printing techniques, direct ink writing has been frequently reported due to its advantage in high mass loading of electrochemically active material and relative facile manufacturing process. Compared with traditional 2D planar structure fabrication techniques, 3D printing provides a new method to solve the issues of ESDs by the 3D design of the electrode architecture. The performance of electrodes and assembled energy storage devices, such as specific power density, energy density, cycling lifetime, mechanical properties and so forth, has been promoted greatly by advanced and rational architectural design. Nevertheless, there are still several challenges that 3D printing must face. One of the most prominent features is the further development of the materials. Due to the limitation of 3D printing techniques such as FDM and SLA, many non-conducting polymers should be added to form stable 3D-printed objects. In consequence, the conductivity and in turn the performance of 3D printed electrodes/devices are negatively affected. The addition of excess liquid electrolyte is another issue. Although they can be replaced by ions-conductive solid-state electrolytes, the development of ultrathin solid-state electrolytes by 3D printing techniques has reached a deadlock. Besides, the post-treatment such as thermal annealing or carbonization is needed to further increase the electrode performance, and manufacturing techniques for the direct fabrication of energy storage devices are scarce. Also, novel and efficient advanced architectures of electrodes need to be designed with the aid of software design and simulation [70]. So far, most of the geometries of 3D-printed electrodes are simple and designed by humans rather than based on scientific theoretical calculations. With the rapid development of machine learning algorithms, more and more advanced architectures of electrodes will be designed and optimized automatically by artificial intelligence, which not only saves a large amount of time but also develops the full potential of electrode architecture design [71]. However, as a revolutionary tool, providing numerous opportunities for the design and manufacturing of high-performance electrodes, 3D printing should be used to address fundamental issues of ESDs.

2.5. Solid oxide fuel cells (SOFCs) and solid oxide electrolysis cells (SOECs)

Solid oxide fuel cells (SOFCs) and solid oxide electrolysis cells (SOECs) are considered among the electrochemical energy storage and conversion devices (EESC). SOFCs convert the chemical energy stored in a fuel (H_2, CO, CH_4, etc.) to electricity directly through an electrochemical reaction (by oxidizing a fuel). SOECs are energy storage units that produce storable hydrogen from electricity and water (electrolysis of water), electrolyze CO_2 to produce CO and oxygen or even co-electrolyze water and CO_2 to produce syngas (CO + H_2) and oxygen [72]. SOFCs and SOECs are highly efficient devices. The efficiency of SOFCs, currently being one of the most efficient energy generation devices, can range from 60% to 90% (in the case of combined heat and power CHP units). The efficiency of SOECs can be over 80%. Applications of SOFCs include use as auxiliary power units in vehicles to stationary power generation, and heat engine energy recovery devices. Applications of SOECs include high-efficiency production of hydrogen/syngas/methane [73]. Hydrogen as a clean energy carrier is promising for next generation power generation and transportation. At the basic level, these electrochemical devices are made of an electrolyte and electrodes (anode and cathode). Interconnects, contact and protective layers and sealing materials are also required for a complete cell and stacked cells. The three main components are made of functional ceramics (electroceramics) and ceramic-metal (cermet) composites.

In an SOFC, the fuel is oxidized at the anode (fuel electrode), the ion conducting electrolyte forces the electrons released during fuel oxidation to power an external circuit before recombining with the oxidant at the cathode. Oxygen is reduced to oxygen ions at the cathode, and these oxygen ions diffuse through the dense solid electrolyte to the anode, where they electrochemically oxidize the fuel. In this reaction, two electrons are released as well as water byproduct. In SOEC, H_2O and CO_2 are reduced to H_2 and CO at the cathode (fuel electrode). The generated oxygen ions diffuse through the electrolyte toward the anode. At the anode, the oxygen ions are oxidized, and this reaction generates oxygen and two electrons. The entire process is driven by an external power supply. In general, operation and fabrication of SOECs are more challenging than SOECs, primarily because the electrodes in SOEC stacks function under harsher conditions.

ZrO_2 (zirconia)-based ceramics are stable under reducing and oxidizing environments. ZrO_2 doped by Y (Yttrium) or Scandia (Sc) provides oxygen conductivity above 800 °C. Currently, yttria-stabilized zirconia (YSZ, a solid solution of a few mol% of yttrium oxide (Y_2O_3) in zirconia) for the electrolyte and YSZ-based composites for electrodes are the state-of-the materials for SOFCs and SOECs. Sc stabilized zirconia (ScSZ) (9 mol% Sc_2O_3 – 9ScSZ) and gadolinium doped ceria (GDC) have been also used as electrolyte [73]. Nickel-YSZ (Ni-YSZ) cermet is used as the fuel electrode (anode in SOFC and cathode in SOEC), in which Ni functions as the catalyst. This is because the high temperature operation of these cells accelerates electrode reaction kinetics and makes the use of

more expensive catalysts (such as Pt) inessential. In addition, Ni is stable under reducing conditions, and is a highly active catalyst for hydrocarbons. The YSZ component of the Ni-YSZ cermet provides the ionic conductivity and serves as the sintering inhibitor of Ni (stops grain growth in Ni). For less-demanding applications, the oxygen electrode (cathode in SOFC and anode in SOEC) is made of abundant Sr (Strontium)-doped $LaMnO_3$ (LSM), while for more demanding applications electrodes based on mixed conductors, such as lanthanum-strontium ferrite cobaltite (LSCF) or lanthanum-strontium cobaltite (LSC) are used. To prevent reaction between the oxygen electrode materials and YSZ, thin (0.1- to 5-mm) layers of gadolinia-doped ceria (CGO) may be utilized [72].

The electrolyte should be sufficiently densified to avoid leakage of the fuel/oxidant gases through the electrolyte to the electrodes and reduce the resistance to oxygen ion diffusion in the electrolyte. The electronic conductivity of the electrolyte should be low to prevent losses due to leakage currents. Flaws, pinholes, and other defects in the electrolyte can drastically reduce the electrochemical performance of the cell. The sintering step of the printed functional ceramics is, therefore, vital. YSZ can be sintered in the range of 1300 – 1500 °C [74]. The densification is often assessed by measurement of the bulk density of the sintered ceramic, as well as by microstructural characterization using electron microscope and X-ray diffraction. For optimal ceramic performance, abnormal grain growth during sintering should be avoided. The density of the electrolyte, which is related to the porosity, plays an important role in the electrical conductivity of the electrolyte. The acceptable electrical conductivity for practical application as SOFC electrolyte is defined to be in the range of $2 - 4 \times 10^{-2}$ S cm^{-1} [75]. Both cathode and anode are required to be porous, electrically conductive and should possess high activities for fuel oxidation and oxygen reduction (high density of electrochemical reactive sites, or triple phase boundaries, TPB). The porosity is required to provide pathways for mass transport (diffusion of gaseous fuels and byproducts). LSM is more common for the oxygen electrode, because of its compatibility and low chemical reactivity with YSZ and their similar coefficient of thermal expansion.

2.6. Traditional fabrications of SOFCs and SOECs, opportunities for additive manufacturing and outlook

SOFCs and SOECs and their stacks are geometrically complex, inherently multimaterial and multilayer devices. The cells are made of thin active elements (~10–50 μm electrolyte and ~50–300 anode and cathode), with different composition and microstructure (porous anode and cathode and dense electrolyte). The microstructure of the functional materials in these devices primarily governs the performance. Currently, the most common geometries are planar and tubular geometries. The current planar cells have higher efficiencies compared to tubular designs (because of lower comparative resistance of the planar design), while the tubular design offers better sealing and faster startup time (minutes compared to ~1 h for planar cells). Modified planar designs may incorporate a wave-like structure (Fig. 9A). Tape casting and screen printing are the most prevalent processing methods used for manufacturing of planar SOFCs and SOECs [76], while physical vapor deposition (PVD) and chemical vapor deposition (CVD) are also being explored, in particular for thin films [77]. However, more than hundred steps could be involved in the manufacturing process of a complete stack, including tape casting, punching, laminating, stacking, firing, etc. [25]. These large number of steps, mostly requiring manual inputs and multiple joints and seals, result in low reliability, low durability, low reproducibility, high cost, and long time to market. Perhaps the high cost of these devices, compared to alternative energy systems, is the single most important factor hindering their wide-spread applications [78].

Currently, there is a shape limitation in the design of these devices, largely due to strict limitation in manufacturing of ceramics with complex geometries. AM is being explored as a promising manufacturing process that may result in lower cost, ease of manufacturing, increased design flexibility, decrease material waste, and more reliable SOFC/SOEC devices. AM may be used to fabricate the entire device or in the production of different components, such as the electrolyte or anode/cathode. If AM technologies can eliminate or reduce the stacking steps, and enable continuous printing of the integrated layers, this can be a significant step forward in manufacturing these devices [79]. Obviously, such AM technologies should also consider the materials compatibility, such as the requirement for co-firing (co-sintering) and matching of the coefficient of thermal expansion of adjacent layers. AM may also result in more favorable geometries (beyond planar and tubular geometries) and controlled layer thicknesses toward enhanced surface area for electrochemical reaction sites and enhanced volumetric current density (specific power), which will result in increased efficiency of the device. As an example, the corrugated devices present ~ 57% performance

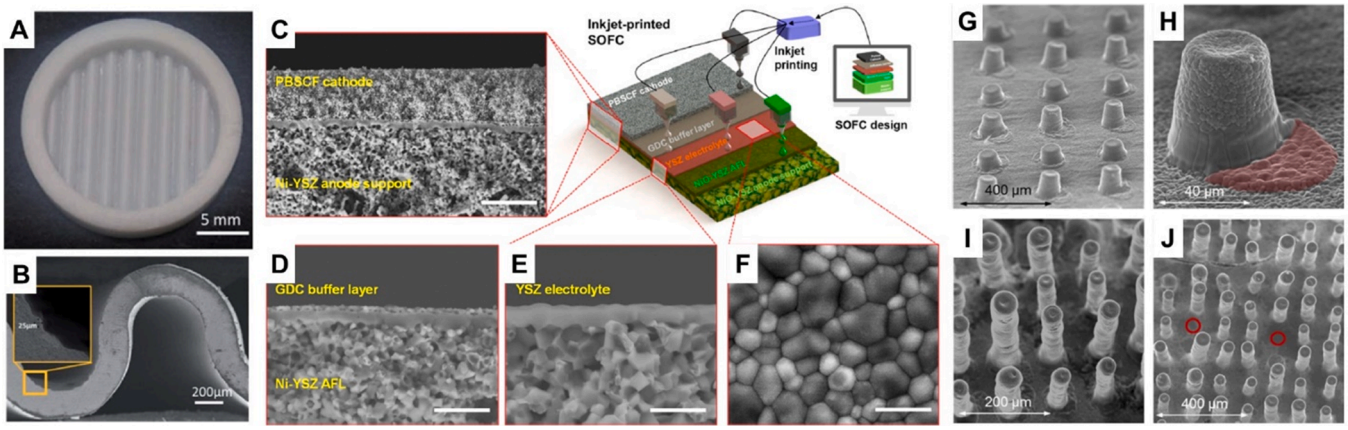

Fig. 9. (A) A top-view image of the self-standing 3D printed corrugated 8YSZ membranes. (B) A cross-section SEM image of the electrolyte. (C) Cross-sectional SEM image of the anode supported SOFC and schematic of the inkjet printing (scale bar: 10 μm). (D) Cross-sectional SEM image of the SOFC with the approximately 0.5 μm thick GDC buffer layer (scale bar: 5 μm). (E) Cross-sectional and (F) surface SEM images of the SOFC with the approximately 0.8 μm thick YSZ electrolyte layer (scale bar: 2.5 μm). SEM images of YSZ pillars on Ni-YSZ substrate. (G) Array of 50-layer pillars at 60 tilt. (H) showing the remnants of a misplaced droplet (red zone) and 50-layer pillar, (I) pillar array 180 layers tall (ca. 300 mm) at 30 tilt, and (J) pillar array showing missing pillars (red circles) due to inactive nozzles. [86]. (For interpretation of the references to colour in this figure, the reader is referred to the web version of this article.)
(a) A and B reproduced from Ref. [80] with permission from the Royal Society of Chemistry. (b) (G) – (J) reproduced from ref. (c) [80] with permission from the Royal Society of Chemistry. (C)-(F) reprinted (adapted) with permission from [83]. Copyright {2020} American Chemical Society. (G)-(J) reproduced from ref. [86].

improvement in fuel cell and electrolysis models, by reducing the area specific resistance ASR [80].

Potential AM technologies should also address the current drive toward lower temperature operation (to ~ 500–600 °C or lower) of SOFCs, which is meant to reduce or resolve some of the outstanding challenges of these devices (such as thermal management and the need for insulation, thermal stress, high degradation rate of current collection and sealings at high operation temperature). A lower operation temperature may result in an increase in the fuel cell efficiency, as well as the possibility of using metals and polymers for these devices. This trend either requires thinner layers to reduce the electrolyte resistance using current materials or discovery of new low temperature oxygen ions conductors. Additionally, microstructural variations such as columnar grains that have less resistance, substitutional doping and defect control, and fabrication of interfaces with less resistance may facilitate lower temperature operations. One way to achieve thinner layers using AM is incorporating (printing) topologically optimized mechanical supports.

Although still at a relatively nascent stage, several AM processes have been used for 3D printing fuel cells or fuel cells electrodes [81,82]. These methods include ink jet printing [83–86], stereolithography [80,87], and DLP [74,79], with ink jet printing being currently the prevalent method. However, perhaps other than printing corrugated surfaces, so far the printed cells and functional layers all have been planar, and no advanced 3D configurations to potentially gain higher specific power has been reported, yet. Pesce et al. fabricated a 250 μm-thick 8YSZ (8 mol% yttria-stabilized zirconia) electrolyte-supported SOFCs with conventional planar and high-aspect ratio corrugated electrolytes using stereolithography, Fig. 9A-B [80]. Cells with corrugated layers showed an increase of 57% in their performance in the fuel cell and co-electrolysis (of CO_2 and steam) modes, in the temperature range of 800 – 900 °C. This enhancement is attributed to the larger area (~60%) compared to the cells with planar layers. The printed cells showed a degradation rate of 0.035 mV h^{-1}. Han et al. used a commercial low-cost office printer (HP inkjet printer) to print an entire anode supported SOFC with a sub-micron thin YSZ electrolyte, Fig. 9C-F [83]. The printed SOFC maintained high open circuit voltage and robust uniform microstructure during electrochemical performance, and in durability test achieved a power output of 730 mW cm^{-2} at 650 °C and a low degradation rate of 0.2 mV h^{-1}. Wei et al. manufactured a dense 8YSZ electrolyte via digital light processing [79]. For this work, the authors used a suspension of 30 vol% 8YSZ powder in a photo-curable resin, and the results showed a dense electrolyte (99.96%) after sintering and debinding. The cell was completed by adding anode and cathode to the printed electrolyte (Ag-GDC/YSZ/Ag-GDC). The cell showed an OCV of 1.04 V, and a peak power density up to 176 mW.cm^{-2} at 850 °C by using hydrogen as the fuel and air as the oxidant. We note that the theoretical OCV for cells with dry hydrogen operation is ~ 1.07–1.15.

Ink jet printing requires inks with certain rheological properties to be printable. Additionally, the ink should have a long-term dispersion stability to prevent agglomeration and sedimentation issues, which makes the choice of suitable dispersant an important step. If the ink does not have the required properties, it may result in nozzle clogging or undesirable printed objects. Han et al. used ceramic particles with size distribution in the range of 0.15 – 0.19 μm, smaller than the nozzle diameter of the printer, to formulate the ink [83]. Ink jet printing is suitable for thin film fabrication (planar cells), which can operate at lower temperature, since the thin electrolyte and electrodes reduce energy loss by ion transport. Another advantage that ink jet printing offers is the porosity control by assigning a “gray scale” in the CAD model. The porosity is required for the electrodes (anode and cathode) in these devices. Additionally, ink jet has a better compatibility for printing various types of materials such as polymers, metals, and ceramics, all in a relatively low cost. However, it has limitation for high aspect ratio structures or tubular cells.

DLP and SL have the advantage of good surface quality and dimensional precision. The resolution of a DLP printer is generally ~50 μm in-plane (XY-plane) [74], with a layer thickness of 25 μm [74] to 50 μm [79]. The main challenge in using DLP and SL for 3D printing ceramics is the preparation of well-dispersed photocurable slurries with high ceramic content (solid loading), which currently are not commercially available at a wide scale. Added to this challenge, is the identification of optimized (often based on thermogravimetric analysis on the green body) debinding (removal of the organic components) and sintering processes. The quality of the photocurable ceramic resin determines the curing depth, precision of green body, and ultimately the electrochemical and mechanical performance of the printed ceramic. A well-dispersed (stable and uniform with no well-defined separated phases) and high solid loading suspension is critical to eliminate or reduce the crack formation, deformation, and delamination when shrinkage occurs during debinding and sintering [79]. Choice of dispersants (such as PEG) is important to achieve a desired dispersion. Solid loadings in the range of 30–50 vol% have been reported for printing solid oxide cells components [74,79]. One method to achieve high solid loading suspension is using powders of the same materials with two or more particle sizes [79]. Generally, a viscosity < 5 Pa at a shear rate of 30 s^{-1} has been necessary for successful printing [88], in addition to preferred low surface tension for self-leveling. Noticeable interfaces from layer-by-layer printing may compromise mechanical and electrical properties of the ceramic and affect the electrochemical performance of the cell. Xing et al. obtained a smaller power density for electrolyte printed by DLP compared to cells with similar electrolyte thickness, which the authors attributed mainly to the layer boundaries between the printed 50 μm layers in the DLP process, in addition to separation of the cathode layer from the electrolyte [74]. This is despite an OCV ~ 1.1 obtained for the cells, which is more indicative of the gas tightness of the printed electrolyte.

If manufacturing of complete SOFCs is intended, SL and DLP have limitations in achieving multi-material printing capability. If the AM process is used to only print a component of the cell (often the electrolyte), the other components should be added by conventional means. For example, NiO-8YSZ slurry and LSM ($La_{0.8}Sr_{0.2}MnO_3$) slurry was applied to the surface of the as-sintered 8YSZ electrolyte plates by using brush (brush painting). The NiO-8YSZ slurry and LSM slurry were prepared using their corresponding commercial powders [74]. Wei et al. sprayed cermets consisting of Ag and GDC ($Ce_{0.8}Gd_{0.2}O_{1.9}$, Gadolinium doped Ceria) as the materials of anode and cathode on the printed electrolyte [79]. After application, the anode and cathode materials were annealed.

We may argue that no single modal printing technology can overcome the above-mentioned limitations, and perhaps the case for development of hybrid multimaterial 3D printers is strong in the case of SOFCs and SOECs [25]. This will require expansion of the list of printable materials such as ceramic interconnects. Since interconnects are exposed to both oxidizing and reducing high temperature environments, ceramic materials can offer a stable and reliable option, albeit at a steep price. Metal based interconnects will be more promising as lower temperature range (600 – 800 °C) devices are developed. The trend toward low temperature and thinner layers (tens of microns) will require printing technologies with better resolution. For example, the thickness of each layer in DLP/SLA process is ~ 50 μm, and perhaps several layers are needed to make a layer with acceptable properties. On the other hand, to keep the ASR < 0.15 Ω.cm^2, the thickness of YSZ should be smaller than 50 μm. One way to circumvent this limitation would be printing an electrolyte with thin and thick sections, in which the former provides the higher electrochemical performance, while the latter provides the mechanical support. This will require complex 3D design of the cells [74].

2.7. Piezoresistive and piezoelectric ceramics as energy harvesters and sensors

Piezoelectric materials transform mechanical stress and deformation into electrical charge by compression/tension/shear of a bulk material,

and piezoresistive materials change electrical resistance when subjected to mechanical stress and deformation. By measuring this electrical energy change, these materials can function as energy harvesters or as sensors. Piezoelectric and piezoresistive ceramic materials have a variety of applications such as piezo generators, sensors, piezo actuators, and transducers. Generally, piezoelectric ceramics are made with powder-based methods and rely on crystal structure and ionic structure for lattice distortion and dipole formation, whereas piezoresistors rely on band structure and electron configuration differences and have mostly been made via preceramic polymer pyrolysis and crystallization. Thus, the distinction and separation will be done in this section.

2.8. *Traditional fabrications of piezoelectric ceramics, opportunities for additive manufacturing and outlook*

Piezoelectricity is the ability of the crystal structure to deform and create a dipole and generate an electrical charge when mechanically loaded with pressure or tension, which is called the direct piezo effect.

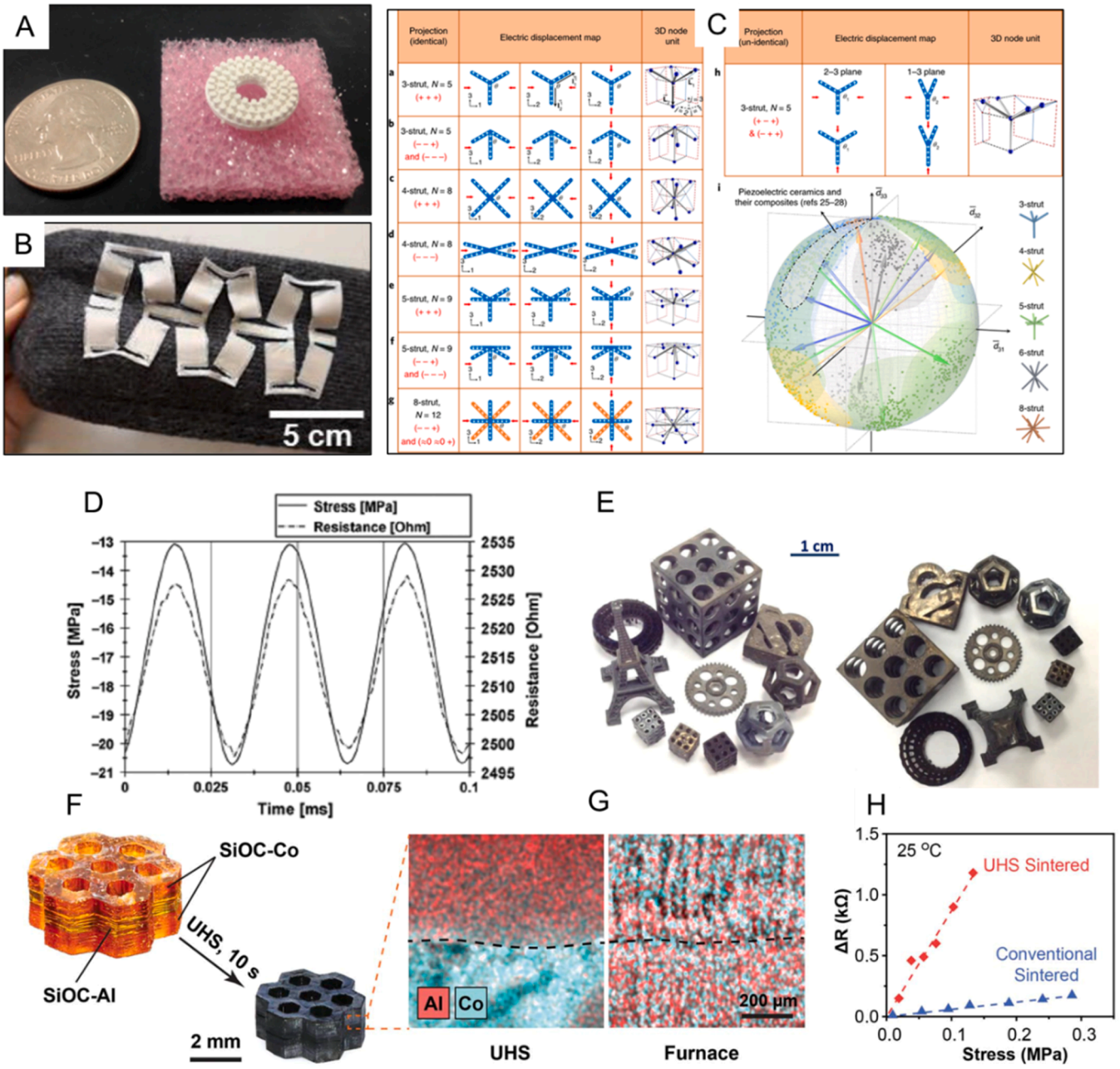

Fig. 10. (A) Barium titanate 3D printed by stereolithography. (B) flexible 3D printed barium titanate, and (C) lattice unit cell and 3D piezoelectric design, reprinted from(100)(D) Piezoresistive response of a polymer derived SiOC upon dynamic loading conditions; the resistivity of the sample (dashed line) exhibits a precise response to the load (continuous line). (E) Preceramic and corresponding pyrolyzed ceramic parts prepared via stereolithographic processing of polysiloxanes. (F) A 3D-printed SiCoOC-SiAlOC-SiCoOC sandwich structure and resulting ceramic part after ultrafast pyrolysis step. (G) elemental mapping of the SiAlOC-SiCoOC interface region showing interdiffusion for the part produced via conventional pyrolysis and a sharp interface in the ultrafast pyrolyzed part. (H) A plot of the change of the resistance of the SiCoOC-SiAlOC-SiCoOC sandwiched parts as function of the applied stress.
(a) Reprinted from [91] Copyright (2016), with permission from Elsevier. (B) reprinted from [94] Copyright (2020), with permission from Elsevier. (C) reprinted from [100], with permission from Springer Nature. (D) [113] with permission from the John Wiley and Sons. (E) Reprinted from [121] Copyright (2017), with permission from Elsevier.(F)-(H) reproduced with permission from ref. [119].

Conversely, these crystals undergo a controlled deformation when exposed to an electric field, a behavior referred to as the inverse piezo effect. The polarity of the charge depends on the orientation of the crystal relative to the direction of the pressure. Piezoelectric ceramic materials include lead zirconate titanate, barium titanate, lead titanate, and potassium sodium niobate and are generally made with powder processing techniques. Traditionally, these materials have been made without additive manufacturing techniques with thin and thick films, single crystal and polycrystalline powder forming techniques. Despite the use of traditional methods, there is room for the use of AM to improve the functionality of piezoelectric ceramics. These methods allow for controlled structures and geometries that can be subject to stress and deformation without catastrophic failure, but also layered structures can tailor the electrical signals though the material.

Gaytan et al. [89] investigated the suitability of binder-jet additive manufacturing to develop barium titanate piezoelectric components for pressure sensing. The authors reported an improved piezoelectric coefficient with increasing sintering temperature. The authors attribute this correlation to decreased grain size and increased density. Kuscer et al. [90] developed an ink with nanometric lead zirconate titanate particles for deposition by ink-jetting onto a corundum substrate to create piezoelectric thick films. Though the printed films showed reduced piezoelectric properties compared to bulk lead zirconate titanate, a similar thickness coupling factor was achieved, thereby indicating the versatility of this method for using inks to print piezoelectric films. Chen et al. [91] used digital light processing to create complex geometry barium titanate components for end use as an ultrasonic generator (Fig. 10A). The authors reported relatively high density (~94%) with increased piezoelectric coefficient over other AM methods, and a comparable loss coefficient to traditionally processed barium titanate. Chen et al. [92] used a similar approach to create potassium sodium niobate (KNN) components using micro-stereolithography. This showed a relatively low piezoelectric coefficient compared to bulk KNN, which was attributed to the low density (92%) of the printed components. However, the authors reported crack-free specimens after debinding of the photopolymer resin used during printing. Hossain et al. [93] used electron beam melting to fabricate lead zirconate titanate components for end use as embedded piezoelectric sensors. Though the study focused more on the development of the assembly that could be used for in-situ monitoring with the printed components, the authors reported high density components. Furthermore, the tested components exhibited excellent response to cyclic loading under a range of frequencies, indicating that these components can be used for in-situ monitoring. Zhou et al. [94] fabricated stretchable piezoelectric nanogenerators by direct ink writing of ink made from barium titanate and polyvinylidene fluoride trifluoroethylene (PVDF), a piezoelectric polymer. These structures were developed for end use as wearable electronics (Fig. 10B). It was found that the addition of 20 wt% barium titanate increased the piezoelectric performance of the PVDF. It was also demonstrated that up to 300% strain of the bulk geometry was achieved without degradation of the output voltage. A similar result was observed for lead zirconate titanate doped PVDF [95]. Walton et al. [96] used direct ink-writing with anisotropic nozzles to align barium titanate particles to increase the electromechanical performance of printed piezoelectric structures. Significant texturing was observed when the nozzle aspect ratio and printing speed were increased.

It has been shown that grain texturing improves the piezoelectric constant and decreases the magnitude of the electric field needed for polarization of piezoelectric materials [97,98]. Depending on thickness, size and material, the piezoelectric materials were polarized in silicon oil for 30–120 min at 20–150 °C with an electric field of 3–50 kV/mm [94,96]. When these structures are polarized, the electric field is homogenous and uni-directional and aligns the dipoles with the electric field. This process works well for materials with simple geometry (plates/films, cylinders/discs, etc.) that are effectively two dimensional. However, AM is capable of fabricating complex three-dimensional shapes with ease, and thus it is important to consider how to control dipole alignment in three-dimensional ceramic structures. With polymer-based AM of piezoelectric materials, printed structures can be manipulated into different shapes using heated molds (or heated press) [99]. With ceramics, this is much more difficult. An interesting approach to encompass three-dimensional piezoelectric properties was developed by Cui et al. [100]. In this study digital light processing (DLP) was utilized to create lead zirconate titanate piezoelectric lattice structures. In this approach each lattice was designed such that each ligament was aligned with the d_{33}, d_{32}, or d_{31} directions within the piezoelectric constant tensor (Fig. 10C). This enabled creating a spatial design that encompassed piezoelectric design space, thus allowing for coupled design of the lattice with the piezoelectric anisotropy. With this method, the authors developed lattice architectures that allowed for multi-dimensional sensing capabilities. Though the mentioned lattice structures were utilized as sensors, these lattices could be further developed as energy harvesting devices that effectively convert mechanical motion in three-dimensions to electricity.

For piezoelectric ceramics, there are many improvements that can help design the materials for the properties and applications. Texturing of piezoelectric ceramic material made with powders has led to increased output voltage at similar levels of strain as compared to components with random grain orientation, so this must be controlled and optimized when designing piezoelectrics. Better ways to incorporate fine grains, texturing, gradation, layering, and large complex shapes should be explored for piezoelectric optimization, and the composites may consist of powders and even PDCs (as with piezoresistors).

2.9. Traditional fabrications of piezoresistive ceramics, opportunities for additive manufacturing and outlook

Typically, there are various classes of piezoresistive materials for sensing, e.g., metallic materials (used for instance in strain gauges), semiconducting materials such as Si, Ge or alloys thereof [325,326], as well as nanocomposite materials relying on an electrically conductive percolative network dispersed within an insulating matrix, such as carbon-containing ceramic (nano)composites [103]. Whereas the piezoresistive response in metallic materials mainly relies on geometric changes upon mechanical loading, applying a mechanical stress on semiconducting piezoresistive materials induces deformation of the energy band structure thereof, and thus alters the charge carrier mass and mobility in the materials. Therefore, the resistivity of the material changes. Due to the direct effect of mechanical loading on the band structure of semiconducting piezoresistive materials, their piezoresistive response is significantly enhanced as compared to that of metals. The gauge factor GF, which is defined cf. $GF = (\Delta R/R_0)/\varepsilon$ (with ΔR being the change of resistivity upon mechanical loading, R_0 being the resistivity of the stress-free material and ε being the strain), has been thus shown to be rather small in metals (e.g., 2.1 in a 60Cu-40Ni alloy); whereas semiconducting piezoresistive materials possess values ranging from 20 to 300. Many piezoresistive materials are made from polymer derived nanocomposites from siloxane and silane preceramic polymers that are pyrolyzed and crystallized.

Significant amount of work and progress has been made in the last few decades within the context of piezoresistive carbon-containing cementitious materials [101,102], as well as polymer-derived ceramics (PDCs) [103]. Both types of composites rely on the presence of a percolative carbon network, which determines the piezoresistive behavior and may be adjusted for volume fraction, aspect ratio, crystallinity/-graphitization etc. Unlike the cement-based composites, in which the disperse carbon phase is introduced within the matrix by mechanical procedures, the phase composition of carbon-containing polymer--derived ceramics can be provided (and modulated) in situ during the ceramization of suitable preceramic polymers [104–106]. The latter approach is highly attractive, as it solves homogeneity and dispersion issues encountered in other processing methods.

Ternary polymer-derived ceramic (PDC) systems, e.g., SiOC and SiCN, as well as quaternary/multinary systems containing additional elements such as boron (B), main group metals, transition metals, and rare earths, have been synthesized within the last decades and their processability and property profiles have been extensively investigated, as summarized in several review articles [105–110]. Their synthesis typically involves the use of suitable preceramic polymers [106,111] that are converted into ceramics in a multi-step procedure involving shaping, cross-linking/curing as well as pyrolysis. The use of polymeric materials as precursors for the ceramics provides a high versatility with respect to the manufacturing of parts; thus, some of the most common shaping techniques include casting, injection molding, pressure- and temperature assisted shaping (warm pressing), electrospinning, fiber drawing (e.g., melt spinning), coating, impregnation, as well as additive manufacturing (AM) procedures (Fig. 10) [108]. The resulting green-bodies are extensively cured to render them infusible (i.e., not meltable) and furthermore to control or even suppress excessive mass loss. The cured green bodies are subsequently thermally treated at elevated temperatures (500–1400 °C) in either reactive or inert atmosphere and converted into ceramics [108].

Within the last 10–15 years, various studies related to the synthesis and piezoresistive behavior of PDCs were reported, as summarized in a recently published review paper [103]. The piezoresistive response in those materials is considered to rely on a sp^2-hybridized carbon phase, which is typically present in the PDCs. As mentioned above, the in-situ generation of the carbon phase within the microstructure of PDCs provides a highly homogeneous dispersion thereof and prevents agglomeration-related issues, which have been reported for other carbon-containing ceramic nanocomposites that are prepared upon mechanically mixing of the carbon phase into the ceramic matrix [103,104]. Additionally, the use of preceramic polymers allows for a tight control and fine tuning of morphological features of the segregated carbon phase, such as content, crystallinity, aspect ratio, etc. [104,109].

The first study reporting on the piezoresistive behavior of a PDC was published in 2008, and described the synthesis of a SiCN-based materials possessing tremendously high gauge factors, in the range of 1000–4000 [112]. Two years later, the piezoresistive effect was demonstrated also in SiOC-based PDCs (Fig. 10D) [113]. In both ternary systems, the piezoresistivity was proposed to be mainly determined by a tunneling-percolation mechanism [114]. Interestingly, the piezoresistive effect was shown to persist in PDCs even upon exposure to temperatures beyond 1000 °C and hostile environments (oxidative, corrosive atmosphere), thus making SiOC and SiCN-based materials highly attractive for high-temperature strain/pressure sensing in harsh environmental conditions [103]. Thus, Terauds et al. reported on piezoresistive SiOCN-based ceramics possessing impressive gauge factor at temperatures beyond 1000 °C, e.g., 322 and 287 at 1400 °C and 1500 °C, respectively [115]. Moreover, Roth et al. reported on the fabrication of a high-temperature piezoresistive C/SiOC-based material showing a reliable gauge factor of ca. 80 at temperatures up to 1300 °C [116]. Also, quaternary PDCs such as SiBCN [117] and SiAlOC [118] were reported possessing piezoresistive behavior with extremely high gauge factor values.

While the extremely large gauge factors reported for several compositions are surprising and not yet clarified, PDCs have been currently recognized as high-potential piezoresistive materials for pressure / strain sensing and are anticipated to be first-choice materials for use at high temperatures and in hostile environments. Recently, few reports on the implementation of piezoresistive PDCs in pressure sensing or strain gauge devices were published. For instance, a pressure sensor based on SiBCN was reported by Shao et al. to exhibit a gauge factor of 5500 along with high accuracy, repeatability as well a stability at pressures up to 10 MPa [117]; also, miniaturized sensing elements based on thin film SiOC were recently shown to possess piezoresistive response in both compressive and tensile loading and exhibited gauge factors of up to 5000 [327]. While there are numerous studies related to the materials synthesis and performance assessment of piezoresistive PDCs, currently there is only one report available in the literature, considering the AM of piezoresistive PDC-based parts [119]. It should be mentioned, though, that the preceramic polymer route for preparing ceramics via additive manufacturing procedures has been increasingly considered in within last years [12,120,121]. Thus, various techniques, such as direct ink writing (Pierin et al. [122]) or digital light processing (Zanchetta et al. [123]) were successfully demonstrated as being suitable to fabricate complex-shaped PDC-based parts (Fig. 10E).

In the study related to additive manufacturing of a PDC-based ceramic part with piezoresistive behavior, a sandwiched SiCoOC-SiAlOC-SiCoOC structure was prepared by using a multi-material stereolithography approach, and converted into ceramic by using either a conventional pyrolysis procedure or an ultrafast pyrolysis method, which used a heating rate of 2400 °C/min and a holding time at 1200 °C of just 10 s (Fig. 10F-H) [119]. Thus, whereas the conventionally pyrolyzed part required many hours of thermal treatment, the conversion using ultrafast pyrolysis procedures took less than one minute. Additionally, it was shown that the ultrafast pyrolyzed structure possesses improved piezoresistive response, exhibiting a gauge factor of 297 (compare to 137 for the structure prepared using conventional pyrolysis). The prepared structure containing the piezoresistive SiAlOC layer sandwiched between two soft-magnetic SiCoOC layers was additionally demonstrated to be suitable for magnetic flux density sensing purposes [119].

Additively manufactured piezoresistive structures are expected to bring significant advantages as compared to piezoresistive sensing devices manufactured by using conventional manufacturing procedures. This has been shown for various 3D-printed strain sensors consisting of carbon-based conductive fillers in polymers, which have been used in, e.g., static and dynamic strain measurements for health and damage monitoring of smart structures in aerospace components [124,125], and medical diagnostics [126]. While one approach addresses integrating strain sensors into 3D-printed structures post 3D-printing step, there is increased activity pointing toward developing materials and manufacturing solutions for multi-material printing, allowing to simultaneously generate the functional sensing part and the structural part [127], where layered and graded parts can provide further tailoring of properties. This indeed makes possible to manufacture complex structures consisting of sensing and structural components in one step and at low-cost. Currently, these concepts which have been demonstrated for polymer-based sensing materials and structures are yet to be implemented.

2.10. Smart glass

Smart glass and smart glass devices are glass-based material constructions that enable active or adaptive response to environmental or interventional stimulation. Most prominently, these can be smart windows or other components of a building envelop with adaptive energy (photovoltaic or heat) harvesting ability, cooling functions or emissivity control and shading [128,129]. Smart glass substrates and surfaces can be generated to enable stimuli response. Target functionality and applications include, for example, thermal, chemical, or optical sensing, adaptive light emission, transmission and scattering, or information display and augmented reality. The term “smart glasses” is also used in a less generic way for wearable devices for computer-aided augmented reality or vision enhancement; for a review on this subject, refer to [130]. While most of these technologies are in their early exploratory stage, they hold promise for future application in holistic energy harvesting, conversion, and transmission systems. Thereby, the glass itself usually provides for the optical and mechanical properties of the construction and, for example, for its overall shape and geometry (such as in window panels, glass-glass solar modules, or glass-based microfluidic elements), and is combined with polymers, ceramics, or other material components to achieve a certain function.

Stimulus response relates to a physical or chemical reaction of the material construction to (local or global) stimulation, for example, caused by changes in temperature, illumination, ambient humidity or other factors [131]. Depending on device design, the response may be global (*e.g.*, in a smart window) or local (*e.g.*, on a glass surface used as smart sensor). In addition, multi-responsivity may be generated, whereby material reactions depend on the simultaneous presence of multiple stimuli. This is illustrated in Fig. 11: color codes "blue" and "rose" indicate the local (A, C) or temporal (B) presence of two different stimuli (for example, illumination and temperature), with material response functions *f*(*A*,*B*) decoded "on"/"off" ("0" / "1"). At stage {11}, both stimuli are present, and a material reaction is triggered.

In practice, such behavior can be realized in, *e.g.*, a chromic window which adapts to the intensity of solar irradiation (or to an intentional switching process by human or automated intervention) by reducing light transmission (single stimulus), or which does the same, but only under the condition of a certain inside or outside temperature (stimulus combination) [132]. As another example, fluidic windows have been reported which combine cooling and heating capability by using a heat transfer liquid circulating within transparent capillaries embedded inside the window sheet [133,134]. In these examples, the triggered function is a result of material combinations, device design and non-glassy components. Although glass itself may exhibit active response (beyond the most common case of light emission by photoluminescence), the structural dynamics and pertinent bond energetics of classical (metal oxide) glasses usually do not allow for pronounced switching processes. Strong stimulus response, on the other hand, may be generated in chalcogenide glasses and phase-change materials [135], ionic glasses [136] or, *e.g.*, from the emerging metal-organic framework glasses [137] and glass-based composites [138,139].

Aside from designing a specific application, there are various challenges associated with smart glass devices, including manufacturing technologies [140], response kinetics [141], sensitivity and selectivity [142], long-term operation, user acceptance, construction logistics and cost. On part of the glass component, while forming and post-processing of large, high-volume glass objects is well-established, there are significant limitations for more intricate and miniaturized designs, small-volume or prototype manufacturing, highly individualized manufacturing, and multi-material integration. These areas offer opportunities for AM processes. AM technology may thus address two aspects: fabricating certain glass objects or components, or enabling integration of active glass parts, glass substrates or disperse glass components within complex material constructions.

2.11. Traditional fabrications of smart glass, opportunities for additive manufacturing and outlook

Interest in glassy materials typically arises from their liquid processing ability, leading to a *universal* fabrication methodology for homogeneous and dense objects. The primary processing parameters are the temperature dependence of viscosity (*viscosity curve*) and the liquidus temperature of the considered glass melt. In processing context, the former is often reduced to the viscosity value at liquidus: glass forming is usually conducted at a temperature above liquidus so that undesired crystal precipitation (*devitrification*) may be avoided. Thereby, a given forming process requires a certain viscosity range and underlies certain temperature limitations in terms of a lower temperature limit (the liquidus temperature of the processed melt) and an upper temperature limit (set through the employed forming tools). These two requirements result in characteristic processing windows: glass-forming is possible *universally*, i.e., towards the broadest variety of shapes and formats (in practical terms) for as long as the viscosity-liquidus characteristics of the glass melt fall within the considered processing window. In some cases, the obtained glass object may further be transformed to a glass ceramic by controlled crystallization, which is conducted during secondary heat treatment [143]. Given the full breadth of glass applications, however, glass ceramics are still relatively rare. On the other hand, by combining the glass forming ability with properties of (polycrystalline) ceramic materials, they offer potential for functional materials, including those formed by additive manufacture. Further post-processing of glass objects may involve, *e.g.*, thermal or chemical strengthening [144], or acid polishing. Such treatments address the surface properties of the glass product, for example, inducing residual mechanical stress or tailoring the surface roughness.

The great advantage of conventional liquid (hot) glass processing lies in production cost and throughput of net-shape objects with a very broad variability of size and shape. These advantages are particularly relevant for mass production of relatively large objects (cm to m –scale). On the other hand, liquid forming underlies various limitations, which impose restrictions on final object geometry. For example, surface tension often prevents net-shaping of sharp edges or certain 2D/3D features; without post-processing or other interventions (e.g., hot drawing), corner and edge radii of glass objects are typically on the mm scale. While uniaxial (re-)drawing can achieve very delicate glass structures (e.g., microstructured/photonic crystal fiber [145], thin and flexible sheet [146]), it is usually limited to 1D or 2D geometry. Alternative methods for 3D shaping (e.g., vacuum/thermoforming techniques, hot embossing) underlie the above limits of surface tension, usually lead to uneven wall thickness distribution, or do not allow for complex internal voids, defects, holes, or concave features.

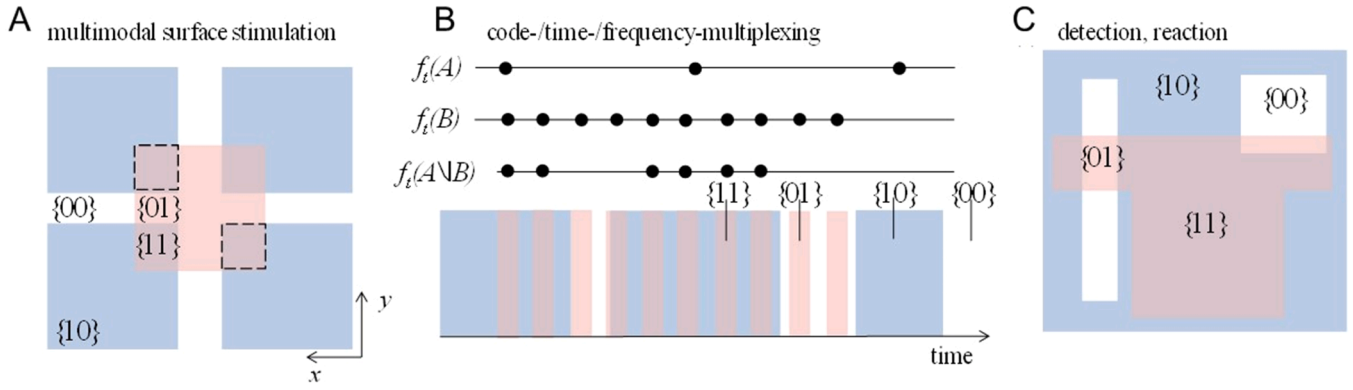

Fig. 11. Schematic of the functionality of a smart material surface with multimodal stimulus response. Blue and rose color codes indicate two independent stimuli {A, B} occurring in space (A and C) and time (B). These trigger stimulus functions f(A, B), whereby state "0" represents "stimulus off" and state "1" represents "stimulus on". The physical response of the substrate material to stimulus combinations enables logical operations (C). (For interpretation of the references to colour in this figure, the reader is referred to the web version of this article.)

Advanced AM methodology provides an opportunity to complement established glass forming techniques by filling some of the above-noted gaps, and some AM examples are shown in Fig. 12. In particular, AM holds significant promise for (*i*) prototype manufacture or the manufacture of individualized (low-volume) glass objects (overcoming the need for complex forming tools, molds, large-scale melting facilities or other adapted processing equipment, (*ii*) manufacture of complex 3D structures with characteristic feature sizes in the sub-mm range towards net-shape objects or preforms, for example, for subsequent secondary forming such as for microstructured fiber and capillary devices, or for transformation into glass ceramics, (*iii*) individualized objects with internal voids (holes, channels, etc.), for example, for microreactor/microfluidic devices [147], preforms for subsequent material infiltration, or scaffold structures, and (*iv*) high-throughput sample deposition methods for accelerated materials discovery.

Aside upscaling, the primary challenges specific to AM of glassy materials relate to achieving glass-like haptics and optical appearance (e.g., optical transparency, surface finish, mechanical performance), the versatility of AM-compatible glass formulations or suitable precursors (e.g., glasses with high refractive index, $n > 1.6$ [148]), material homogeneity (effects of powder or filament vs. bulk processing, for example, in the desired manufacturing of glass ceramics, or in the undesired surface/interface crystallization), and – when precursor materials are used – property variations between precursor and melt-processed glasses, or – when melt-processed glasses are used – achieving processing timescales and temperatures which enable high-quality forming and avoid devitrification. Notwithstanding these specific aspects, the main challenges of AM for ceramic materials (see Section 1) apply also for AM of glasses.

A specialist review on AM technologies applied to glassy materials was provided by Zhang et al. [149]. The presently employed technologies can roughly be divided into two groups: melt-deposition, whereby a precursor glass is used which already exhibits a composition equivalent or very similar to the final object, or reactive deposition, where the final glass is created from chemical reactions in the precursor batch (and, eventually, melted in a consolidation treatment). The obtained objects are either a result of viscous powder sintering at relatively high viscosity (~10^8 Pa·s) or melting (~10^2 – 10^5 Pa·s), eventually affected by preceding pyrolysis of organic binders and other additives.

At present, related research and development work is still focusing on obtaining transparent (in visible or IR spectral range) objects of various shapes, sizes, and chemical compositions. The primary aim is to reproduce glass-like haptics, visual appearance and structural features by AM, with less emphasis on functional properties, whereby optical functionality represents an important exception [150]. Some of this started with the pioneering work of Klein et al. [151] in which large area glass structures were printed with heated nozzles. In view of the established efficiency of large-scale/high-volume glass production and lamination technologies, the advantages of upscaling AM to m^2-scale glass devices or functional sheet remain unclear, although architectural-scale glass objects by AM have already been demonstrated [152]. In this latter field, AM has the potential to replace specialized molding techniques used to fabricate certain kinds of structural glasses or cast glass bricks [153]. Similarly, AM manufacturing of functional glass ceramic materials (e.g. [154]) or glass-ceramic-composites (e.g. [155]) remain nascent fields as shown in Fig. 12A. DIW and SLA were used to create 3D printed translucent alumino-borosilicate glass scaffolds from fine powders and resins or slurries as shown in Fig. 12C [156]. 3D printing of transparent fused silica glass was achieved using two-photon lithography with tens of micrometer resolution and a surface roughness of $R_a \sim 6$ nm as shown in Fig. 12E [157]. As another example, $As_{40}S_{60}$ chalcogenide glasses ($T_g = 188$ °C) were fabricated as shown in Fig. 12 F using filament FDM methodology at a temperature around 140 °C above the glass transition temperature [158]. Similar materials may achieve importance in various electrical and optical applications (such as thermoelectrics, further discussed in Section 2f).

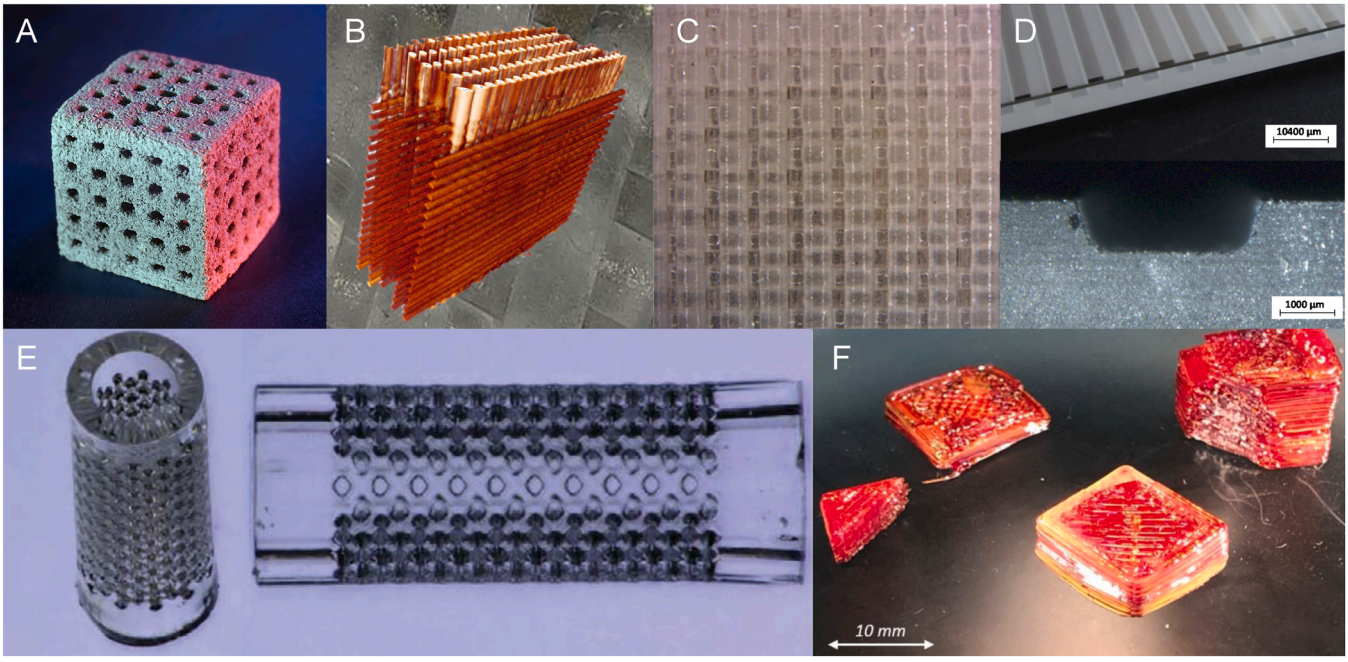

Fig. 12. Examples of smart glass objects manufactured by 3D methodologies. (a) Glass-ceramic composite scaffold produced by binder jetting and subsequent sintering of a cube with width ~ 17 mm [155]; (b) CT-scan of a silica glass fiber stack for 3D volumetric light delivery with an individual fiber thickness of 200 µm; (c) translucent scaffold produced from an aluminoborosilicate glass by DIW using a 800 µm nozzle; (d) laminate glass sheet device with internal capillary channels of depth ~ 961 µm ; (e) micron-scale silica glass objects (diameter ~ 0.5 mm) produced by two-photon DLW from a photoresponsive precursor resin; (f) chalcogenide glass objects manufactured by filament FDM .
(c) (reproduced from Fig. 5a of Ref. (156) under CC-BY license), (d)(reproduced from Fig. 10a-b of Ref. (140) under CC-BY license), (e) (reproduced from Fig. 2c-d of Ref. (157) under CC-BY license), (f) (reproduced from Fig. 3a of Ref. (158)under the terms of the OSA Open Access Publishing Agreement © 2019 Optical Society of America).

Conventional glasses often act as passive substrates or containments, light-guides, support structures, containers, windows and covers, gas-tight seals, or components of material composites which provide mechanical robustness and structural stability [159]. Most of today's research efforts in AM of glasses relate to similar applications, whereby the AM technology offers enhanced individualization and flexibility of shapes, integration ability with other materials, miniaturization, and, on the scale of individual or prototype objects, rapid manufacturing. All of these can add to sustainable manufacture of glasses and glass ceramics, so the opportunity to produce glass ceramics at lower cost exists. By tailoring material properties and device architectures, improved performance can be obtained, eventually contributing to higher material payback and device efficiency, from building technology to applications of energy storage, conversion and conservation.

2.12. Thermoelectrics

Thermoelectric devices are solid-state energy conversion devices that convert heat to electricity and vice versa. Thermoelectric devices are commonly used for highly localized heating and cooling. The most notable application for power generation is radioisotope thermoelectric generators powering space vehicles [160,161]. There has been extensive interest in thermoelectric waste heat recovery where thermoelectric devices are used for power generation by converting excess heat directly into electricity. Proposed applications include heat-to-power conversion in automotive exhaust, industrial processes, and sensors [162]. However, the relatively low device efficiencies, high device costs, and need for application-specific customization have limited widespread adoption of the technology.

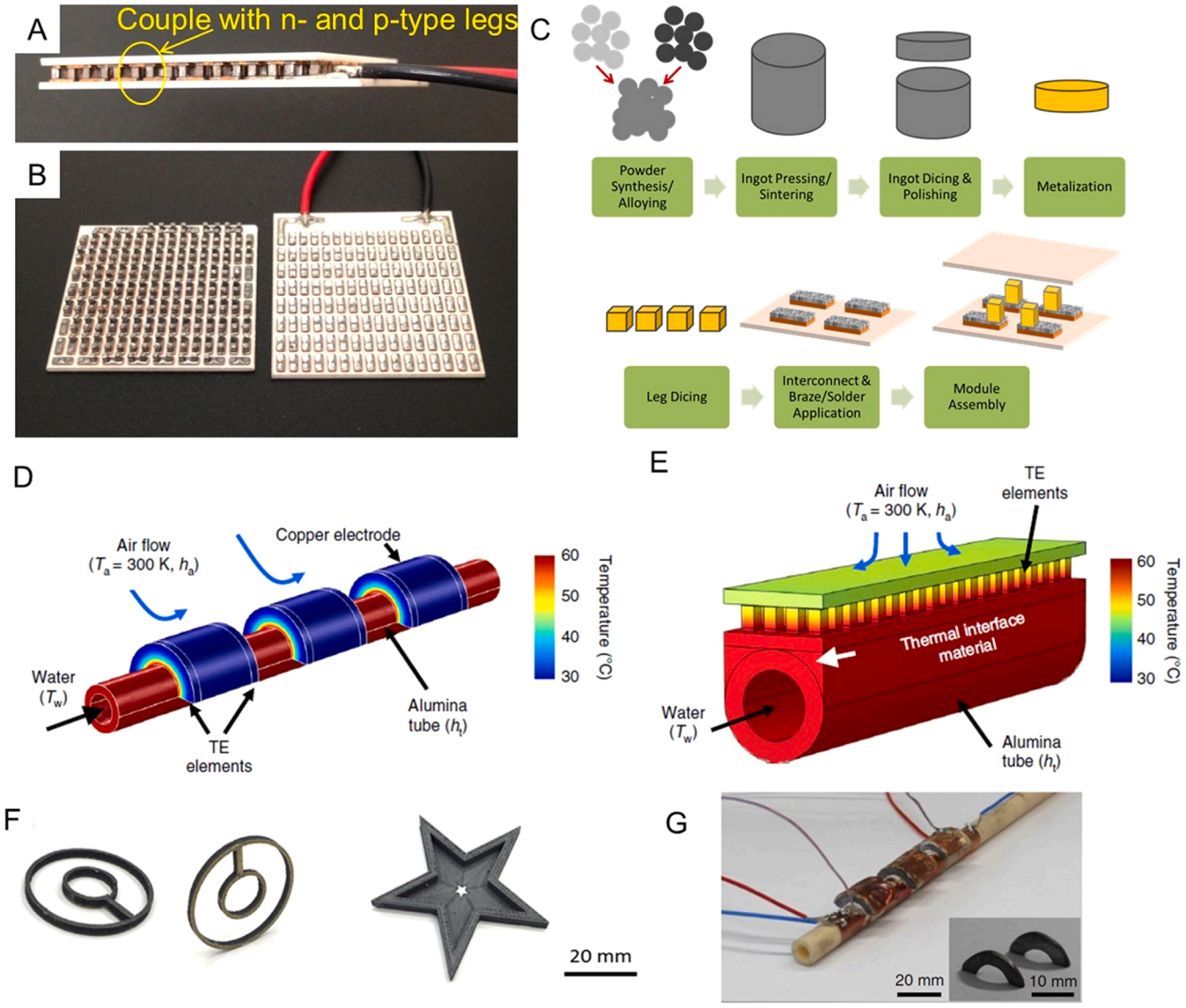

Fig. 13. Commercially available, off-the-shelf thermoelectric module. (A) Side-view of the assembled module shows the series of n- and p-type leg couples. (B) Top view of the disassembled module shows the electrical interconnects with the joining material that connects the legs to the interconnects. (C) The typical process for traditional manufacturing of thermoelectric modules involves multiple steps, including formation of an ingot, dicing, and assembly. Thermoelectric devices that conform to surfaces as shown in (D) reduce the parasitic thermal resistance between the application surface and the thermoelectric device. Traditional devices are not conformal and thus have a lower temperature gradient across the thermoelectric legs or elements as shown in (E). (F) Thermoelectric elements of varying shapes printed with fused filament fabrication. (G) Thermoelectric elements printed with an extrusion process in a shape that conforms to a pipe. (G)
(C) Reprinted from [163], Copyright (2014), with permission from Elsevier. (D) [166] with permission from Springer Nature. (F) Reprinted from [167], Copy right 2019, with permission from Elsevier. (d) Reproduced from ref. ([166] with permission from Springer Nature.

2.13. Traditional fabrications of thermoelectrics, opportunities for additive manufacturing and outlook

Thermoelectric units are commercially available as off-the-shelf thermoelectric modules. Fig. 13A and B show pictures of typical thermoelectric modules [163]. These modules must be integrated into the applications where they are used. They must be attached to a surface that will be heated/cooled or from which heat will be converted to electrical power. Often, the thermoelectric modules must be integrated into more extensive devices for use in applications; the modules will be attached to heat exchangers that then interface with hot gas streams on the device hot side and coolant streams on the device cold side. Notably, this module-to-device integration for many applications introduces system-level, parasitic thermal and electrical resistances that hinder the thermoelectric heating/cooling or power generation potential.

The oft-touted thermoelectric figure-of-merit is $ZT = (S^2\sigma/k)T$ where S, σ, k, and T are the Seebeck coefficient, electrical conductivity, thermal conductivity, and average temperature of the thermoelectric material. Based on intrinsic material properties, this figure-of-merit provides an understanding of thermoelectric materials performance, but it does not communicate the performance of a device. Thermoelectric device performance depends on extrinsic properties that are, in part, geometry or shape dependent. For example, Ebling et al. and Yee et al. reformulated the figure-of-merit and developed device metrics to determine the system-level performance of thermoelectric devices [164,165].

Thermoelectric materials used in devices are semiconductor materials alloyed to provide high ZT values. The relevant intrinsic material properties (namely S, σ, and k) are temperature-dependent, so the optimal performance of each type of thermoelectric material is temperature-dependent. Sootsman et al. and Tritt et al. provide a thorough reviews of thermoelectric materials, including the optimal operating temperatures of each material [168,169]. For low temperature (e.g., near room temperature) applications, bismuth telluride alloys are the dominant option. Many more options such as half-Heusler, skutterudite, and silicide materials are available for mid-temperature ranges (e.g., 300 – 700 °C), and the options are more limited to lead telluride and silicon germanium for high temperatures (~900 – 1000 °C). Other material properties besides S, σ, and k are relevant within the context of device fabrication and manufacturing. Bulk thermoelectric materials are brittle and thus prone to cracking and fracture both during manufacturing and in operation. Operations such as dicing or uneven compression during module assembly thus reduce yield during manufacturing. The mismatch in thermal expansion between the thermoelectric material and the surrounding device materials can also lead to stress concentration and cracking.

Because thermoelectric materials are typically high purity materials, and some require rare earth elements, the cost of the thermoelectric material alone can be high. The added cost of the other device components results in high thermoelectric device costs that are hard to offset with the current performance levels. The technology needs a radically different approach to bring down overall costs and improve application readiness and performance.

Traditional thermoelectric device fabrication generally follows the multi-step process shown in Fig. 13C [163]. The first step is often a powder synthesis or alloying step in which elemental powders are combined (e.g., via ball milling) to form the thermoelectric compound. The powder is then consolidated to form an ingot. Various methods such as hot pressing or current-assisted hot pressing can form an ingot. In some fabrication processes, these first two steps are replaced by a melt-growth process to directly form the ingot. The ingot is then diced into wafers, which are polished and metalized. The wafer is diced into "legs," and the legs are mounted onto electrical interconnects (typically copper shunts) with a braze or solder material and process selected specifically for compatibility with the thermoelectric material to provide good mechanical adhesion and prevent diffusion at the metal-semiconductor interface. The mounting of the legs onto the electrical interconnects can be done manually, with automated pick-and-place, or using vibration feeding and placement. Finally, the module is assembled with the thermoelectric legs sandwiched between electrically insulating barriers often consisting of ceramic plates, such as aluminum nitride sheets.

The traditional device fabrication process presents both benefits and limitations. A key benefit is the scalability of the process and resulting device size: the process generally remains the same whether the final module is small (the size of a coin) or large (the size of a book). The current process results in good uniformity; there is nothing inherent to the fabrication process that causes variation within the leg or across the module. The dicing results in legs of uniform size and shape, and the legs are all mounted into the module in the same way. On the other hand, the traditional fabrication process presents many limitations to device performance and cost. For example, the kerf loss in the multiple dicing steps of the traditional manufacturing process causes significant material waste with up to (and sometimes more than) 50% of the high purity, costly thermoelectric material lost and unrecoverable. Additionally, the multi-step assembly process producing a discrete module leads to parasitic thermal and electrical resistances within the module as well as when the device is integrated into an application. Fig. 13D and E show an example of the significantly higher temperature gradient that can be achieved across a thermoelectric device that conforms to the application surface compared to the traditional, rigid devices [166]. The interfaces between the thermoelectric leg and the electrical interconnect, the interconnects and the electrically insulating plates, as well as the insulating plates and the heat exchanger all contribute parasitic resistances and can negatively impact device performance.

Perhaps most significantly, there is a distinct gap between fabrication and device design; the fabrication process greatly limits the design degrees of freedom. The traditional fabrication process limits the device shape to flat, rigid squares or rectangles. However, many applications require thermal management or waste heat recovery on curved surfaces such as pipes and ducts, so using a thermoelectric device entail attaching a flat, rigid device to a curved surface, thus introducing significant thermal resistances between the thermoelectric device and the application surface. Moreover, thermoelectric legs are overwhelmingly rectangular prisms, although cylindrical devices have been shown in specialized applications [170,171]. Thus, the geometric design parameters are the leg aspect ratio and device fill factor (the amount of device area covered by thermoelectric legs). These minimal design parameters are particularly limiting because tuning the leg thermal and electrical resistances is critical to optimizing device performance, and the resistances are extrinsic parameters dependent on geometry or shape. The critical role thermoelectric leg shape plays in device performance was demonstrated in recent work that explored trapezoidal (or tapered) legs [172], and legs with circular and triangular cross-sections as well as hollow interiors, and significant changes in aspect ratio along the length of the leg [173,174]. The simulations showed power generation on a per unit area basis was 35–55% higher for hollow and layered leg shapes [173]. The impact of novel leg shapes was even more pronounced when the thermal boundary conditions replicated realistic conditions for many applications. For an hourglass shape with the leg cross-sectional area large at the top and bottom but narrow in the middle, the power output more than doubles compared to the traditional rectangular prism when the device experiences heat flux boundary conditions similar to applications like waste heat recovery from combustion exhaust [174]. Such work suggests additive manufacturing can be used to achieve thermoelectric leg structures with higher thermal resistance (and thus better thermoelectric performance). There are obvious benefits to fabricating thermoelectric legs and devices with techniques that enable geometries other than the current rectangular prism legs and flat, rigid modules, so additive manufacturing emerges as a promising approach for thermoelectric device fabrication.

Adaptable form factors for thermoelectric devices are explored through various advanced manufacturing techniques. These techniques

can be classified into to two themes: techniques for thin/thick film devices and techniques for bulk devices. Thin/thick film techniques enable adaptable device shapes in 2D. Several examples of flexible, lightweight devices have been demonstrated such as reviewed by Bahk et al. [175] and Du et al. [176], and the thin/thick film printing techniques and results for thermoelectric devices are summarized by Orrill et al. [177]. The discussion here will focus instead on additive manufacturing results that support fabrication of bulk devices where the techniques enable adaptable form factors in 3D. A myriad of AM techniques exists and are in development, and some of the most widespread have been applied to thermoelectric materials. Table 1 shows an early comparison of AM techniques compared within the context of feasibility for thermoelectric device fabrication [178]. Since the publication of that comparison, thermoelectric parts have been fabricated using extrusion and powder sintering/melting approaches.

Several additive manufacturing techniques require some form of binder or filler, often to create a printable ink, slurry, or filament that can be extruded. For example, Oztan et al. used fused filament fabrication with Bi_2Te_3 in an acrylonitrile butadiene styrene (ABS) polymer matrix for the filament, and they printed unique thermoelectric part shapes shown in Fig. 13F [167]. However, burning off the polymer binder with post-processing sintering resulted in significant porosity in the final part as well as substantial oxidation. He et al. used a stereolithography approach in which $Bi_{0.5}Sb_{1.5}Te_3$ particles were integrated with photocurable resins, cured during the 3D printing process, and thermally annealed to remove the resin [179]. After the thermal annealing step, residual amorphous carbon and oxygen remained in the samples. Their 3D printing process resulted in parts with low thermal conductivity (as low as 0.2 W/(m-K)), but the electrical conductivity was quite low, resulting in a peak *ZT* of only 0.12, which is about one order of magnitude less than the state-of-the-art for bulk bismuth telluride thermoelectric alloys. Qui et al. and Wu et al. demonstrated dispenser printing of a Bi_2Te_3 based slurries followed by selective laser melting (rather than thermal annealing) to synthesize the final bulk material [180,181]. Kim et al. devised a clever solution to the challenge posed by organic binders; they created an inorganic binder with Sb_2Te_3 chalcogenide metallic ions surrounding Bi_2Te_3 powder particles. They were able to extrude conformable part geometries as shown in Fig. 13 G and obtain ZT values as high as 0.9 [166].

Multiple investigators have attempted laser powder bed fusion (also known as selective laser melting) of thermoelectric materials. El Desouky et al. showed processing of bismuth telluride powder compacts on a commercial laser powder bed fusion tool [182], and Carter et al. performed single melt track studies comparing experimental and computational results of melt width and depth [183]. Zhang et al. showed layer-by-layer laser powder bed fusion to create bulk bismuth telluride parts without the use of binders/additives or post-processing [184]. Within the technique of laser additive manufacturing, high temperature thermoelectric materials have been processed in addition to the low temperature bismuth telluride alloys. Yan et al. demonstrated selective laser melting of a $CoSb_{2.85}Te_{0.15}$ skutterudite with a peak *ZT* of 0.56 at 823 K [185]. Several investigators have even attempted to synthesize the high temperature thermoelectric material alloy in situ during laser processing. Yan et al. attempted this approach with ZrNiSn and achieved at ZT of 0.39 at 873 K [186]. Thimont et al. showed the approach applied to higher manganese silicide results in formation of the pure HMS phase and powder densification [187]. These myriad endeavors begin the exploration of the process-structure-property relationships for laser additive manufacturing of thermoelectric materials, and they demonstrate the potential to achieve the same outcomes and advancements shown with the more widespread laser powder bed fusion of metals such as 316 L stainless steel and Ti-6Al-4 V.

Key challenges and opportunities remain for additive manufacturing of thermoelectric devices. Most results to date show significant porosity in the final parts, and the porosity appears detrimental to the thermoelectric performance. Moreover, remnants of carbon or formation of thin/small oxide layers and regions significantly reduces the electrical conductivity. Few studies have shown additively manufactured parts with *ZT* values as high as those of traditionally manufactured parts, and it is unclear whether any benefits from geometric adaptability or complexity will overcome subpar thermoelectric properties. Moreover, there is limited exploration of which part and device shapes are most desirable. The printing resolution is tied to the additive manufacturing technique, so the resolution and complexity of the final part must be considered alongside the selection of the appropriate additive manufacturing technique. Additionally, thermoelectric devices will require electrical interconnects, joining materials (brazing/solder materials), and, in many cases, electrically insulating layers and thermal interface materials between the device and the application surface. Whether and how the entire device can be made via additive manufacturing must be determined. Nevertheless, additive manufacturing provides a breakthrough in thermoelectric device development that has the potential to enable the technology to overcome the challenges that have kept it on the sidelines in limited niche applications for many decades.

2.14. Thermionic emission

Energy harvesting is typically achieved with solar cells or photovoltaic cells and thermoelectrics, which are useful devices for collecting solar energy and waste heat to produce useful electricity. These materials and modular device technologies are still evolving to achieve higher conversion efficiency in power systems. Direct thermal energy to electricity conversion is achievable through thermoelectrics, and they are advantageous because they eliminate losses due to mechanical work during the conversion process, which reduces the overall efficiency. Thermoelectrics inherently have a lot of material loss and high entropy, but thermionic energy converters (TECs) have the potential for less

Table 1
Comparisons of traditional thermoelectric module manufacturing process to various additive manufacturing processes. Several of the additive manufacturing techniques have advantages with respect to the part geometry/shape, required assembly, and material loss. The table is reproduced from [178].

	Materials		Assembly	Geometry	Post-processing	Material Losses
	Common Materials	**Processing Temperature**				
Traditional Thermoelectric Manufacturing	Semiconductor thermoelectric materials	Low – High	Manual or automated	Limited to simple geometries (rectangular)	Dicing, soldering/ brazing	High
Stereolithography	Polymers, metals and ceramics	Low – High	Direct assembly	Free form	Required for binder burnout and sintering	Low
Fused Deposition Modeling	Polymers, composites and low-temperature alloys	Low	Direct assembly	Free form	Optional	Low
Binder Jetting	Metals, polymers, ceramics and composites	Low – High	Direct assembly	Free form	Required for binder burnout and sintering	Low
Selective Laser Melting	Metals, ceramics, and composites	Low – High	Direct assembly	Free form	Optional	Low

material loss and higher conversion efficiency. TECs are heat engines that convert very high-temperature heat directly into electricity by driving electrons across a vacuum gap, as shown in Fig. 14A, allowing for high efficiencies without any moving parts [188]. The devices operate at high temperatures by accepting heat directly from sources such as hydrocarbon combustion, concentrated sunlight, or nuclear generation processes [189,190]. Like thermoelectrics, the lack of moving parts gives TECs inherently long lifetimes with little associated maintenance and lets them avoid some irreversible loss mechanisms such as friction and turbulence. Additionally, TECs have relatively small sizes as shown in Fig. 14B that can provide high specific power outputs up to ~100 Wcm^{-2} [189].

2.15. Traditional fabrications of thermionics, opportunities for additive manufacturing and outlook

Although the technology was discovered in the 1950s [191], the progress in the development of thermionic energy converters (TECs) has been limited due to the lack of advanced technology and fabrication techniques. However, a significant amount of research on TECs has occurred to improve materials, manufacturing, and making of modular devices with adequate power density output [192,193]. Even though there have been recent studies on thermionic emitting devices, few modern TECs have demonstrated efficiencies close to the technology's potential or have achieved power densities of more than tens of $mWcm^{-2}$. Thus, materials that can provide power density outputs ($P > 1$ Wcm^{-2}) are needed for heat-to-electricity conversion efficiencies of interest in modular devices ($\eta > 10\%$). There are some ceramic and composite configurations that must be researched further for use in devices.

Currently, there are several ceramic-based systems that show promise. Ceramic oxides of the mayenite electride clathrates made via spark plasma sintering show low work function and can be composited with carbon [194,195]. Tungsten (W) and tungsten ceramic composites have been made and used for years [196]. The Ba-Sr-Ca-O system offers low work function material as well as compositing with W [197]. Ba-Sc-O and perovskites of this system can be used or composited with W [198]. SiC and its composite with W is an important system for thermionic emission, and some SiC emitters have been investigated [199,200]. Additive manufacturing of SiC has been carried out with binder jet 3D printing and various densification methods [201–203]. Also, since there is a need for improved emitters in thermionic devices, the shape and manufacturing of the materials is important [204], so AM could help improve the material emitting properties and thus efficiencies. This is seen in Fig. 14 C, where the tungsten emitter geometry benefits from AM [204]. Also, insulators are needed and used in TECs, so AM of the basic ceramics for modules can and should be used where needed. Not only are thermionic emitters useful for a device, but they can also be used in hot structures to provide passive cooling without making a device through electron transpiration cooling or thermionic emission at the hot surface [205,206]. Thermionic materials made via AM should be used in devices and hot structures for increased efficiencies and cooling effects.

2.16. Emissions control (catalytic converters) and carbon capture for negative carbon emissions

Combustion engines, a popular pathway to convert fossil fuel energy to mechanical and electrical energy, are used in many engineering applications such as vehicles, industrial plants, generators, marine powertrain, and mining equipment across the world because they are low-cost, efficient, and easy to operate with barely any training. At the same time, environmental concerns and climate challenges have forced many regions around the world to pass strict emission control regulations. Amongst such regulatory examples one can point to the US Clean Air Act of 1963, repeatedly revised to the present day, similar regulations in Europe known as Euro I through 6, regulations in China known as China 1 through 6, Bharat 1 through 6 in India, and wide variations of the US and European regulations adopted in South America and Africa. All such global attempts are aimed at bringing emissions of combustion engines under control. These regulations have focused on three notable engine pollutants: nitrogen oxides (NO, NO_2), carbon monoxide (CO) and unburn fuel fractions most notably in the form of hydrocarbon (HC) emissions. In many diesel and gasoline vehicles, also soot more commonly called particulate matter (PM), is under strict regulations. Recent engine emission regulations specially in California have also

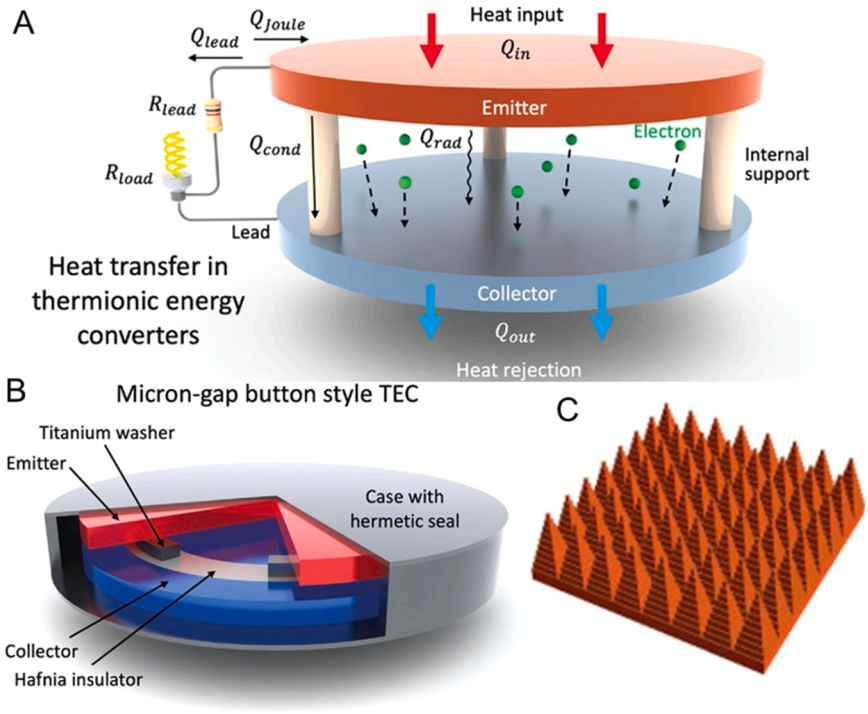

Fig. 14. (A) Schematic and configuration of a diode thermionic energy converter. Heat transferred into the emitter $Q_{in}$is transferred out by the flow of thermionic electrons to the collector Q_{therm}. (B) Schematic diagram of a twentieth century micron-gap button-style thermionic energy converter [189]. (C) Illustration of tungsten pyramid absorber that can be made via AM techniques.
(A) and (B) from ref. [189] under open access CC BY license. (C) from ref. [204] under open access CC BY license.

included formaldehyde. A good summary of emission regulations in the US and major worldwide regions was reported in reference [207].

Due to stringent regulations, emission control technologies have evolved remarkably. A modern catalytic converter on a mainstream car can reduce 99.9% of the engine's regulated emissions, while a diesel soot filter could conveniently trap up to 99.9% of the emitted soot from diesel engines. Selective Catalytic Reduction (SCR), a catalyst used predominantly for control of diesel engine NO_x, can easily operate in the 98% efficiency space, often with 99% or more efficiency. A typical catalytic reactor, shown in Fig. 15 is a combination of three technologies: a ceramic honeycomb, a catalyst solution coated on the honeycomb channels encompassing precious metals (platinum, palladium, and rhodium), and a metal shell enclosing the honeycomb mainly for packaging and protection purposes.

2.17. *Traditional fabrications of catalytic converters and carbon capture, opportunities for additive manufacturing and outlook*

Here we focus on the honeycomb, the substrate for the catalytic coating ultimately responsible for the reducing the engine emissions. The honeycomb acts as a building foundation hosting the catalytic coating on its structure, where reactions of pollutant species (NO_x, CO, HC, etc.) take place, converting to inert species (N_2, CO_2, H_2O, etc.) Over the last nearly four decades, a variety of honeycombs, one example of which is shown in Fig. 15B, have been proposed for use as catalytic substrates for emission control purposes, varying across geometry, material, surface area, durability target and so on. Amongst all ceramic honeycombs, the type displayed in Fig. 15B has remained dominant and forms more than 90% of honeycombs currently used worldwide on combustion engines, the remaining fraction mainly being metal honeycombs having nearly the same geometry with modest variations. The key attributes of honeycombs making them ideal for catalytic coating (and hence for emission control) are several: one is that they make a substantially large surface area available in a very small volume. A typical catalytic converter for a 2-liter engine, only 4 or 5 in. in diameter and/or in length, has several square meters of surface area. Next, when coated with the highly porous catalytic wash coat, the very same surface area extends to the area of a football field [208], ideal for the complex emission control reactions required to take place downstream of an engine. Further, ceramic honeycombs are relatively easily producible via low-cost extrusion. Exceeding majority of such ceramic emission control honeycombs are made of cordierite, an extremely low-cost refractory oxide ceramic capable of withstanding substantial temperature variations downstream of an engine without a detriment, sometimes near a temperature change of 500–1000 °C taking place within seconds or minutes. Thanks to their porous ceramic structure, they are also lightweight.

The automotive market worldwide includes one billion cars nearly all equipped with emission control honeycombs. Further tailpipe emission regulations signal growing needs for diversity and flexibility in manufacturing techniques. Thus far, additive manufacturing (AM) has not been widely used in producing ceramic emission control honeycombs. The dominant reason for lack of AM penetration into such industry sector appears to be such major requirements as low cost and high production speeds. While thousands of such ceramic honeycombs can be produced in a single day each costing a few dollars (single digits) via standard extrusion, such numbers and high production cost are still unadoptable in AM techniques. Although binder jet 3D printing and direct ink writing may reach the production rates of traditional extrusion, there must be more research and scale-up to overtake traditional methods. One example of AM taking over production is with steel parts made via binder jet 3D printing for the automotive industry.

There have been recent advances targeting lowering the cost of emission control components via reducing their expensive precious metals contained in the catalytic wash coat (platinum, palladium and rhodium), also making such honeycombs smaller, better fit-able in tight automotive spacing [209]. This has resulted in novel honeycomb designs having non-linear flow channels [209], shown in Fig. 15C and D. This is a major departure from mainstream honeycombs dominating the automotive sector since their inception nearly half a century ago [210], as their geometries has remained nearly unchanged ever since. Unlike conventional honeycombs utilizing simple, straight channels, the novel honeycomb design includes proprietary, enhanced structures and flow patterns substantially enhancing mass transport of toxic species to the catalyst layer via faster convection, thus augmenting the otherwise slow, diffusive transport. Twisted channels (Fig. 15 D and E) thus not only make honeycombs more efficient than conventional ones having straight channels, but they also make such honeycombs smaller (downsized), easing their fitting in tight spaces near engine or underbody spaces in a vehicle. This is shown in Fig. 15D and E. Such twisted channel

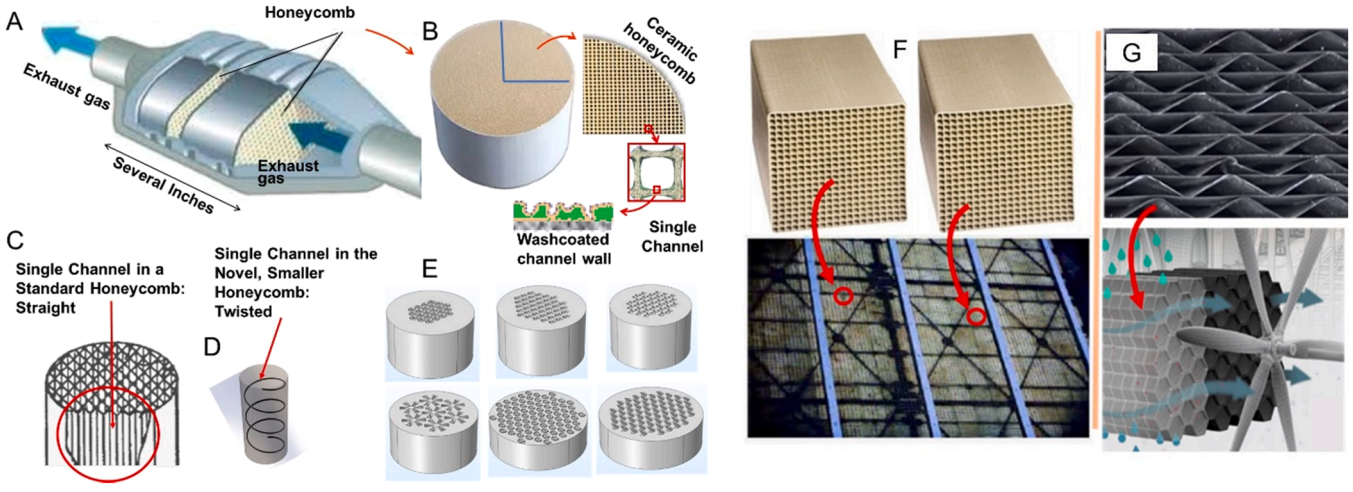

Fig. 15. . (A) A common catalytic converter used in a vehicle emission control system. (B) A honeycomb, used in the catalytic converter, its single channel and catalytically coated channel walls (C) Straight channels in a standard honeycomb. (D) A twisted channel in the novel honeycomb (one channel shown for comparison purposes), requiring reduced precious metals, hence markedly lowering their cost. (E) Examples of small-scale, helical channel honeycomb prototypes produced via additive manufacturing for R&D purposes. (F) Top: Ceramic honeycomb contactors (several liters in volume) used for carbon capture by Global Thermostat LLC. Bottom: A large stack of the honeycomb contactors at the Global Thermostat pilot plant. (G) Top: Carbon Engineering's array of metallic contactors, honeycomb-like structures (one section shown only) for air flow (bottom) and CO_2 removal using a solvent.
Image A modified from ref. [217].

honeycombs, proposed as a novel concept, are possibly best suited to non-extrusion techniques, making them thus ideal candidates for AM production pathways. Indeed, during its entire research and development process, AM was used for rapid prototyping of such honeycombs, its resulting prototypes shown to be easily coatable with appropriate catalytic wash coat and testable on test benches and in microreactors [211]. Sample AM-produced prototypes are shown in Fig. 15E. Further, AM techniques must be comparable to mid-level production quantities and costs with that of die extrusion, so careful consideration of the costs is warranted.

Recently, there has been development of technologies to extract CO_2 from industrial sources or from the air around us. The former, a 'point source' approach, deals with carbon capture from higher CO_2 concentration streams typically in the range 100,000 – 150,000 ppm, while the latter extracts CO_2 from the air around us having a concentration of about 420 ppm of CO_2 hence called 'Direct Air Capture (DAC) of CO_2' or negative carbon emission. In a DAC process, air is pulled into a 'contactor', many are honeycomb-type coated with a sorbent, sort of a sponge, where CO_2 is adsorbed. Contactors used for CO_2 is selectively capture are ceramic honeycombs much like those used for emission control purposes downstream of engines. Fig. 15F displays a ceramic contactor used in a DAC pilot plant by Global Thermostat LLC; in an actual CO_2 capture practice, the contactor could be coated (not shown) with a sorbent such as poly(ethyleneimine) or PEI for short, a CO_2 adsorption material coated on the honeycomb channel walls typically functionalized on alumina [212]. Fig. 15G displays a metallic honeycomb for use with a solvent (not shown) used in Carbon Engineering Inc. operations. Solid sorbent coated in such contactors, the chemical coating that adsorbs the CO_2, is much the same as the wash coats coating the honeycomb channel surfaces for catalytic converters.

The need to develop novel, process-intensified contactors via additive manufacturing was recognized and emphasized in a report by the National Academy of Science and Medicine [213]. AM was used in design and construction of an adsorbent for post-combustion CO_2 capture applications, focused on an electrically conductive 3D-printed monolith adsorbent [214]. Two honeycomb monoliths composed of 70% of zeolite 13X and 30% of activated carbon were manufactured and tested for mechanical properties. The aim was to develop a viable adsorbent for Electric Swing Adsorption (ESA) process, in turn capturing the feed stream CO_2. It was demonstrated that 3D-printed monolith (honeycomb/ contactor) material can be successfully utilized for CO_2 capture using an ESA process. One group has demonstrated that the presence of binder reduces the adsorption capacity during CO_2 capture (materials were 65 wt% zeolite ZSM-5 and 35 wt% of binder (bentonite and colloidal silica)) [215]. Using a mixture of zeolite (13X or 5A), binders and other additives, Thakkar et al. have tried 3D-printing of composite monolith for point-source CO_2 capture, reporting a lower CO_2 adsorption capacity in the AM prototype because of its low zeolite content [216].

For catalytic converters, a collection of large surface area, low cost of material and manufacturing, high thermal durability, and ease in coatability, amongst other attributes, make AM design ideal for ceramic honeycombs for emission control applications. It is viable to predict that extrusion, an archaic technique for producing emission control honeycombs, is reaching its limits and could be replaced by AM to enter the said sector of emission control honeycombs and its associated energy field. Most CO_2 capture contactors are made of some type of a ceramic, a material acting inert during CO_2 capture (it does not adsorb or desorb CO_2 on its own). It is then wise to, judiciously increase or optimize the contactor's wall porosity, easily manageable via AM, especially considering that, relatively speaking, contactors' operational environment are not that harsh (have modest temperature fluctuations, minor vibrations and are free from harsh contaminants), thus reducing the overall contactor thermal mass [218]. This is especially helpful during thermally induced desorption, which allows lowering the needed thermal energy to heat the contactor, hence saving energy and its associated costs. All evidence indicates use of AM in CO_2 capture in general and in contactor design in particular is receiving wide attention and is expected to grow in the coming years.

2.18. Heat exchangers

A heat exchanger is broadly defined as a device that transfers energy from one fluid stream to another. Heat exchangers (like boilers and recuperators etc.) have been identified as critical components in power generation systems since they help to maximize the energy efficiency of an entire system. Also, heat exchangers can be used in various other systems that release heat to capture some of the energy lost and reuse elsewhere. Energy efficient power generation has been a challenge since the advent of steam or gas driven power plants, and incremental changes have been introduced to improve the components performance which can be translated into a gain in overall system efficiency. The fundamental laws of thermodynamics indicate that process efficiency increases as the heat source temperature increases [219]. The importance of the impact of a higher source temperature is evident from the second law of thermodynamics, as the Carnot efficiency ($\eta_f = 1 - T_{sink}/T_{source}$) of a process can increase by almost 2% with every 100 °C increase in source temperature. The efficiency increases as the temperature increases, so several power generation applications will achieve higher efficiency if higher temperatures are achieved. That makes the demand for ceramics high in power generation, and specifically, ceramic solutions are still sought for high temperature heat exchangers.

Maximum combustion temperatures are much higher than those being used in the actual processes. For example, combustion of coal in air can provide temperatures higher than 2150 °C [220]. Similarly, the maximum limit for natural gas combustion is 1950 °C; for coal-natural gas combustion with a higher oxygen concentration, it can approach 3000 °C [221]. The unavailability and reliability of materials that can withstand the extreme environment has limited the application to much lower temperature than desired. Thus, ceramics have been used and researched to reach such high temperatures and increase the efficiency. High-temperature heat exchangers (HTHXs) are described in the literature as operating above an arbitrary value of 500 °C, but the need for heat exchangers in temperatures well passed 750 °C are needed to increase efficiencies. During the 1970 s, the development of high-temperature solutions was motivated by a sudden reduction in oil supply, which resulted in several initiatives to develop technologies via which energy can be saved and maximum power generated while fuel combustion is minimized [222]. Since then, continuous efforts have been focused on the development of heat exchanger technologies for a broad range of applications, including recuperators for gas turbine engines, aviation, renewable energy conversion, waste heat recovery, sCO_2 power cycles, and high-temperature fuel cell systems [223–225].

2.19. Traditional fabrications of heat exchangers, opportunities for additive manufacturing and outlook

Typically, the best materials for high temperature heat exchangers are ceramics that have high thermal conductivity to transfer heat effectively and have high strength to obtain thin tubular shapes or channels. The thin-walled structures help attain effective heat transfer, so high strength materials are needed. Ceramics materials such as metal oxides, nitrides, and carbides can provide these properties. Namely, WC, SiC, Si_3N_4, and Al_2O_3 are all very good candidates for heat exchangers [21]. These materials also have corrosion resistance better than any metal alloy, but the reasons that they are not use more often reflects their fracture toughness and fracture modes and ability to be formed and processed as monoliths or composites.

While the compatible materials development is a critical area, the manufacturing processes are equally critical. Ceramics are more difficult to process compared to metals because they typically do not melt, nor do they sinter well. It has been obvious that emergence of advanced

manufacturing has led to new materials developments where base metals have been compounded with additives to alter the physical properties and even improve the manufacturing of parts. Traditionally, ceramics can be processed with casting or pressure-assisted methods with slurries and dry powders, respectively. These techniques are more expensive because of tooling, cannot reach high levels of geometric complexity, and typically need to be machined in green or final state.

Although most of the use of oxide ceramics is in thermal barrier coatings [226,227], they can be used as bulk materials where high thermal conductivity is not needed. Several researchers have made oxide-based ceramic heat exchangers in different configurations and with different processing methods. Oxide ceramics have excellent corrosion resistance and can be used at high temperature; however, their thermomechanical properties are poor, which is not wanted for high-temperature heat exchangers because the efficiency is maximized with high thermal conductivity. Also, poor thermomechanical properties can lead to structural failure of the heat exchangers during cycling. To ensure efficiency and effective heat exchange at higher temperature, carbide ceramics, especially SiC, have been developed. Even though silicon carbide presents itself as an ideal candidate in heat exchange, there are other materials that can perform well under the same conditions such as carbon, nitrides, silicides, silicates, and borides.

In terms of improving heat exchanger efficiencies, there is a lot that AM can do to help achieve structures that mix flow and spread heat better than any traditionally made ceramic part. Namely, triply period minimal surface (TPMS) structures like the gyroid made from SiC in Fig. 16A are achievable [201]. Limited concepts for high-temperature, ceramic heat exchangers made via additive manufacturing or 3D printing have been developed. However, there are some studies on making ceramic material with AM for heat exchangers. One group used lithography to design complex heat exchanger parts out of alumina and zirconia as shown in Fig. 16B and C, but no heat exchanger test nor thermal-mechanical properties were measured [228]. A concept based on AlN-ZrO_2 ceramic composites was explored for high temperature heat exchangers and recuperators [229]. A 3D printed direct winding heat exchanger made from alumina was designed with micro-features to enhance convection heat transfer in motor stators as seen in Fig. 16D and E [230], and the inner structures were optimized to minimize the overall system losses due to pumping and increased winding temperature. A ceramic heat exchanger was optimized for a concentrating solar power (CSP) electric power plant with a corrosive molten salt at atmospheric pressure and temperatures from 750 °C to 540 °C [231]. Alumina heat exchangers were made and modeled using stereolithography techniques based on DLP printing as shown in Fig. 16 F [232]. In recent work, material and architecture selections were performed to develop an innovative compact gas-to-gas heat exchanger with improved flow channels by using a Kelvin lattice system as shown in Fig. 16G [233].

2.20. Fission energy

Use of ceramic materials in fission energy systems is extensive and driven by the same performance requirements that motivate their selection in other fields. Nuclear reactors impose high temperatures, aggressive corrosion requirements, and high radiation fluxes on materials that must serve several applications [234]. Uranium dioxide (UO_2), the ubiquitous nuclear fuel form, is the most obvious ceramic material used in nuclear applications. However, the most promising near-term application of advanced manufacturing to the field of energy generation from fission will likely be in application to advanced fuel forms and high-performance structural materials. Discussion of ceramic materials focuses primarily on light water reactor (LWR) designs given that they are responsible for generating most of the world's electricity that comes from nuclear power. However, application of advanced manufacturing methods to enable advanced reactor designs is a major area of current research [235].

2.21. Traditional fabrications for fission energy, opportunities for additive manufacturing and outlook

The choice of nuclear fuel is driven by reactor type as well as design and performance tradeoffs. Uranium dioxide is the best understood nuclear fuel form, possessing extensive performance data, industrial and regulatory familiarity, ease of fabrication, and other favorable attributes. The ubiquitous nuclear fuel architecture as deployed for electricity generation is ~10 mm right cylinder pellets stacked into rods. These rods, generally multiple meters in length, are collected into

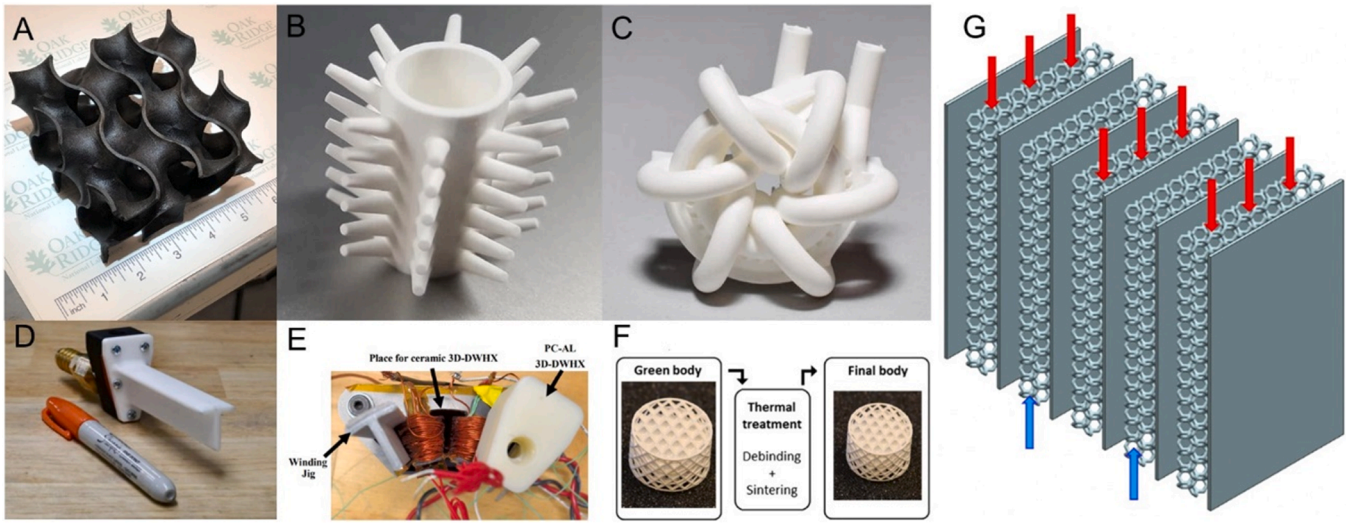

Fig. 16. (A) A gyroid part processed by binder jet 3D printing followed by PIP. [201] under open access CC BY license. under open access CC BY license. (B) LCM printing of alumina heat exchanger parts with extended surfaces, and (C) complex channel paths. (D) alumina heat exchanger insert, and (E) installation of motor and heat exchanger. (D) and (E) (F) example of a complex alumina cellular structure. (F) Reprinted from ref. (G) a complex lattice heat exchanger configuration. [233] under open access license.
(a) Reproduced from ref. [201] under open access CC BY license. (B) and (C) Reproduced from ref. [228] with permission from Springer Nature. (D) and (E) Reproduced from [230] with permission from IEEE. (F) Reprinted from ref. [232], Copyright 2019, with permission from Elsevier. (G) reproduced from ref. [233] under open access license.

assemblies, which are then arranged to optimize a wide range of parameters to construct the reactor core. The basic UO_2 pellet geometry is shown in Fig. 17A.

In all present commercial fuel fabrication facilities, UO_2 pellets are fabricated using conventional methods: cold pressing followed by sintering at temperatures above 1900 K. This process is well understood and produces highly repeatable fuel performance, but also limits possibilities for incorporation of advanced microstructures or other enhancements. Commercial nuclear fuel vendors may modify their UO_2 fuel with various additives to control the fuel microstructure with the goal of improving fuel performance [236] or introduce burnable absorbers or neutron poisons such as Gd_2O_3 to control reactivity early in service [237]. Other material modifications such as boron-contain coatings (typically zirconium diboride or boron nitride) may also be applied to the pellet surfaces for similar aims of improving reactivity control [238].

Non-oxide ceramic nuclear fuels have received more limited development. The most familiar are monocarbide (UC) and mononitride (UN) fuels. Compared to UO_2, these systems offer improved properties at the expense of more challenging manufacturing processes as well as a more limited irradiation performance database [239]. The greatest fabrication challenge of non-oxide ceramic fuels is that they must be handled in inert atmosphere gloveboxes if processed using traditional means due to thermodynamic favorability of uranium oxidation. Glovebox processing is commonplace in research environments but presents a challenge if UC or UN are considered for energy production applications.

Monolithic pellet fuel forms have been the focus of most nuclear fuel development activities due to their widespread usage. However, homogeneous pellets are also the simplest possible fuel form; service requirements are little more than retaining a reasonably stable geometry throughout service and limiting fission product mobility to an acceptable level. In service, UO_2 fuel pellets undergo extensive restructuring, fracture, and release of radioactive fission gasses into the fuel rod plenum. In the event of a beyond design basis accident such as Three Mile Island or Fukushima, the cladding will fail, and radioactive fission products release to the primary containment vessel. While the primary containment vessel retained integrity at Three Mile Island in 1979 and prevented radioactivity release to the public, this did not occur at Fukushima in 2011. Extensive research has been devoted to advancement of fuel forms that improve upon this fundamental vulnerability. Most notably, tristructural isotropic (TRISO) fuel architectures implement a SiC barrier designed to retain fission products in the event of an accident [240]. The key features of a TRISO particle fuel are shown in Fig. 17B. The most widely considered use of TRISO fuels have been for a high temperature gas cooled reactor (HTGR), but TRISO fuel concepts for light water reactors have also received more limited study [241, 242].

The matrix (the non-fissile material that provides a cohesive structural component to the TRISO fuel particles and conducts heat to the coolant) is graphite for HTGR applications, but technologies for fabricating SiC matrices are of significant interest. Silicon carbide provides the same advantages (irradiation tolerance, corrosion, and oxidation resistance, etc.) when used for a fuel matrix as for other in core components as discussed below. However, conventional SiC matrix fabrication processes using cold pressing and sintering methods are limited in attainable packing fraction [243]. Particle packing fraction is a critical metric for particle fuels, as this parameter ultimately determines the uranium density and therefore attainable power density and core lifetime. Packing fractions of 30–40% are typical for historic HTGR TRISO [244]. Attempts to increase this using conventional fabrication are limited by the cold pressing technique; too high of particle packing fraction will result in particle-to-particle contact and failure of the SiC layer that is relied upon for fission product retention [245].

Metal alloys are commonly used for most structural components within the reactor core. Familiar corrosion-resistant metallic alloys such as stainless steels and nickel superalloys are generally used for core structural components, ductwork, and pressure vessels. In pressurized or boiling water-cooled reactors, zirconium alloys are used as cladding that

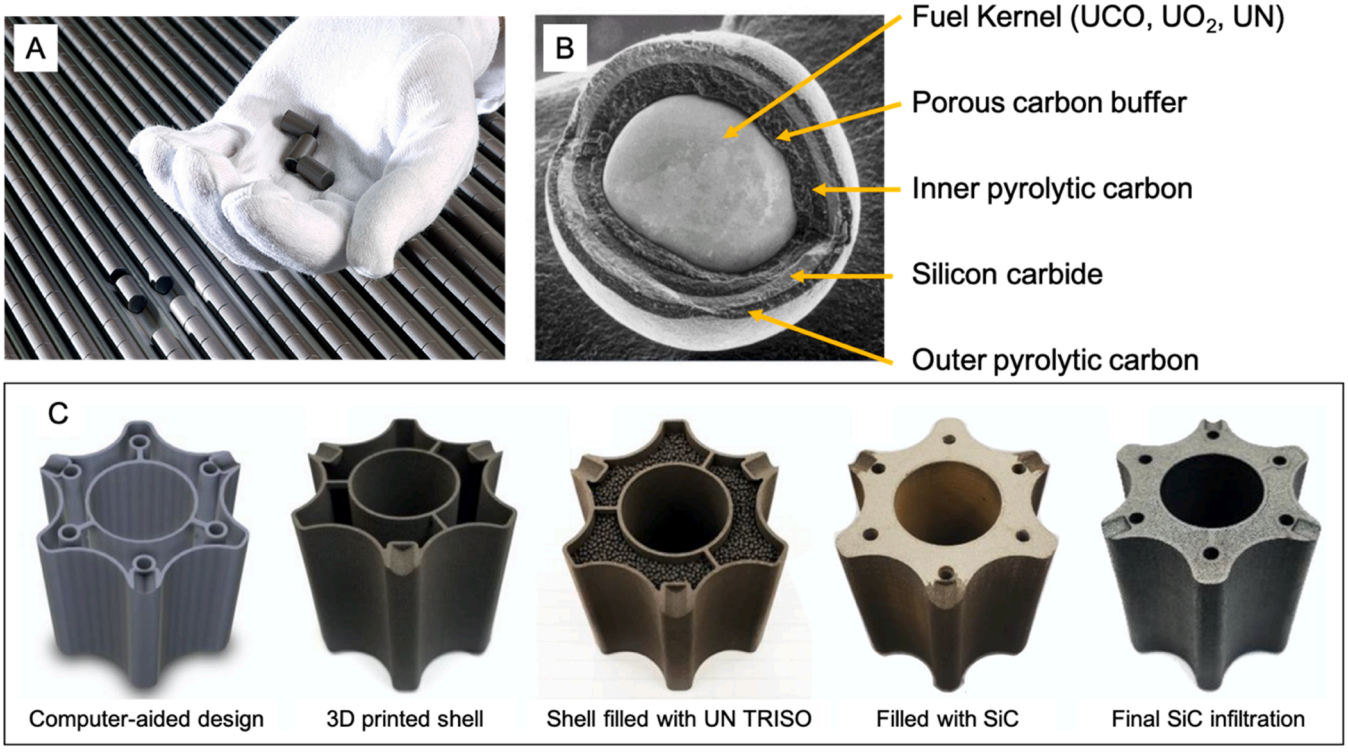

Fig. 17. . (A) An example of standard UO_2 fuel pellet. (B) Features of a TRISO fuel kernel. (C) Progression of Transformational Challenge Reactor (TCR) fuel cog design from computer-aided design through final densification.
(C) reproduced from ref. [259], copyright 2021, with permission from Elsevier.

surrounds the fuel pellets. The cladding is responsible for both retaining radioactive fission products and retaining core thermal hydraulic performance. The previous decade has seen significant worldwide interest in development of cladding materials that are more resilient to high temperature steam oxidation as would be experienced in many design-basis and beyond design-basis nuclear accidents [246]. While multiple approaches have received attention [247], silicon carbide (SiC) fiber reinforced SiC matrix composite (SiC_f/SiC) cladding offers the potential to both overcome the high temperature oxidation vulnerability of Zr alloys [248] as well as offer performance advantages due to its high temperature strength [249]. The challenges in deployment of SiC_f/SiC cladding have been chronicled by multiple authors [250,251]. Foremost include improvement of methods for fabrication, joining and sealing methods that can produce hermetically sealed cladding geometries (e.g. tubes exceeding four meters in length), and improved understanding of mechanical property evolution, corrosion, and microcracking under service conditions. SiC_f/SiC is also proposed for use in channel box assemblies due to the reduced neutron cross section of SiC compared to Zr [252].

The final major ceramic component of fission reactors are the control rods. Control rods are important to tune the neutronic profile of nuclear reactors and must rapidly terminate the chain reaction when called to do so. Isotopes possessing high neutron absorption cross sections (e.g. Boron-10) are necessary for this purpose. Boron carbide (B_4C) is a commonly used ceramic for this purpose, but alternatives including hafnium, cadmium, and others have been proposed. The most critical design criteria for these are a high melting point and lack of deleterious interactions with Zr cladding or water in the event of an off-normal condition.

Development of advanced manufacturing methods for ceramic materials in the fission energy field remains in early stages of assessment. A major hurdle to successful deployment is the extended time necessary for qualification of new materials for nuclear applications, which historically covers many decades due to the time required for dose or burnup to accumulate to service lifetimes in test reactors [253]. Qualification of fabrication processes for nuclear materials often relies on setting tolerances for all controllable aspects of the fabrication process, as well as easily observable features or properties of the final product [254]. This has often dissuaded development of new materials, but recent approaches to accelerate qualification propose to reduce this timeline through use of both accelerated irradiation methodologies and leveraging of modern modeling and simulation tools [255].

Application of advanced manufacturing to monolithic nuclear fuel are largely only hypothesized at present [256]. The design of current reactor fuels employs minor variations on geometries of UO_2 readily achieved by conventional fabrication. Use of additive manufacturing has been proposed for development of ceramic composite fuel systems that retain UO_2 as the fuel material. Additive manufacturing of refractory metal inserts to improve thermal conductivity of UO_2 is one example of this approach [257]. More advanced application of advanced manufacturing to pellet fuel geometries may be possible, if approaches are identified that can provide spatial control over poisons (e.g., Gd, B) or U-235 enrichment. Either would provide economic advantages by reducing fuel cycle costs. For example, reference conventional fabrication of UO_2-Gd_2O_3 using conventional methods results in uniform distribution of Gd poison throughout the pellet. Duplex pellet fabrication is possible using current techniques, but significant advances would be needed to produce a nuclear fuel pellet with a thin (less than 1 mm) annulus of Gd_2O_3 surrounding UO_2.

Significant recent progress has occurred through application of additive manufacturing to fabrication of the particle fuel matrix. Conventional processing methods inherently limit the maximum packing fraction of fuel particles to avoid particle contact and failures. Application of 3D printing of SiC [202,258] to SiC-matrix TRISO fuels has enabled revolutionary fuel forms that could not be fabricated using conventional means [259]. As shown in Fig. 17 C, use of 3D printed SiC methodologies can greatly expand options for coolant channel geometries and overall flexibility of design. Beyond the fuel design itself, opportunities abound for incorporation of sensing and monitoring within ceramic components that would be challenging if not impossible using conventional methods [260]. Ongoing test irradiations will demonstrate the irradiation performance of SiC fabricated using 3D printing methods [261].

Beyond SiC, zirconium carbide (ZrC) is the next logical extension for this approach, offering an even higher melting point than SiC and intriguing application spaces in advanced reactors [262] and possessing demonstrated method of synthesis via chemical vapor deposition [263]. Finally, hybrid methods that pair particle fuel synthesis, variations on particle coating methodologies, and analogous gas phase precursor manufacturing routes to build the fuel matrix will likely yield a new generation of particle fuel concepts optimized for various reactor applications and performance requirements.

2.22. Fusion energy

Among many fusion reactor concepts, those burning the deuterium-tritium (D-T) fuels in confined plasma are considered the most feasible technically, so a great deal of research effort is presently active. For the magnetically confined D-T fusion energy systems such as Tokamaks and stellarators, continuously heating and fueling the plasma, breeding tritium fuel, and converting kinetic energy of the fusion reaction products into a usable form are the most essential functional requirements Powering the Future: Fusion & Plasmas [264]. Moreover, since the burning plasma must be maintained at temperatures exceeding a hundred million Kelvin while emitting high energy neutrons and other radiations, the surrounding components have to survive the extremely harsh operating environments [264,265].

Ceramic materials are essential for enabling fusion energy. In fact, many fusion reactor concepts require the use of ceramics, in monolithic or composite forms, for various components due to their high temperature severe environment capabilities and the unique functionality. Such components include the flow channel inserts (FCI) in liquid metal blankets [266], tritium breeders [267], the radio frequency plasma heating window, diagnostic mirrors, the blanket and first wall structures [268], and those for more generic functions such as electrical insulation and heat resistance. Here, we discuss two examples of ceramic material applications unique to fusion energy: the FCI and the ceramic breeders.

The FCI is a component that magneto-hydrodynamically detaches a flowing liquid metal from the conductive structure of liquid metal-cooled and/or -bred blankets [266,269,270]. The primary purposes of FCI, which are used as the lining in the internal flow channel in the steel structure Fig. 18A and B, are to minimize the pressure loss in a liquid metal flow system and the reduce the impact of liquid metal corrosion of the steel. The FCI is required to provide adequate thermal and electrical insulation (typically <5 W/m-K and <20 S/m, respectively, through a wall thickness of several millimeters), minimize neutronic impact on fuel breeding, be chemically compatible with the liquid metal (most commonly Pb-Li eutectic), be tight against the leak, and maintain integrity in a high radiation nuclear environment [271]. Continuous fiber composite is a preferred form of the ceramic for this application since a catastrophic failure of the FCI will not be tolerated.

Fusion reactors must continuously produce the tritium fuel. To accommodate this need by nuclear reactions ^{7}Li (n, T) $^{4}He^{+n}$, lithium must be externally supplied as either a liquid metal, a molten salt, or a solid ceramic. A fusion blanket using a ceramic breeder is classified as a solid breeding blanket. The solid breeding blanket concepts are most commonly cooled by helium [272,273]. Requirements to the solid breeder are many-fold: tritium must be efficiently extracted using a purge gas; generate significantly more tritium than the arriving neutrons (tritium breeding ratio > 1.0, this requires a combined use of neutron multiplier like beryllium); maintain purgeable and coolable structure as lithium burns progressively. Using a pebble bed of millimeter size

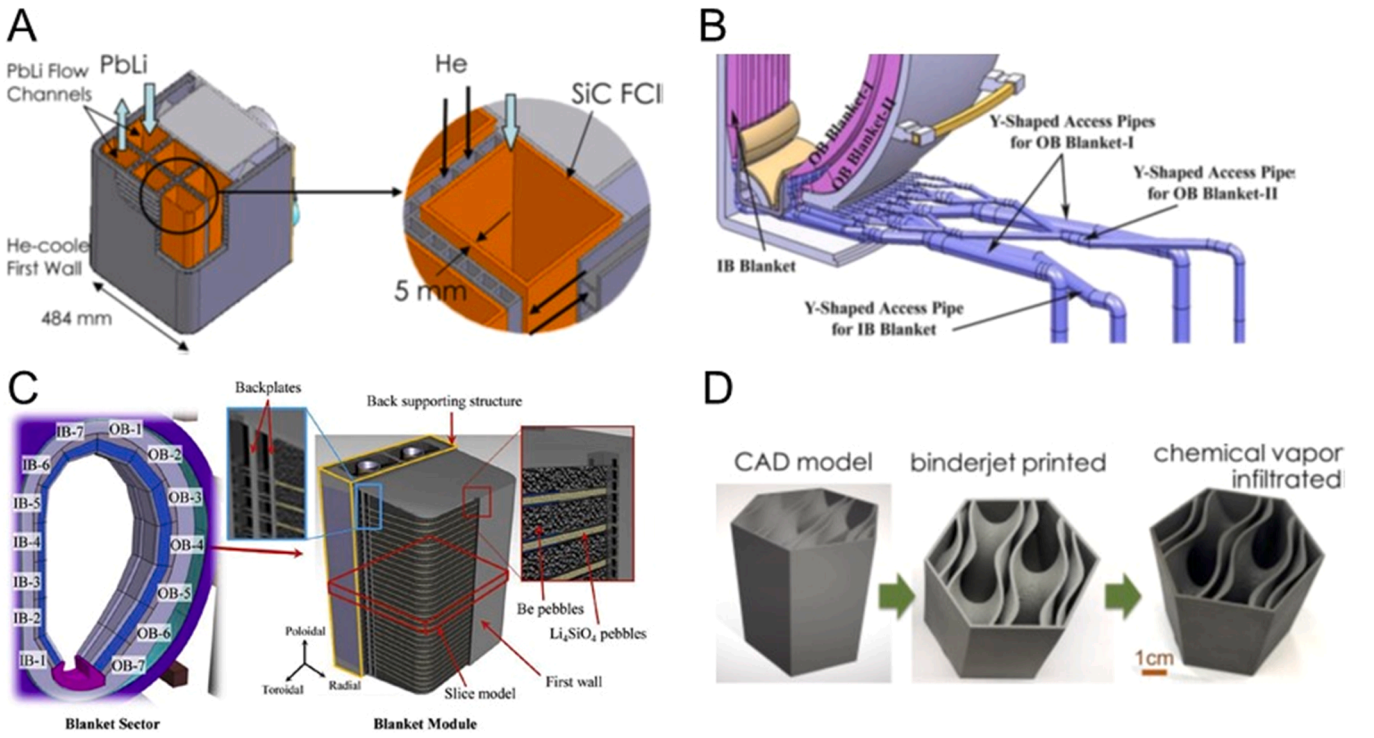

Fig. 18. Examples of ceramic components in fusion reactor blanket concepts: (A) the dual-cooled lead lithium (DCLL) blanket concept with Pb-Li coolant/breeder and ceramic flow channel inserts. (B) A manifold section of DCLL blanket. (C) A solid breeding blanket concept utilizing pebble beds of ceramic breeder and neutron multiplier. (D) additively manufactured SiC component for nuclear fuel assembly.
(A) (reproduced from [322]). (B) (reproduced from [323]). (C) Reprinted from [275], copyright 2017, with permission from Elsevier. (D) [324].

spherical particles of a lithium-bearing oxide ceramic is the common approach to design the solid breeding blankets Fig. 18C [274,275].

2.23. Traditional fabrications for fusion energy, opportunities for additive manufacturing and outlook

For the FCI of liquid metal breeding fusion blankets, such as the dual-cooled lead lithium (DCLL) and helium-cooled lead lithium (HCLL) concepts, the primary choice of material is silicon carbide (SiC) due mainly to the widely recognized radiation tolerance [276], the demonstrated chemical compatibility with lead lithium [277], the negligible neutronic penalty, and the low-activation/low-decay heat properties. While a continuous fiber-reinforced composite is a preferred form due to its damage tolerance [278], a microporous foam has also been considered [279]. Alternatively to SiC, the use of metal-cladded oxide ceramics is considered for a near-term demonstration of the liquid metal blanket, i.e., the ITER Test Blanket Module (TBM) [280]. The European TBM program is studying an FCI design with aluminum oxide insulator cladded in a reduced-activation ferritic/martensitic steel (RAFMS). The metal cladded FCI option limits risks associated with matrix microcracking, semiconducting nature, and the manufacturing challenges with the SiC composite, while it poses new challenges including the severely limited operating temperature window, radiation tolerance, and manufacturing of the cladded structure.

For the ceramic breeders, the materials historically considered include lithium oxide and variants of lithium silicate, titanate, zirconate, aluminate, and other ternary to quadruple compounds. Among them, lithium metatitanate (Li_2TiO_3) and orthosilicate (Li_4SiO_4) are considered the leading candidates across all the ceramic breeding ITER TBM developments [281]. Ternary compounds present a clear advantage over LiO_2 for structural stability as lithium burns into gas species. Choices of the preferred ceramic compounds are based primarily upon comparative evaluations of known properties such as lithium density, tritium release, thermomechanical stability, and thermal conductivity.

The continuous fiber SiC composite FCIs are manufactured by a conventional fabrication route involving preparation of woven fiber preforms followed by a matrix densification through the chemical vapor infiltration (CVI) process [282]. Among the mainstream SiC matrix densification approaches, CVI is the only demonstrated method to produce the SiC composites that are stable in a nuclear environment [278]. The alternative, microporous SiC FCI is manufactured through the CVI onto a preform made of an open-porous carbon foam [279]. The carbon core may be burned off after the deposition of SiC to mitigate erratic behavior of carbon in a high radiation environment. The challenges to fabrication of the SiC-based FCIs are the large dimensions and the complex geometries (particularly for the manifold sections) that need to be assembled to line the metallic flow channels. While the existing state of the art of CVI SiC composite technology allows the near-net shaping of the required geometries, the manufacturing will be very expensive and time-consuming. The alternative option of the microporous foam may eliminate fiber costs and the very long infiltration time; however, net shaping of the foam is even more challenging and, more importantly, the ability of open-porous foam-based FCI to meet the performance requirements is questionable [283].

AM presents the potential to print the complex 3D structure of SiC to replace the conventional approaches to fabricate the FCIs, which may be designed to use a form of fiber-reinforced composite and/or microporous ceramic. While a continuous fiber composite is ideal to minimize the risk of a catastrophic failure, a short fiber composite may prove adequate. AM is suitable to create a closed microporous structure, which is preferred over the open-porous structure that can be achieved by the CVI route. Moreover, AM will be capable of realizing a combination of the fiber composite and the microporous ceramic matrix to achieve the requirements of mechanical and insulating properties at the same time. AM Capabilities to manufacture fine features such as for fitting components together and retaining components in place would be of great benefit to this application.

The primary form of ceramic breeders is a pebble bed. Typical

designs assume the use of ~1 mm diameter spherical pebbles in a steel or ceramic composite compartment. The lithium metal oxide ternary pebbles are made via various processes including the sol-gel, melt-spraying, extrusion-spheronization, and reactive sintering [281]. In general, the technologies of pebble fabrications are mature with reasonable quality controls and production scaleup pathways identified, whereas the desired set of pebble attributes (e.g., density, open vs. closed porosity, stoichiometry) are yet to be established.

The pebble bed is a simple and well-established concept of the solid breeding fusion blanket with the challenges established as well. To name a few, while maximizing the lithium loading is desired to warrant an adequate tritium breeding performance, the packing density of pebbles is limited by their spherical geometry. Increasing the packing density is attainable, however, that jeopardizes the ability of tritium recovery with the gas purge. Even without maximizing the packing density, pebbles gradually sinter to compromise the tritium recovery. The poor thermal conductivity of a pebble bed challenges the temperature management and expedite the pebble sintering. It would be more advantageous to have macro scale controlled over the geometry to make architectures that mitigate heat fluxes well.

AM technologies are promising solutions to these engineering challenges for two main reasons. The flexibility of generating complex, porous structures is ideal to achieve the maximized volume fraction of the breeding material, securing efficient purge gas passages, minimized tritium diffusion path length through the solid material, and adequate removal of volumetric heat to the coolant at the same time. AM may enable, or help enable, to realize a clever integration of the breeding ceramics with the structural substrate or skeleton that is made of a material known to be stable in the operating nuclear environment.

AM development for SiC-based ceramics has recently been active. However, the applicable technical approaches are limited because of the requirement of radiation-tolerance. In general, high crystallinity and stoichiometric chemical composition make SiC resistant to atomic displacement damage. In addition, beta-phase SiC is considered more stable in a temperature range where anisotropic defect clusters form in the hexagonal polytypes. For these reasons, the AM technologies relying on the vapor deposition processes are considered promising to manufacture SiC components for fusion energy, as overviewed by Koyanagi, et al. [258]. One successful example of applying AM to print SiC for nuclear applications is the combined binder jet 3D printing-CVI method reported by Terrani et al. [202]. Encouragingly, the recent work by Karakoc et al. implies the potentials of other approaches, including the laser powder bed fusion, to print SiC without using additives that form the second phases, as in Fig. 18D [284].

Applications of the modern AM technologies to fabricate SiC composites for fusion energy have not been reported to our knowledge. For non-nuclear components, the approaches of using preceramic polymer precursor with inert or reactive fillers is perhaps the most mature technologies to form the SiC composites by AM (e.g., [285]). The technology of achieving the radiation-tolerant form of SiC matrix, defined above, remains a critical challenge.

The first step of AM applications to the solid breeders may be printing an open-microporous and/or microchannel structure with the relevant lithium ceramics. A recent attempt by Sharafat et al. to develop cellular Li_2ZrO_3 aligns with this direction [286]. In a more recent work by Liu et al., a similar cellular structure of Li_4SiO_4 was fabricated through stereolithography ceramic AM route [287].

2.24. Turbines and superalloy casting cores and molds

Higher temperature turbine operation for air/fuel Brayton open cycle turbines could be described as an on-going, key objective in turbine development to enable higher fuel efficiency [288–291]. This includes particularly hot section turbine blades, vanes, and other components formed from high temperature nickel alloys. Failure of these components poses a significant risk to catastrophic failure and could lead to significant costs, loss of power production, and human life, which necessitates a high level of quality assurance in the fabrication of these components. Various approaches including highly developed superalloys blades and turbine components, film cooling and internal cooling passages, and thermal barrier coating materials have been extensively applied to this challenge [288–293], all of which provide self-evidence of the commercial importance of reaching higher temperatures to improve the thermal efficiency [288–291]. Further, the components used at highest temperatures are typically made from nickel superalloys that are directionally solidified as single crystals to increase the high temperature resistance to creep strain [289–291]. The casting process traditionally used is investment casting or the "lost-wax" process incorporating porous ceramic cores for the cooling passages within the casting mold design [289–291]. Casting cores are a necessity within blades and vanes to provide internal cooling passages to allow the highest operating temperatures that provide increased thermodynamic efficiency [290]. The cooling passageways also allow air exit points to provide film cooling over the surface of the turbine blades and vanes [291]. Exacting tolerances are applied in the placement and dimensions of the cooling passageways to assure the required thermal and mechanical performance; these cores are usually made by injection molding a polymer and ceramic mixture into metal molds [292,294,295]. The cores are then typically encased within the solidified wax patterns used to create the exterior ceramic casting mold for the turbine components. The ceramic mold and core components for casting these nickel-based superalloy components must tolerate the casting temperatures used for the superalloys [291,292].

While the exterior surfaces of turbine components can be machined and surface inspected, the internal passageways that are critical to the cooling performance must be maintained with close tolerances throughout the high temperature casting process typically without any post-casting machining. Consequently, the internal casting cores used to maintain those passageways during casting and the exterior molds must be maintained to tight tolerances as well [292,294]. Turbine component cooling passageways can be quite complicated as can be seen from the cores in Fig. 19A-C including various flow paths to balance the cooling throughout the entire volume of the turbine component. Surface features are included on the cores to disrupt boundary layers to enable better heat transfer to the cooling air, and these features must be transferred to the casting by the core. These cores generally contain fine porosity, must remain dimensionally stable during the molten metal casting to preserve passageways down to the solidification temperatures, and then ideally become weak (partially due to the porosity) closer to room temperature to facilitate dissolution/removal of the casting cores [291,294,296]. This combination of dimensional stability and porosity requirements becomes particularly challenging with the high temperatures during casting of the molten nickel alloys.

2.25. Traditional fabrications of turbine molds and cores, opportunities for additive manufacturing and outlook

Given the high requirements for quality assurance in the composition of the cast superalloy turbine components, compositions of the core and mold materials are restricted tightly to limit potential contamination of the metal alloys by trace elements from the molds and cores. The selection of compositions of the core materials frequently includes silica, alumina, and zircon [292,294,297] although exact compositions often involve trade secrets as to the amount of each component, purity, and particle size distributions. The amount of silica and constituents are also carefully selected to control the phase transformations in the silica phase [296–298] during the lifecycle of the molds and cores including potential use of disruptive phase transformations upon cooling below alloy solidification temperatures to break up the porous cores. The compositions typically used are frequently greater than 80% silica [294]. Some amount of alumina and zircon can be used to increase bonding between grains, control grain growth, and to influence the phase transformations

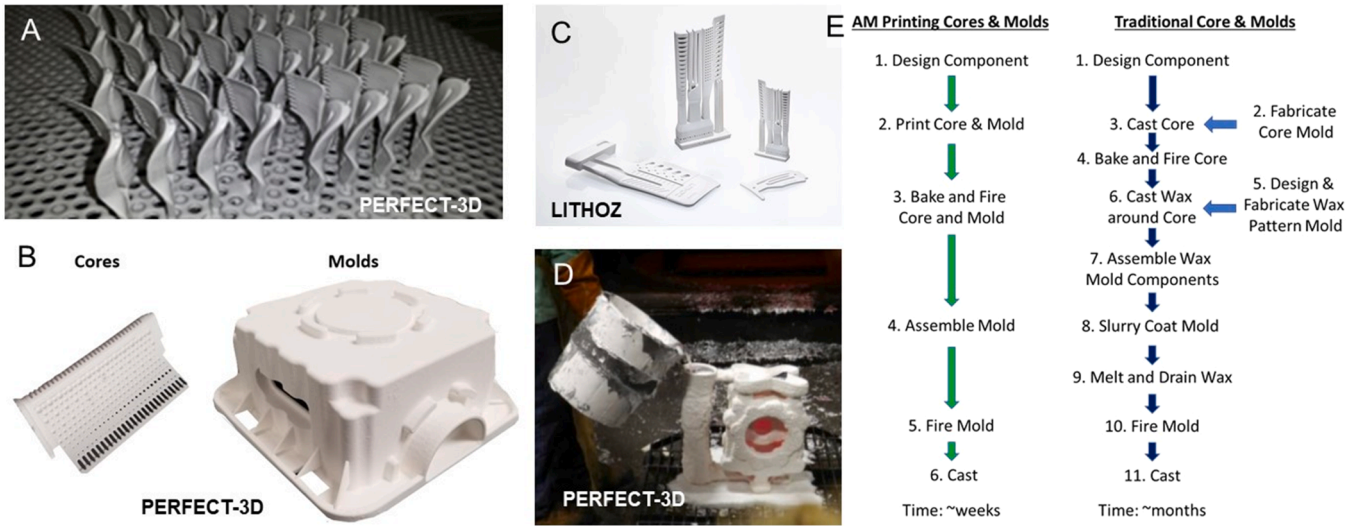

Fig. 19. (A) Image of a large number of concurrently printed additively manufactured turbine casting cores, (B) core and mold components after thermal treatments, (C) image showing various sizes of complex printed cores, (D) casting into an assembled mold obtained from ceramic AM printing, (E) Comparison of nominal Design and Manufacturing Flow Process with AM Printing of Cores and Molds and Traditional Process.
[Photos reproduced with permission of PERFECT-3D, Fairborn, OH and Lithoz, GmbH as indicated on the images].

in the silica upon cooling [297]. To some extent, it can be expected that the material selection is limited by the constraint of dimensional control through the range of heating and cooling that occurs during the core and mold fabrication and the casting process. Trace impurity limits are also applied to protect the alloy composition, e.g., sodium [295]. This ensures that the constituent elements in the mold and cores do not affect the creep and structural performance of the super alloys and to preserve the corrosion, oxidation, and erosion performance of the castings. It is also important that the subsequent bond coatings and thermal barrier coatings that are applied to high performance turbine components are not affected by contaminates from the mold materials. The desired stability and avoidance of dissolution and transfer of contaminating elements from the mold or core into the casting make the material selection choices for molds and cores quite complex and challenging.

The cores are typically formed by injection molding of primarily silica particles with alumina and zircon particles added along with any other additives that may be used to control the properties of the core material [292]. Typically, the injection molded cores that are used must be de-binded and partially sintered to have sufficient strength [292, 295]. Investment casting molds with cores typically involves placing the cores within a machined steel die and casting the wax pattern around the core (see Fig. 19E). Due to the importance of dimensional control, these wax patterns containing the cores are usually subjected to radiography techniques to assure proper positioning of the core within the wax pattern. Palladium pins are driven through the wax pattern to help assure that the core remains in position within the mold when the wax is removed and later during the mold heat treatment and the casting process [295]. Additional ancillary wax components are added to the pattern to form pour cups, runners, and vents for the liquid metal along with the fixturing for seed crystals and mold features to select a single crystal to grow in the turbine component during solidification of the casting, if desired [295]. The complete wax pattern assembly is then coated with a fine slurry of typically a silica powder suspension that also may contain alumina, zircon, and other trace additives. This is followed by successive dip coatings in slurries with successively larger ceramic particles that often culminates with slurry coatings and depositions of coarse ceramic powders and/or flakes to strengthen the mold. The wax is then removed by inverting the mold and heating, which is followed by heat treatments to strengthen the mold for casting [292,295]. The material selection and heat treatments of the mold are controlled usually to obtain a specific (casting and vendor specific) amount of cristobalite silica in the core material prior to the casting. Selected ceramic slurry coatings may be applied to the interior of the mold to further limit interaction of the molten alloy with the molds and cores [292].

Several primary benefits accrue from the use of ceramic additive manufacturing that particularly can benefit turbine development work. These include the ability to rapidly cycle and iterate on prototype designs of cores and molds for turbine and airfoil components without having to pursue extensive time and costs in designing, machining, and iteratively refining master metal molds for the cores, wax molding, and the processes for the exterior mold formation [292]. Even more complicated and efficient cooling channel designs could be contemplated with more rapid core fabrication and possibly alternate architectures than are not easily fabricated within the constraints of injection molded cores. Additive Manufacturing (AM) of cores as well as molds for turbine components can significantly reduce the development cost of cores and molds for turbine components and significantly shorten the development time to test new designs [292]. This can reduce the risks to cost and schedule for a new turbine component development effort. The combination of printing molds and cores for casting in some cases can avoid all the steps for forming the wax patterns and proceed directly to mold assembly and casting – an example of a completed AM ceramic mold used for casting is shown in Fig. 19D. Stereolithography AM techniques tend to allow high precision and good surface finish in the prototype cores and molds. Binder Jet printing techniques also might be considered. Advanced approaches for additive manufacturing of cores may also allow grading of the materials within the core to improve strength, mitigate stresses, save cost, or facilitate improved leachability for removal of the cores after casting [292]. The additive techniques can enable such improvements in development time such that greater improvements in turbine components may be attempted because of the lower cost of the development process.

Another important economic opportunity through additive manufacturing of ceramic molds and cores is the savings on potentially large mold and core development efforts for replacement aerospace parts requiring low-run numbers but careful start-to-finish Quality Control. With dimensional control provided by the additive manufacturing process, the Quality Assurance can be applied on the finished mold, cores, or parts and iterations are made more easily without the costs of developing the whole traditional production process for making molds for the cores, molds for the wax forms, and the process lines for the multi-layered dip coating of the wax mold patterns. Items

such as gearboxes and related castings in aerospace applications may not have the same alloy and casting complexity as turbine components, but the quality assurance required is still high to protect human life. Risk aversion for performance of manned aircraft often requires the continued use of investment casting in components originally produced by investment casting once those specific components have been approved and proven in service for a specific aircraft. This means that, for short runs of components, an additive manufacturing approach for the molds and cores could be cost competitive, since with control of the mold materials and dimensions through the printing process the alloy composition and the dimensional accuracy of the parts are likely to be obtained. A challenge in the additive manufacturing of cores and molds is the precision of printing and the control of distortion during binder burnout and sintering, which requires care in material selection and thermal profiles in subsequent processing [299]. The quality of surface finish and dimensional precision appears to have made stereolithography printing methods more commonly used for ceramic cores for turbine components. Examples of ceramic cores and molds printed using ceramic additive manufacturing are shown in Fig. 19A-C. Some molds, runners, and pour cups have been pieced together with ceramic paste for casting in Fig. 19D. The cost savings are partially enabled because the quality control is typically on the composition of the metal alloy and the finished dimensions of the component.

2.26. Ceramic turbine components requirements

Traditional ceramic turbine blades and vanes could be considered a particular ideal goal to further improve turbine efficiency owing to the refractive ceramic properties including higher melting temperature, potentially high creep resistance, potential for high corrosion resistance at elevated temperatures, and low density which has been explored with several traditional ceramic fabrication processes in large scale gas turbines [300,301]. However, these components can suffer from the potential for brittle fracture, difficulties in performing non-destructive evaluations to predict failure life, thermal shock susceptibility, increased machining costs, extreme stresses at the blade root and attachment points, and potentially more extensive levels of quality control required compared to superalloy blades and components. As can be expected, this has not led to significant efforts to form individual ceramic blades by additive manufacturing methods, as few of these challenges for individual blades may be improved by AM techniques. Silicon Carbide (SiC) and chopped SiC_f/SiC Ceramic Matrix Composites have been attempted by Binder Jet AM printing of vane components through a NASA program, although the report noted that fiber bridging of crack surfaces was not observed and high relative densities were not obtained [302]. Applications of ceramics to insulation, combustor liners, and exhaust flaps are more likely applications, owing to slightly reduced risk and structural demands, but these applications are not addressed here, although, work has been done to consider cost advantages of various turbine engine components that could be made from ceramics by additive manufacturing methods [303].

Monolithic ceramic turbines including ceramic microturbines such as those illustrated in Fig. 20 are an exception where research and development efforts for ceramic additively manufactured components have been applied. Government funding has supported development of monolithic microturbines using traditional ceramic processing methods [304,305]. Conventional metal alloy microturbines have applications to distributed power, auxiliary power units, backup power, and potentially as low-emission range extenders for electric vehicles, among other interests [306–308]. These applications benefit from operation on a variety of fuels, small size, potentially low NO_x emissions, and the suitability to co-generation with exhaust gases [306–308]. Ceramic microturbines could increase efficiency through increased operating temperatures which is difficult with metal alloy microturbines due to limitations for turbine cooling channels in the compact monolithic design [309]. In a related design application, ceramic turbocharger rotors have been evaluated and deployed into production road vehicles due to the benefit in improved responsiveness in boosting engine power [310]. The improved responsiveness results from the lower rotational inertia of the ceramic turbocharger rotor primarily because of the lower ceramic density compared to a metal turbocharger rotor [310,311]. One reference recently reported that up to 300,000 ceramic turbocharger rotors have been built into gasoline vehicles, although this number is still dwarfed by metal turbocharger rotors [312]. A drawback in microturbine designs is that, in shrinking the size, the turbine speed generally must increase to very high speeds [306], similar to turbochargers, to obtain reasonable efficiencies. Operational speeds of microturbines appear to range from 60,000 to well over 100,000 rpm. The advantages of low density and good thermal properties of ceramic materials will be a trade off to the challenges of increased stress at high speeds in the development efforts with ceramic microturbines.

Fig. 20. β-SiAlON impeller created by Digital Light Processing after de-binding and sintering. The features indicate a part built to net shape that is not easily fabricated by conventional ceramic processing or machining techniques. The diameter is approximately 45 mm.
Photo Credit: Photo Credit: Lithoz, GmbH., used with permission.

2.27. Traditional fabrications of turbine components, opportunities for additive manufacturing and outlook

The materials considered for traditional hot section turbine components often involve high temperature nickel superalloys. Ceramic materials proposed for these applications are typically those with relatively lower thermal expansion coefficients, higher thermal conductivity, preferably lower elastic modulus, low density, and lower heat capacity to mitigate against thermal shock. Silicon carbide (SiC) and silicon nitride (Si_3N_4) are the more common ceramics used in development thus far, with silicon nitride tending to be preferred [310–314]. While examples of sintered oxide microturbine shapes exist, it is not expected that oxides are good candidates for microturbines, based on thermo-mechanical properties. Early design work on ceramic turbine components that considered short-term use tended to utilize shorter and smaller blades and vanes to minimize stresses and assessed, based on properties, that reaction-bonded Si_3N_4 in the blade application would be more reliable than SiC for that application [300].

The traditional turbine blades, vanes, and other turbine components are made of high temperature nickel alloys including the nickel superalloys, which are typically fabricated by investment casting as detailed in the prior description of casting cores and molds. Ceramic turbine components have been formed by injection molding [312,314], pressure slip-casting [315,316], and gel-casting [317] among other ceramic processing techniques to produce the nominal green shapes. It is highly

preferable to shape ceramic parts closer to the final shape prior to sintering/densification processes, to avoid significant costs of machining; however, this is often not completely practical. Controlled atmosphere sintering and in some cases subsequent Hot Isostatic Pressing (HIP) are used for consolidation [316]. Balancing of rotor components for high-speed use will usually require some machining along with machining to support attachment to metal shafts [310,312].

Various approaches to additively manufactured ceramic microturbines have been undertaken [318–320]. The likely advantages of a ceramic microturbine are the potential higher operating temperatures leading to improved efficiency [305]. As with other ceramic additive manufacturing applications, the advantages of rapid prototyping by additive manufacturing are likely to be significant with ceramic microturbine development, as the design and fabrication of molding for traditional ceramic processes are expensive and time consuming. An attempt to compare gel-casting type approaches to Selective Laser Sintering (SLS) of alumina in generating a complete turbine disk and blades yielded a suitable structure after sintering; however, the limited measurements of mechanical properties were judged to be insufficient to report relative to better properties from more traditional gel-casting approaches [319]. Printing demonstrations of turbine impeller components have been shown in β-SiAlON by lithography printing of ceramic suspensions [321]. A basic Silicon infiltrated Silicon Carbide (SiSiC) turbine rotor has also been fabricated by Selective Laser Sintering of SiC followed by pyrolysis of residual organics to produce carbon with a subsequent infiltration by silicon to react to form additional SiC in the pore space by established ceramic processing techniques [320]. An example of a β-SiAlON impeller produced by a selective optical-curing lithography technique is shown in Fig. 20. While there are examples of demonstrations of components, the commercial deployment of ceramic additively manufactured components in high-speed microturbines presently appears to be limited. Future research will need to determine if the accuracy, uniformity, and surface finish quality after subsequent sintering steps will provide reliability comparable to other ceramic forming processes.

2.28. Outlook and future considerations for additive manufacturing of ceramics for energy applications

Ceramics are a unique class of materials that possess many structural and functional properties needed for energy applications. In energy applications where metals and polymers cannot be used, ceramics typically are called upon to provide improved properties including thermal stability, wear and corrosion resistance, strength, and electrical conductivity, among others. Ceramics are typically difficult to process, but many AM techniques are under development to improve manufacturing and reduce the associated cost. In addition, AM helps to control the local material microstructure and macro-architecture, which leads to improved properties for many energy applications where the engineering design requirements are aggressive and stringent. However, leaps of progress have already been seen and tested in many energy applications utilizing ceramics. Coincidentally, many ceramics engineering applications in energy require very similar materials, processing, and properties; so, there are many opportunities for the energy sector to grow and leverage AM of ceramics among the various applications presented in this review. Additionally, some applications require functional and structural properties, so there is some overlap among the various applications and materials, and more engineering and processing to consider. For the more functional ceramics, slips and pastes can be used, but the balance between rheology to print and final properties must be considered. Slurry media and dispersing will be important. Achieving very thin layers and using multimaterial will aid this development. For the more structural ceramics, the density, microstructure, and methods to achieve high strength with some improvements to fracture toughness will be crucial. In general, it is a recommended to select material for the properties and decide on the best manufacturing technique to achieve said properties, whether it is traditional techniques or AM. Cost, and sustainability are areas to keep in mind while selecting the materials and manufacturing routes (i.e., does the manufacturing save time and cost and will it make the application more effective or efficient?). For ceramics, AM is not as popular or widely used as for metals and polymers, so it is important to understand all the literature that is already present and continue to build from it. It is also prudent to consider hybridization of different AM technologies as well as new techniques to process the ceramics materials of the future for energy applications. We note that each AM technique has its own unique advantages, disadvantages, and characteristics, in terms, for instance, of the type of ceramic materials that can be processed successfully with it, the minimum and maximum feature size achievable, the size of the printing envelope, the surface quality of the parts, the cost of the equipment and the cost of the overall printing-to-sintered part process. Although many materials can be processed with different AM technologies, when we consider the making of parts, we should be careful in selecting the AM technique(s) that can afford the characteristics required for the specific application for which the part is being manufactured.

Energy applications have stringent requirements, and ceramics have the properties needed for these applications.AM of ceramics has a great opportunity to improve energy applications from design, materials, and properties. Here, several functional and structural energy applications utilizing ceramics are presented. There are some areas of improvements for AM techniques, however the benefits from AM are worth exploring and pushing the boundaries to achieve parts with improved properties. A review of work in AM of ceramics for energy is presented, where the functional ceramics are in batteries, supercapacitors, solid oxide fuel cells, piezoelectrics, smart glass, thermoelectrics, thermionics, catalytic converters; and the thermal/structural ceramics are heat exchangers, fission reactors, fusion reactors, turbines, and casting cores and molds. There are cases where functional and structural properties are needed, and some of the same AM techniques are used among all the applications utilizing ceramics, whether functional or structural. Several examples of ceramics AM in each application show promise. For many energy applications, ceramics AM should be used where necessary and be explored for further improvements.

Declaration of Competing Interest

The authors declare that they have no known competing financial interests or personal relationships that could have appeared to influence the work reported in this paper.

Acknowledgements

This material is based upon work supported by the United States (US) Department of Energy (DOE), Office of Energy Efficiency and Renewable Energy, Office of Advanced Manufacturing, Office of Vehicle Technology, Office of Nuclear Energy through the Transformational Challenge Reactor (TCR) program, and Office of Fusion Energy Sciences through the Fusion Materials Science program under contract number DE-AC05-00OR22725 with UT-Battelle LCC. In addition, this work is supported by the United States National Science Foundation, grant # 2152732 and the United States Air Force of Scientific Research grant # FA9550-20-1-0280 (PI, Majid Minary-Jolandan). Material contributed by S.L. is based upon work supported by the National Science Foundation under Grant No. CMMI-1943104. EI acknowledges funding from the German Research Foundation (DFG) within the Heisenberg program. LW acknowledges funding from the Carl Zeiss Foundation (Durchbrueche 2019). Jeffery J. Haslam acknowledges his contributions were prepared by Lawrence Livermore National Laboratory under Contract DE-AC52-07NA27344.

Summary

Ceramics are a unique class of materials that possess many structural and functional properties needed for energy applications. In energy applications where metals and polymers cannot be used, ceramics typically are called upon to provide improved properties including thermal stability, wear and corrosion resistance, strength, and electrical conductivity, among others. Ceramics are typically difficult to process, but many AM techniques are under development to improve manufacturing and reduce the associated cost. In addition, AM helps to control the local material microstructure and macro-architecture, which leads to improved properties for many energy applications where the engineering design requirements are aggressive and stringent. However, leaps of progress have already been seen and tested in many energy applications utilizing ceramics. Coincidentally, many ceramics engineering applications in energy require very similar materials, processing, and properties; so, there are many opportunities for the energy sector to grow and leverage AM of ceramics among the various applications presented in this review. Additionally, some applications require functional and structural properties, so there is some overlap among the various applications and materials, and more engineering and processing to consider. In general, it is a recommended to select material for the properties and decide on the best manufacturing technique to achieve said properties, whether it is traditional techniques or AM. Cost and sustainability are areas to keep in mind while selecting the materials and manufacturing routes (i.e. does the manufacturing save time and cost and will it make the application more effective or efficient?). For ceramics, AM is not as popular or widely used as for metals and polymers, so it is important to understand all the literature that is already present and continue to build from it. It is also prudent to consider hybridization of different AM technologies as well as new techniques to process the ceramics materials of the future for energy applications. Ultimately, AM of ceramics has a great opportunity to improve energy applications. We note that each AM technique has its own unique advantages, disadvantages, and characteristics, in terms for instance of the type of ceramic materials that can be processed successfully with it, the minimum and maximum feature size achievable, the size of the printing envelope, the surface quality of the parts, the cost of the equipment and the cost of the overall printing-to-sintered part process. Although many materials can be processed with different AM technologies, when we consider the making of parts, we should be careful in selecting the AM technique(s) that can afford the characteristics required for the specific application for which the part is been manufactured.

References

[1] Global Advanced Ceramic Market Size Report, 2020–2027 [Internet]. [cited 21 Jul 2021]. Available from: ⟨https://www.grandviewresearch.com/industry-analysis/advanced-ceramics-market⟩.

[2] Battery Pack Prices Cited Below $100/kWh for the First Time in 2020, While Market Average Sits at $137/kWh | BloombergNEF [Internet]. [cited 2021 Aug 1]. Available from: ⟨https://about.bnef.com/blog/battery-pack-prices-cited-below-100-kwh-for-the-first-time-in-2020-while-market-average-sits-at-137-kwh/⟩.

[3] Department of Energy U. Energy Storage Grand Challenge: Energy Storage Market Report [Internet]. 2020 [cited 1 Aug 2021]. Available from: ⟨https://energy.gov/energy-storage-grand-challenge/downloads/energy-storage-⟩.

[4] Batteries, Charging , and Electric Vehicles | Department of Energy [Internet]. [cited 1 Aug 2021]. Available from: ⟨https://www.energy.gov/eere/vehicles/batteries-charging-and-electric-vehicles⟩.

[5] Y. Katoh , T. Nozawa , L. Snead , KO-J of N, 2011 undefined. Stability of SiC and its composites at high neutron fluence. Elsevier [Internet]. [cited 2022 Jan 13]; Available from: ⟨https://www.sciencedirect.com/science/article/pii/S0022311510009104⟩.

[6] L. Zhou, Y. Huang, Z. Xie, Gelcasting of concentrated aqueous silicon carbide suspension, J. Eur. Ceram. Soc. 20 (1) (2000) 85–90.

[7] Z. Zhang , Y. Zhang , H. Gong , X. Guo, Y. Zhang, X. Wang, et al. Influence of Carbon Content on Ceramic Injection Molding of Reaction-Bonded Silicon Carbide. Int J Appl Ceram Technol [Internet]. 2016 Sep 1 [cited 5 Apr 2020;13 (5):838–43. Available from: ⟨http://doi.wiley.com/10.1111/ijac.12570⟩.

[8] J.M.F. Ferreira, H.M.M. Diz, Effect of Solids Loading on Slip-Casting Performance of Silicon Carbide Slurries, in: J. Am. Ceram. Soc., 82, 2020, pp. 1993–2000. Available from: http://doi.wiley.com/10.1111/j.1151-2916.1999.tb02031.x.

[9] W. David Richarson, Modern Ceramic Engineering: Properties, Processing, and Use in Design, CRC Press, 2005.

[10] N. Bansal , J. Lamon , Ceramic matrix composites: materials, modeling and technology. John Wiley & Sons; 2014.

[11] Ceramics Additive Manufacturing Markets 2018–2027-SmarTech Report [Internet]. [cited 27 Jul 2021]. Available from: ⟨https://www.smartechanalysis.com/reports/ceramics-additive-manufacturing-markets-2017–2028/⟩.

[12] A. Zocca, P. Colombo , CM Gomes , J. Günster , Additive Manufacturing of Ceramics: Issues, Potentialities, and Opportunities. Green DJ, editor. J Am Ceram Soc [Internet]. 2015 Jul 1 [cited 2019 Jan 23];98(7):1983–2001. Available from: ⟨http://doi.wiley.com/10.1111/jace.13700⟩.

[13] Z. Chen, Z. Li, J. Li, C. Liu, C. Lao, Y. Fu, et al., 3D printing of ceramics: a review, J. Eur. Ceram. Soc. 39 (4) (2019) 661–687.

[14] M. Schwentenwein, J. Homa, Additive manufacturing of dense alumina ceramics, Int J. Appl. Ceram. Technol. 12 (1) (2015) 1–7.

[15] J. Schlacher, T. Lube, W. Harrer, G. Mitteramskogler, M. Schwentenwein, R. Danzer, et al., Strength of additive manufactured alumina, J. Eur. Ceram. Soc. (2020).

[16] C.L. Cramer, J.K. Wilt, Q.A. Campbell, L. Han, T. Saito, A.T. Nelson, Accuracy of stereolithography printed alumina with digital light processing, Open Ceram. 8 (2021), 100194.

[17] C.L. Crame , P. Nandwana , R.A. Lowden , A.M. , Elliott Infiltration studies of additive manufacture of WC with Co using binder jetting and pressureless melt method. Addit Manuf [Internet]. [15 Apr 2019]; Available from: ⟨https://www.sciencedirect.com/science/article/pii/S2214860419301903⟩.

[18] E. Sachs , M. Cima , P. Williams , D. Brancazio , J. Cornie , Three Dimensional Printing: Rapid Tooling and Prototypes Directly from a CAD Model. J Eng Ind [Internet]. 1992 Nov 1 [cited 2019 Jun 2];114(4):481. Available from: ⟨http://manufacturingscience.asmedigitalcollection.asme.org/article.aspx?articleid=1447635⟩.

[19] J. Pelz, N. Ku, W. Shoulders, Multi-material additive manufacturing of functionally graded carbide ceramics via active, in-line mixing, Addit. Manuf. (2022).

[20] T. Chu , S. Park , K. Fu , (Kelvin) 3D printing-enabled advanced electrode architecture design. Carbon Energy [Internet]. 2021 Jul 1 [cited 2021 Aug 6];3 (3):424–39. Available from: ⟨https://onlinelibrary.wiley.com/doi/full/10.1002/cey2.114⟩.

[21] F. Michael Ashby, Materials Selection in Mechanical Design, third ed., Elsevier, 2005.

[22] P. Chang , H. Mei , S. Zhou , K.G. Dassios , L. Cheng , 3D printed electrochemical energy storage devices [Internet]. Vol. 7, Journal of Materials Chemistry A. Royal Society of Chemistry; 2019 [cited 2021 Jul 1]. p. 4230–58. Available from: ⟨https://pubs.rsc.org/en/content/articlehtml/2019/ta/c8ta11860d⟩.

[23] M.P. Browne , E. Redondo , M. Pumera , 3D Printing for Electrochemical Energy Applications. Chem Rev [Internet]. 2020 Mar 11 [cited 2021 Jul 1];120(5): 2783–810. Available from: ⟨https://dx.doi.org/10.1021/acs.chemrev.9b00783⟩.

[24] A. Chen, C. Qu, Y. Shi, F. Shi, Manufacturing Strategies for Solid Electrolyte in Batteries, Front. Energy Res. 3 (2020) 8.

[25] C. Ruiz-Morales J. A Tarancón, J. Canales-Vázquez, J. Méndez-Ramos, L. Hernández-Afonso, P. Acosta-Mora, et al. Three dimensional printing of components and functional devices for energy and environmental applications. Energy Environ Sci [Internet]. 2017 Apr 12 [cited 2021 Jul 9];10(4):846–59. Available from: ⟨https://pubs.rsc.org/en/content/articlehtml/2017/ee/c6ee03526d⟩.

[26] S. Mooraj , Z. Qi , C. Zhu , J. Ren , S. Peng , L. Liu , et al. , 3D printing of metal-based materials for renewable energy applications. Nano Res 2020 147 [Internet]. 2020 Dec 4 [cited 2021 Jul 9];14(7):2105–32. Available from: ⟨https://link.springer.com/article/10.1007/s12274–020-3230-x⟩.

[27] M. Cheng, R. Deivanayagam, R. Shahbazian-Yassar, 3D printing of electrochemical energy storage devices: a review of printing techniques and electrode/electrolyte architectures, Batter Supercaps (2020) 130–146. ⟨https://chemistry-europe.onlinelibrary.wiley.com/doi/full/10.1002/batt.201900130⟩.

[28] D.M. Soares, Z. Ren, S.Bin Mujib, S. Mukherjee, C.G.M. Real, M. Anstine, et al., Additive manufacturing of electrochemical energy storage systems electrodes, Adv. Energy Sustain. Res. (2021). ⟨https://onlinelibrary.wiley.com/doi/full/10.1002/aesr.202000111⟩.

[29] C. Sun, Y. Wang, M.D. McMurtrey, N.D. Jerred, F. Liou, J. Li, Additive manufacturing for energy: a review, Appl. Energy 282 (2021), 116041.

[30] Y. Pang, Y. Cao, Y. Chu, M. Liu, K. Snyder, D. MacKenzie, et al., Additive manufacturing of batteries, Adv. Funct. Mater. (2021). ⟨https://onlinelibrary.wiley.com/doi/full/10.1002/adfm.201906244⟩.

[31] A. Zhakeyev, P. Wang, L. Zhang, W. Shu, H. Wang, J. Xuan, Additive manufacturing: unlocking the evolution of energy materials, Adv. Sci. (2021). ⟨https://onlinelibrary.wiley.com/doi/full/10.1002/advs.201700187⟩.

[32] S. Tagliaferri, A. Panagiotopoulos, C. Mattevi, Direct ink writing of energy materials, Mater. Adv. 2 (2) (2021) 540–563. ⟨https://pubs.rsc.org/en/content/articlehtml/2021/ma/d0ma00753f⟩.

[33] S.-W. Kim, D.-H. Seo, X. Ma, G. Ceder, K. Kang, Electrode materials for rechargeable sodium-ion batteries: potential alternatives to current lithium-ion batteries, Adv. Energy Mater. (2021) 710–721. ⟨https://onlinelibrary.wiley.com/doi/full/10.1002/aenm.201200026⟩.

[34] L. Peng, Y. Zhu, R.S. Ruoff, G. Yu, Two-dimensional materials for beyond-lithium-ion batteries, Adv. Energy Mater. (2016).

[35] C. Fang, Y. Huang, W. Zhang, J. Han, Z. Deng, Y. Cao, et al., Routes to high energy cathodes of sodium-ion batteries, Adv. Energy Mater. (2021). ⟨https://onlinelibrary.wiley.com/doi/full/10.1002/aenm.201501727⟩.

[36] L. Zeng, P. Li, Y. Yao, B. Niu, S. Niu, B. Xu, Recent progresses of 3D printing technologies for structural energy storage devices, Mater. Today Nano 12 (2020), 100094.

[37] J. Wang, Q. Sun, X. Gao, C. Wang, W. Li, F.B. Holness, et al., Toward high areal energy and power density electrode for Li-Ion Batteries via optimized 3D printing approach, ACS Appl. Mater. 10 (46) (2021) 39794–39801 (Available from), ⟨https://pubs.acs.org/doi/abs/10.1021/acsami.8b14797⟩.

[38] Zhang C. (John), M.P. Kremer, A. Seral-Ascaso, S.-H. Park, N. McEvoy, B. Anasori, et al., Stamping of flexible, coplanar micro-supercapacitors using MXene inks, Adv. Funct. Mater. (2021). ⟨https://onlinelibrary.wiley.com/doi/full/10.1002/adfm.201705506⟩.

[39] X. Tang, C. Zhu, D. Cheng, H. Zhou, X. Liu, P. Xie, et al., Architectured leaf-inspired Ni0.33Co0.66S2/graphene aerogels via 3D printing for high-performance energy storage, Adv. Funct. Mater. (2021). ⟨https://onlinelibrary.wiley.com/doi/full/10.1002/adfm.201805057⟩.

[40] J. Song, Y. Chen, K. Cao, Y. Lu, J.H. Xin, X. Tao, Fully controllable design and fabrication of three-dimensional lattice supercapacitors, ACS Appl. Mater. 10 (46) (2021) 39839–39850 (Available from), ⟨https://pubs.acs.org/doi/abs/10.1021/acsami.8b15731⟩.

[41] B. Chen, Y. Jiang, X. Tang, Y. Pan, S. Hu, Fully packaged carbon nanotube supercapacitors by direct ink writing on flexible substrates, ACS Appl. Mater. 9 (34) (2021) 28433–28440 (Available from), ⟨https://pubs.acs.org/doi/abs/10.1021/acsami.7b06804⟩.

[42] C.M. Costa, R. Gonçalves, S. Lanceros-Méndez, Recent advances and future challenges in printed batteries, Energy Storage Mater. 28 (2020) 216–234.

[43] K. Narita, M.A. Citrin, H. Yang, X. Xia, J.R. Greer, 3D architected carbon electrodes for energy storage, Adv. Energy Mater. (2021). ⟨https://onlinelibrary.wiley.com/doi/full/10.1002/aenm.202002637⟩.

[44] K. Narita, M.A. Citrin, H. Yang, X. Xia, J.R. Greer, Carbon electrodes: 3D architected carbon electrodes for energy storage, Adv. Energy Mater. (2021). ⟨https://onlinelibrary.wiley.com/doi/full/10.1002/aenm.202170019⟩.

[45] R.E. Sousa, C.M. Costa, S. Lanceros-Méndez, Advances and future challenges in printed batteries, ChemSusChem (2021) 3539–3555. ⟨https://chemistry-europe.onlinelibrary.wiley.com/doi/full/10.1002/cssc.201500657⟩.

[46] S.M.H. Hashemi, U. Babic, P. Hadikhani, D. Psaltis, The potentials of additive manufacturing for mass production of electrochemical energy systems, Curr. Opin. Electrochem 20 (2020) 54–59.

[47] V. Egorov, C. O'Dwyer, Architected porous metals in electrochemical energy storage, Curr. Opin. Electrochem 21 (2020) 201–208.

[48] Yanyan Zhang Yuxin Tang, Bing Ma Wenlong Li, Xiaodong Chen, Rational material design for ultrafast rechargeable lithium-ion batteries, Chem. Soc. Rev. 44 (17) (2021) 5926–5940 (Available from), ⟨https://pubs.rsc.org/en/content/articlehtml/2015/cs/c4cs00442f⟩.

[49] D.L. Wood, J. Li, C. Daniel, Prospects for reducing the processing cost of lithium ion batteries, J. Power Sources 275 (2015) 234–242.

[50] A. Maurel, S. Grugeon, M. Armand, B. Fleutot, M. Courty, K. Prashantha, et al., Overview on lithium-ion battery 3D-printing by means of material extrusion, ECS Trans. 98 (13) (2021) 3 (Available from), ⟨https://iopscience.iop.org/article/10.1149/09813.0003ecst⟩.

[51] F. Liu, D.Z. Zhang, P. Zhang, M. Zhao, S. Jafar, Mechanical properties of optimized diamond lattice structure for bone scaffolds fabricated via selective laser melting, Materials 11 (2018) 374 [Internet]. 2018 Mar 3 [cited 2021 Aug 7]; 11(3):374. Available from, ⟨https://www.mdpi.com/1996-1944/11/3/374/htm⟩.

[52] M. Li, J. Lu, Z. Chen, K. Amine, 30 years of lithium-ion batteries, Adv. Mater. (2021). ⟨https://onlinelibrary.wiley.com/doi/full/10.1002/adma.201800561⟩.

[53] J. Hu, Y. Jiang, S. Cui, Y. Duan, T. Liu, H. Guo, et al., Lithium-ion batteries: 3D-printed cathodes of LiMn1−xFexPO4 nanocrystals achieve both ultrahigh rate and high capacity for advanced lithium-ion battery, Adv. Energy Mater. (2021). ⟨https://onlinelibrary.wiley.com/doi/full/10.1002/aenm.201670105⟩.

[54] K. Fu, Y. Wang, C. Yan, Y. Yao, Y. Chen, J. Dai, et al., Graphene oxide-based electrode inks for 3D-printed lithium-ion batteries, Adv. Mater. (2021) 2587–2594. ⟨https://onlinelibrary.wiley.com/doi/full/10.1002/adma.201505391⟩.

[55] C. Chen, Y. Zhang, Y. Li, Y. Kuang, J. Song, W. Luo, et al., Highly conductive, lightweight, low-tortuosity carbon frameworks as ultrathick 3d current collectors, Adv. Energy Mater. (2021). ⟨https://onlinelibrary.wiley.com/doi/full/10.1002/aenm.201700595⟩.

[56] K. Sun, T.-S. Wei, B.Y. Ahn, J.Y. Seo, S.J. Dillon, J.A. Lewis, 3D printing of interdigitated Li-ion microbattery architectures, Adv. Mater. (2021) 4539–4543. ⟨https://www.onlinelibrary.wiley.com/doi/full/10.1002/adma.201301036⟩.

[57] E. Cohen, S. Menkin, M. Lifshits, Y. Kamir, A. Gladkich, G. Kosa, et al., Novel rechargeable 3D-microbatteries on 3D-printed-polymer substrates: Feasibility study, Electro Acta 265 (2018 1) 690–701.

[58] D.W. McOwen, S. Xu, Y. Gong, Y. Wen, G.L. Godbey, J.E. Gritton, et al., 3D-printing electrolytes for solid-state batteries, Adv. Mater. (2021). ⟨https://onlinelibrary.wiley.com/doi/full/10.1002/adma.201707132⟩.

[59] A.M. Gaikwad, G.L. Whiting, D.A. Steingart, A.C. Arias, Highly flexible, printed alkaline batteries based on mesh-embedded electrodes, Adv. Mater. (2021 8) 3251–3255. ⟨https://onlinelibrary.wiley.com/doi/full/10.1002/adma.201100894⟩.

[60] A.M. Gaikwad, A.C. Arias, D.A. Steingart, Recent progress on printed flexible batteries: mechanical challenges printing technologies, and future prospects, Energy Technol. (2021) 305–328. ⟨https://onlinelibrary.wiley.com/doi/full/10.1002/ente.201402182⟩.

[61] D. Jie Liu, D.G. Galpaya, Yan Lijing, Sun Minghao, Lin Zhan, Yan Cheng, et al., Exploiting a robust biopolymer network binder for an ultrahigh-areal-capacity Li–S battery, Energy Environ. Sci. 10 (3) (2021) 750–755 (Available from), ⟨https://pubs.rsc.org/en/content/articlehtml/2017/ee/c6ee03033e⟩.

[62] K. Shen, H. Mei, B. Li, J. Ding, S. Yang, 3D printing sulfur copolymer-graphene architectures for Li-S batteries, Adv. Energy Mater. (2021). ⟨https://onlinelibrary.wiley.com/doi/full/10.1002/aenm.201701527⟩.

[63] X. Gao, Q. Sun, X. Yang, J. Liang, A. Koo, W. Li, et al., Toward a remarkable Li-S battery via 3D printing, Nano Energy 56 (2019 1) 595–603.

[64] S. Huang, X. Zhu, S. Sarkar, Y. Zhao, Challenges and opportunities for supercapacitors, APL Mater. (2021). ⟨https://aip.scitation.org/doi/abs/10.1063/1.5116146⟩.

[65] J. Li, F. Ye, S. Vaziri, M. Muhammed, M.C. Lemme, M. Östling, Efficient inkjet printing of graphene, Adv. Mater. (2021) 3985–3992. ⟨https://onlinelibrary.wiley.com/doi/full/10.1002/adma.201300361⟩.

[66] A. González, E. Goikolea, J.A. Barrena, R. Mysyk, Review on supercapacitors: technologies and materials, Renew. Sustain Energy Rev. 58 (2016 1) 1189–1206.

[67] B. Yao, S. Chandrasekaran, J. Zhang, W. Xiao, F. Qian, C. Zhu, et al., Efficient 3D printed pseudocapacitive electrodes with ultrahigh MnO2 loading, Joule 3 (2) (2019) 459–470.

[68] W. Yang, J. Yang, J.J. Byun, F.P. Moissinac, J. Xu, S.J. Haigh, et al., 3D printing of freestanding MXene architectures for current-collector-free supercapacitors, Adv. Mater. (2021). ⟨https://onlinelibrary.wiley.com/doi/full/10.1002/adma.201902725⟩.

[69] K. Shen, J. Ding, S. Yang, 3D printing quasi-solid-state asymmetric micro-supercapacitors with ultrahigh areal energy density, Adv. Energy Mater. (2021). ⟨https://onlinelibrary.wiley.com/doi/full/10.1002/aenm.201800408⟩.

[70] J. Park, J. Li, W. Lu, A.M. Sastry, Geometric consideration of nanostructures for energy storage systems, J. Appl. Phys. (2021). ⟨https://aip.scitation.org/doi/abs/10.1063/1.4939282⟩.

[71] T.I. Zohdi, Dynamic thermomechanical modeling and simulation of the design of rapid free-form 3D printing processes with evolutionary machine learning, Comput. Methods Appl. Mech. Eng. 331 (2018) 343–362.

[72] A. Hauch, R. Küngas, P. Blennow, A.B. Hansen, J.B. Hansen, B.V. Mathiesen, et al., Recent advances in solid oxide cell technology for electrolysis, Science 370 (6513) (2021).

[73] Y. Shi , N. Cai , T. Cao , J. Zhang , High-temperature Electrochemical Energy Conversion and Storage: Fundamentals and Applications [Internet]. 2017 [cited 2021 Jul 20]. Available from: ⟨https://books.google.com/books?hl=en&lr=&id=rmhQDwAAQBAJ&oi=fnd&pg=PP1&dq=Yixiang+Shi,+N.C.,+Tianyu+Cao,+Jiujun+Zhang,+High-Temperature+Electrochemical+Energy+Conversion+and+Storage:+Fundamentals+and+Applications&ots=TYbEM-fta_&sig=PgxqPHdVWgt4LOgfpjICQ7n59YQ⟩.

[74] B. Xing, C. Cao, W. Zhao, M. Shen, C. Wang, Z. Zhao, Dense 8 mol% yttria-stabilized zirconia electrolyte by DLP stereolithography, J. Eur. Ceram. Soc. 40 (4) (2020) 1418–1423.

[75] J.W. Fergus, Electrolytes for solid oxide fuel cells, J. Power Sources 162 (1) (2006) 30–40.

[76] F. Salari, A.B. Najafabadi, M. Ghatee, M. Golmohammad, Hybrid additive manufacturing of the modified electrolyte-electrode surface of planar solid oxide fuel cells, Int. J. Appl. (2021) 1554–1561. ⟨https://ceramics.onlinelibrary.wiley.com/doi/full/10.1111/ijac.13527⟩.

[77] M. Cassidy, Trends in the processing and manufacture of solid oxide fuel cells, Rev. Energy Environ. (2021), e248. ⟨https://onlinelibrary.wiley.com/doi/full/10.1002/wene.248⟩.

[78] M. Weimar , L. Chick , D. Gotthold , G. Whyatt , Cost study for manufacturing of solid oxide fuel cell power systems [Internet]. 2013 [cited 2021 Jul 20]. Available from: ⟨https://www.osti.gov/biblio/1126362⟩.

[79] L. Wei, J. Zhang, F. Yu, W. Zhang, X. Meng, N. Yang, et al., A novel fabrication of yttria-stabilized-zirconia dense electrolyte for solid oxide fuel cells by 3D printing technique, Int J. Hydrog. Energy 44 (12) (2019) 6182–6191.

[80] Aitor Hornés Arianna Pesce, Alex Morata Marc Núñez, Albert Tarancón Marc Torrell, 3D printing the next generation of enhanced solid oxide fuel and electrolysis cells, J. Mater. Chem. A 8 (33) (2021) 16926–16932 (Available from), ⟨https://pubs.rsc.org/en/content/articlehtml/2020/ta/d0ta02803g⟩.

[81] Adriano Ambrosi, R.R. Sheng Shi, D. Webster R, 3D-printing for electrolytic processes and electrochemical flow systems, J. Mater. Chem. A 8 (42) (2021) 21902–21929 (Available from), ⟨https://pubs.rsc.org/en/content/articlehtml/2020/ta/d0ta07939a⟩.

[82] X.Y. Tai, A. Zhakeyev, H. Wang, K. Jiao, H. Zhang, J. Xuan, Accelerating fuel cell development with additive manufacturing technologies: state of the art, opportunities and challenges, Fuel Cells (2021) 636–650. ⟨https://onlinelibrary.wiley.com/doi/full/10.1002/fuce.201900164⟩.

[83] G.D. Han, K. Bae, E.H. Kang, H.J. Choi, J.H. Shim, Inkjet printing for manufacturing solid oxide fuel cells, ACS Energy Lett. 5 (5) (2021) 1586–1592 (Available from), ⟨https://pubs.acs.org/doi/abs/10.1021/acsenergylett.0c00721⟩.

[84] A.M. Sukeshini, F. Meisenkothen, P. Gardner, T.L. Reitz, Aerosol Jet® Printing of functionally graded SOFC anode interlayer and microstructural investigation by low voltage scanning electron microscopy, J. Power Sources 224 (2013) 295–303.

[85] N.M. Farandos, T. Li, G.H. Kelsall, 3-D inkjet-printed solid oxide electrochemical reactors. II, LSM - YSZ Electrodes Electro Acta 270 (2018) 264–273.

[86] N.M. Farandos, L. Kleiminger, T. Li, A. Hankin, G.H. Kelsall, Three-dimensional inkjet printed solid oxide electrochemical reactors. I. Yttria-stabilized zirconia electrolyte, Electro Acta 213 (2016) 324–331.

[87] S. Masciandaro, M. Torrell, P. Leone, A. Tarancón, Three-dimensional printed yttria-stabilized zirconia self-supported electrolytes for solid oxide fuel cell applications, J. Eur. Ceram. Soc. 39 (1) (2019) 9–16.

[88] Y. De Hazan, J. Heinecke, A. Weber, T. Graule, High solids loading ceramic colloidal dispersions in UV curable media via comb-polyelectrolyte surfactants, J. Colloid Interface Sci. 337 (1) (2009) 66–74.

[89] S.M. Gaytan, M.A. Cadena, H. Karim, D. Delfin, Y. Lin, D. Espalin, et al., Fabrication of barium titanate by binder jetting additive manufacturing technology, Ceram. Int. 41 (5) (2018) 6610–6619 (Available from), ⟨https://linkinghub.elsevier.com/retrieve/pii/S0272884215001558⟩.

[90] D. Kuscer, S. Drnovšek, F. Levassort, Inkjet-printing-derived lead-zirconate-titanate-based thick films for printed electronics, Mater. Des. 198 (2021), 109324.

[91] Z. Chen, X. Song, L. Lei, X. Chen, C. Fei, C.T. Chiu, et al., 3D printing of piezoelectric element for energy focusing and ultrasonic sensing, Nano Energy 27 (2016) 78–86.

[92] W. Chen, F. Wang, K. Yan, Y. Zhang, D. Wu, Micro-stereolithography of KNN-based lead-free piezoceramics, Ceram. Int. 45 (4) (2019) 4880–4885.

[93] M.S. Hossain, J.A. Gonzalez, R.M. Hernandez, M.A.I. Shuvo, J. Mireles, A. Choudhuri, et al., Fabrication of smart parts using powder bed fusion additive manufacturing technology, Addit. Manuf. 10 (2016) 58–66.

[94] X. Zhou, K. Parida, O. Halevi, Y. Liu, J. Xiong, S. Magdassi, et al., All 3D-printed stretchable piezoelectric nanogenerator with non-protruding kirigami structure, Nano Energy 72 (2020), 104676.

[95] X. Qiao, W. Geng, Y. Sun, J. Yu, X. Chen, Y. Yang, et al., Preparation of high piezoelectric and flexible polyvinylidene fluoride nanofibers via lead zirconium titanate doping, Ceram. Int. 46 (18) (2020) 28735–28741.

[96] R.L. Walton, M.J. Brova, B.H. Watson, E.R. Kupp, M.A. Fanton, R.J. Meyer, et al., Direct writing of textured ceramics using anisotropic nozzles, J. Eur. Ceram. Soc. 41 (3) (2021) 1945–1953.

[97] Z.H. Zhao, M.Y. Ye, H.M. Ji, X.L. Li, X. Zhang, Y. Dai, Enhanced piezoelectric properties and strain response in ⟨001⟩ textured BNT-BKT-BT ceramics, Mater. Des. 137 (2018) 184–191.

[98] H. Leng, Y. Yan, H. Liu, M. Fanton, R.J. Meyer, S. Priya, Design and development of high-power piezoelectric ceramics through integration of crystallographic texturing and acceptor-doping, Acta Mater. 206 (2021), 116610.

[99] R. Tu, E. Sprague, H.A. Sodano, Precipitation-printed high-β phase poly (vinylidene fluoride) for energy harvesting, ACS Appl. Mater. Interfaces 12 (52) (2021) 58072–58081, https://doi.org/10.1021/acsami.0c16207.

[100] H. Cui, R. Hensleigh, D. Yao, D. Maurya, P. Kumar, M.G. Kang, et al., Three-dimensional printing of piezoelectric materials with designed anisotropy and directional response, Nat. Mater. 18 (3) (2021) 234–241, https://doi.org/10.1038/s41563-018-0268-1.

[101] D.D.L. Chung, Piezoresistive cement-based materials for strain sensing, J. Intell. Mater. Syst. Struct. 13 (9) (2021) 599–609. Available from: https://journals.sagepub.com/doi/abs/10.1106/104538902031861.

[102] B. Han, S. Ding, X. Yu, Intrinsic self-sensing concrete and structures: a review, Measure. J. Int. Measure.Confed. (2015) 110–128.

[103] E. Ricohermoso, F. Rosenburg, F. Klug, N. Nicoloso, H.F. Schlaak, R. Riedel, et al., Piezoresistive carbon-containing ceramic nanocomposites – a review, Open Ceram. 5 (2021), 100057.

[104] Q. Wen, Z. Yu, R. Riedel, The fate and role of in situ formed carbon in polymer-derived ceramics, in: Progress in Materials Science, Vol. 109, Elsevier Ltd, 2020.

[105] G. Mera, M. Gallei, S. Bernard, E. Ionescu, Ceramic nanocomposites from tailor-made preceramic polymers, Nanomaterials 5 (2) (2021) 468–540. ⟨www.mdpi.com/journal/nanomaterials⟩.

[106] G. Mera , Ionescu E. Silicon-Containing Preceramic Polymers. In: Encyclopedia of Polymer Science and Technology [Internet]. John Wiley & Sons, Inc.; 2013 [cited 2021 Jun 26]. Available from: ⟨https://onlinelibrary.wiley.com/doi/full/10.1002/0471440264.pst591⟩.

[107] R. Riedel, G. Mera, R. Hauser, A. Klonczynski, Silicon-based polymer-derived ceramics: Synthesis properties and applications-a review, J. Ceram. Soc. Jpn. Ceram. Soc. Jpn. (2021) 425–444. ⟨www.colorado.edu⟩.

[108] P. Colombo, G. Mera, R. Riedel, G.D. Sorarù, Polymer-derived ceramics: 40 Years of research and innovation in advanced ceramics, J. Am. Ceram. Soc. 93 (7) (2010) 1805–1837.

[109] C. Stabler, E. Ionescu, M. Graczyk-Zajac, I. Gonzalo-Juan, R. Riedel, Silicon oxycarbide glasses and glass-ceramics: "All-Rounder" materials for advanced structural and functional applications, J. Am. Ceram. Soc. (2021) 4817–4856. ⟨https://ceramics.onlinelibrary.wiley.com/doi/full/10.1111/jace.15932⟩.

[110] E. Ionescu, S. Bernard, R. Lucas, P. Kroll, S. Ushakov, A. Navrotsky, et al., Polymer-derived ultra-high temperature ceramics (UHTCs) and related materials, in: Advanced Engineering Materials, vol. 21, Wiley-VCH Verlag, 2019, https://doi.org/10.1002/adem.201900269.

[111] Encyclopedia of Inorganic and Bioinorganic Chemistry. Encyclopedia of Inorganic and Bioinorganic Chemistry. Wiley; 2011.

[112] L. Zhang, Y. Wang, Y. Wei, W. Xu, D. Fang, L. Zhai, et al., A silicon carbonitride ceramic with anomalously high piezoresistivity, J. Am. Ceram. Soc. (2021) 1346–1349. ⟨https://ceramics.onlinelibrary.wiley.com/doi/full/10.1111/j.1551-2916.2008.02275.x⟩.

[113] R. Riedel, L. Toma, E. Janssen, J. Nuffer, T. Melz, H. Hanselka, Piezoresistive effect in SiOC ceramics for integrated pressure sensors, J. Am. Ceram. Soc. (2021) 920–924. ⟨https://ceramics.onlinelibrary.wiley.com/doi/full/10.1111/j.1551-2916.2009.03496.x⟩.

[114] Y. Wang, L. Zhang, Y. Fan, D. Jiang, L. An, Stress-dependent piezoresistivity of tunneling-percolation systems, J. Mater. Sci. (2021) 2814–2819. ⟨https://link.springer.com/article/10.1007/s10853-009-3371-5⟩.

[115] K. Terauds, P.E. Sanchez-Jimenez, R. Raj, C. Vakifahmetoglu, P. Colombo, Giant piezoresistivity of polymer-derived ceramics at high temperatures, J. Eur. Ceram. Soc. 30 (11) (2010) 2203–2207.

[116] F. Roth, C. Schmerbauch, E. Ionescu, N. Nicoloso, O. Guillon, R. Riedel, High-temperature piezoresistive C / SiOC sensors, J. Sens. Sens Syst. 4 (1) (2015 31) 133–136.

[117] G. Shao, J. Jiang, M. Jiang, J. Su, W. Liu, H. Wang, et al., Polymer-derived SiBCN ceramic pressure sensor with excellent sensing performance (Available from), J. Adv. Ceram. 2020 (3) (2021) 374–379, https://doi.org/10.1007/s40145-020-0377-6.

[118] Y. Cao , X. Yang , R. Zhao , Y. Chen , N. Li , L. An , Giant piezoresistivity in polymer-derived amorphous SiAlCO ceramics. Vol. 51, Journal of Materials Science.

[119] C. Wang , W. Ping , Q. Bai , H. Cui , R. Hensleigh , R. Wang et al. , A general method to synthesize and sinter bulk ceramics in seconds. Science (80-) [Internet]. 2020 May 1 [cited 2021 Jun 30];368(6490):521–6. Available from: ⟨http://science.sciencemag.org/⟩.

[120] Z.C. Eckel , C. Zhou , J.H. Martin , A.J. Jacobsen , Carter WB , Schaedler TA. Additive manufacturing of polymer-derived ceramics. Science (80-) [Internet]. 2016 Jan 1 [cited 2021 Jun 30];351(6268):58–62. Available from: ⟨http://science.sciencemag.org/⟩.

[121] Y. de Hazan, D.Si.C. Penner, and SiOC ceramic articles produced by stereolithography of acrylate modified polycarbosilane systems, J. Eur. Ceram. Soc. 37 (16) (2017) 5205–5212.

[122] G. Pierin, C. Grotta, P. Colombo, C. Mattevi, Direct ink writing of micrometric SiOC ceramic structures using a preceramic polymer, J. Eur. Ceram. Soc. 36 (7) (2016) 1589–1594.

[123] E. Zanchetta, M. Cattaldo, G. Franchin, M. Schwentenwein, J. Homa, G. Brusatin, et al., Stereolithography of SiOC ceramic microcomponents, Adv. Mater. (2020) 370–376. ⟨https://onlinelibrary.wiley.com/doi/full/10.1002/adma.201503470⟩.

[124] F. Yin , D. Ye , C. Zhu , L. Qiu , YA. Huang , Stretchable, highly durable ternary nanocomposite strain sensor for structural health monitoring of flexible aircraft. Sensors (Switzerland) [Internet]. 2017 Nov 20 [cited 2021 Jun 30];17(11):2677. Available from: ⟨www.mdpi.com/journal/sensors⟩.

[125] B. Stark , B. Stevenson , K. Stow-Parker , Y. Chen , Embedded sensors for the health monitoring of 3D printed unmanned aerial systems 2014 International Conference on Unmanned Aircraft Systems, ICUAS 2014 - Conference Proceedings 2014 IEEE Computer Society, 175 180.

[126] L.A. Hockaday, K.H. Kang, N.W. Colangelo, P.Y.C. Cheung, B. Duan, E. Malone, et al., Rapid 3D printing of anatomically accurate and mechanically heterogeneous aortic valve hydrogel scaffolds, Biofabrication 4 (3) (2021), 035005 (Available from), ⟨https://iopscience.iop.org/article/10.1088/1758-5082/4/3/035005⟩.

[127] A. Dijkshoorn, P. Werkman, M. Welleweerd, G. Wolterink, B. Eijking, J. Delamare, et al., Embedded sensing: integrating sensors in 3-D printed structures, J. Sens. Sens. Syst. 7 (1) (2018) 169–181.

[128] Y. Wang, E.L. Runnerstrom, D.J. Milliron, Switchable materials for smart windows, Annu Rev. Chem. Biomol. Eng. 7 (2016) 283–304.

[129] C.G. Granqvist, M.A. Arvizu, Pehlivan Bayrak, H.Y. Qu, R.T. Wen, G.A. Niklasson, Electrochromic materials and devices for energy efficiency and human comfort in buildings: a critical review, Electro Acta 259 (2018) 1170–1182.

[130] D. Kim , Y. Choi , Applications of Smart Glasses in Applied Sciences: A Systematic Review. Appl Sci 2021, Vol 11, Page 4956 [Internet]. 2021 May 27 [cited 2021 Sep 13];11(11):4956. Available from: ⟨https://www.mdpi.com/2076–3417/11/11/4956/htm⟩.

[131] M.A.C. Stuart, W.T.S. Huck, J. Genzer, M. Müller, C. Ober, M. Stamm, et al., Emerging applications of stimuli-responsive polymer materials, Nat. Mater. 9 (2) (2021) 101–113 (Available from), ⟨https://www.nature.com/articles/nmat2614⟩.

[132] C.G. Granqvist, P.C. Lansåker, N.R. Mlyuka, G.A. Niklasson, E. Avendaño, Progress in chromogenics: new results for electrochromic and thermochromic materials and devices, Sol. Energy Mater. Sol. Cells 93 (12) (2009 1) 2032–2039.

[133] B.P.V. Heiz, L. Su, Z. Pan, L. Wondraczek, Fluid-integrated glass–glass laminate for sustainable hydronic cooling and indoor air conditioning, Adv. Sustain. Syst. (2021). ⟨https://onlinelibrary.wiley.com/doi/full/10.1002/adsu.201800047⟩.

[134] L. Su, M. Fraaß, L. Wondraczek, Design guidelines for thermal comfort and energy consumption of triple glazed fluidic windows on building level, Adv. Sustain. Syst. (2021). ⟨https://onlinelibrary.wiley.com/doi/full/10.1002/adsu.202000194⟩.

[135] M. Wuttig, N. Yamada, Phase-change materials for rewriteable data storage, Nat. Mater. 6 (11) (2021) 824–832 (Available from), ⟨https://www.nature.com/articles/nmat2009⟩.

[136] C. Calahoo, L. Wondraczek, Ion. Glass.: Struct., Prop. Classif. J. Non-Cryst. Solids X 8 (2020), 100054.

[137] T.D. Bennett , S. Horike , Liquid, glass and amorphous solid states of coordination polymers and metal–organic frameworks. Nat Rev Mater 2018 311 [Internet]. 2018 Sep 7 [cited 2021 Sep 13];3(11):431–40. Available from: ⟨https://www.nature.com/articles/s41578–018-0054–3⟩.

[138] L. Longley, C. Calahoo , R. Limbach , Y. Xia , J.M. Tuffnell , A.F. Sapnik , et al. , Metal-organic framework and inorganic glass composites. Nat Commun 2020 111 [Internet]. 2020 Nov 16 [cited 2021 Sep 13];11(1):1–12. Available from: ⟨https://www.nature.com/articles/s41467–020-19598–9⟩.

[139] V. Nozari, C. Calahoo, J.M. Tuffnell, D.A. Keen, T. Bennett, L. Wondraczek, Ionic liquid facilitated melting of the metal-organic framework ZIF-8, Nat. Commun. 12 (5703) (2021).

[140] B.P.V.Heiz , Z. Pan , G. Lautenschläger , C. Sirtl , M. Kraus , L. Wondraczek , Ultrathin Fluidic Laminates for Large-Area Façade Integration and Smart

Windows. Adv Sci [Internet]. 2017 Mar 1 [cited 2021 Sep 13];4(3):1600362. Available from: ⟨https://onlinelibrary.wiley.com/doi/full/10.1002/advs.201600362⟩.
[141] M. Casini, Active dynamic windows for buildings: a review, Renew. Energy 119 (2018) 923–934.
[142] L. Wondraczek , G. Pohnert , F.H. Schacher , A. Köhler , M. Gottschaldt , U.S. Schubert , et al. , Artificial Microbial Arenas: Materials for Observing and Manipulating Microbial Consortia. Adv Mater [Internet]. 2019 Jun 1 [cited 2021 Sep 13];31(24):1900284. Available from: ⟨https://onlinelibrary.wiley.com/doi/full/10.1002/adma.201900284⟩.
[143] J. Deubener, M. Allix, M.J. Davis, A. Duran, T. Höche, T. Honma, et al., Updated definition of glass-ceramics, J. Non Cryst. Solids 501 (2018) 3–10.
[144] L. Wondraczek , J. C Mauro , J. Eckert , U. Kühn , J. Horbach , J. Deubener , et al. Towards Ultrastrong Glasses. Adv Mater [Internet]. 2011 Oct 18 [cited 2021 Sep 13];23(39):4578–86. Available from: https://onlinelibrary.wiley.com/doi/full/10.1002/adma.201102795.
[145] P. Russell , PHOTONIC CRYSTAL FIBRES. Opt Fiber Commun Conf Natl Fiber Opt Eng Conf (2009), Pap OTuC1 [Internet]. 2009 Mar 22 [cited 2021 Sep 13]; OTuC1. Available from: ⟨https://www.osapublishing.org/abstract.cfm?uri=OFC-2009-OTuC1⟩.
[146] S. Garner , S. Glaesemann , X. Li , Ultra-slim flexible glass for roll-to-roll electronic device fabrication. Appl Phys A 2014 1162 [Internet]. 2014 May 15 [cited 2021 Sep 13];116(2):403–7. Available from: ⟨https://link.springer.com/article/10.1007/s00339–014-8468–2⟩.
[147] Gal-Or Eran , Yaniv Gershoni , E. Gianmario Scotti , SM Nilsson , Jukka Saarinen , Ville Jokinen , et al. Chemical analysis using 3D printed glass microfluidics. Anal Methods [Internet]. 2019 Mar 28 [cited 2021 Sep 13];11(13):1802–10. Available from: ⟨https://pubs.rsc.org/en/content/articlehtml/2019/ay/c8ay01934g⟩.
[148] K. Sasan , A. Lange , T.D. Yee , N. Dudukovic , D.T. Nguyen , M.A. Johnson , et al. , Additive Manufacturing of Optical Quality Germania–Silica Glasses. ACS Appl Mater Interfaces [Internet]. 2020 Feb 5 [cited 2021 Sep 13];12(5):6736–41. Available from: ⟨https://pubs.acs.org/doi/abs/10.1021/acsami.9b21136⟩.
[149] D. Zhang , X. Liu , J. Qiu , 3D printing of glass by additive manufacturing techniques: a review. Front Optoelectron 2020 [Internet]. 2020 Jul 10 [cited 2021 Sep 13];1–15. Available from: ⟨https://link.springer.com/article/10.1007/s12200–020-1009-z⟩.
[150] A. Camposeo , L. Persano , M. Farsari , D. Pisignano , Additive Manufacturing: Applications and Directions in Photonics and Optoelectronics. Adv Opt Mater [Internet]. 2019 Jan 1 [cited 2021 Sep 13];7(1):1800419. Available from: ⟨https://onlinelibrary.wiley.com/doi/full/10.1002/adom.201800419⟩.
[151] J. Klein, M. Stern, G. Franchin, M. Kayser, C. Inamura, S. Dave, et al., Additive manufacturing of optically transparent glass, 3D Print. Addit. Manuf. 2 (3) (2015) 92–105.
[152] M. Bechthold , J.C. Weaver , Materials science and architecture. Nat Rev Mater 2017 212 [Internet]. 2017 Dec 5 [cited 2021 Sep 13];2(12):1–19. Available from: ⟨https://www.nature.com/articles/natrevmats201782⟩.
[153] F. Oikonomopoulou , T. Bristogianni , F.A. Veer , R. Nijsse , The construction of the Crystal Houses façade: challenges and innovations. Glas Struct Eng 2017 31 [Internet]. 2017 Apr 11 [cited 2021 Sep 13];3(1):87–108. Available from: ⟨https://link.springer.com/article/10.1007/s40940–017-0039–4⟩.
[154] A. Zocca, C.M. Gomes, E. Bernardo, R. Müller, J. Günster, P. Colombo, LAS glass–ceramic scaffolds by three-dimensional printing, J. Eur. Ceram. Soc. 33 (9) (2013) 1525–1533.
[155] A. Winkel , R. Meszaros , S. Reinsch , R. Müller , N. Travitzky , T. Fey , et al. , Sintering of 3D-Printed Glass/HAp Composites. J Am Ceram Soc [Internet]. 2012 Nov 1 [cited 2021 Sep 13];95(11):3387–93. Available from: ⟨https://onlinelibrary.wiley.com/doi/full/10.1111/j.1551–2916.2012.05368.x⟩.
[156] A. Dasan , P. Ożóg ,J. Kraxner , H. Elsayed , Materials EC-, 2021 undefined. Up-Cycling of LCD Glass by Additive Manufacturing of Porous Translucent Glass Scaffolds. mdpi.com [Internet]. [cited 2021 Sep 17]; Available from: ⟨https://www.mdpi.com/1996–1944/14/17/5083⟩.
[157] F. Kotz , A.S. Quick , P. Risch , T. Martin , T. Hoose , M. Thiel , et al. , Two-Photon Polymerization of Nanocomposites for the Fabrication of Transparent Fused Silica Glass Microstructures. Adv Mater [Internet]. 2021 Mar 1 [cited 2021 Sep 17];33(9):2006341. Available from: ⟨https://onlinelibrary.wiley.com/doi/full/10.1002/adma.202006341⟩.
[158] E. Baudet , P. Larochelle , S. Morency , Y. Ledemi , Y. Messaddeq , 3D-printing of arsenic sulfide chalcogenide glasses. Opt Mater Express, Vol 9, Issue 5, pp 2307–2317 [Internet]. 2019 May 1 [cited 2021 Sep 17];9(5):2307–17. Available from: ⟨https://www.osapublishing.org/viewmedia.cfm?uri=ome-9–5-2307&seq=0&html=true⟩.
[159] L. Wondraczek, E. Bouchbinder, A. Ehrlicher, J.C. Mauro, R. Sajzew, M. M. Smedskjaer, Advancing the mechanical performance of glasses: perspectives and challenges, Adv. Mater. (2021), 2109029.
[160] J.-P. Fleurial, Thermoelectric power generation materials: technology and application opportunities, JOM 61 (4) (2009) 79–85.
[161] J.P. Fleurial , T. Caillat , B.J. Nesmith , R.C. Ewell , D.F. Woerner , G.C.Carr , et al. Thermoelectrics: From Space Power Systems to Terrestrial Waste Heat Recovery Applications. In: 2nd Thermoelectrics Applications Workshop. San Diego, CA; 2011.
[162] D. Champier, Thermoelectric generators: a review of applications, in: Energy Conversion and Management, vol. 140, Elsevier Ltd, 2017, pp. 167–181.
[163] S. LeBlanc, Thermoelectric generators: Linking material properties and systems engineering for waste heat recovery applications, Sustain Mater. Technol. 1–2 (2014) 26–35.
[164] D. Ebling, K. Bartholomé, M. Bartel, M. Jägle, Module geometry and contact resistance of thermoelectric generators analyzed by multiphysics simulation, J. Electron Mater. 39 (9) (2010) 1376–1380.
[165] S.K. Yee, S. LeBlanc, K.E. Goodson, C. Dames, $ per W metrics for thermoelectric power generation: beyond ZT, Energy Environ. Sci. (2013).
[166] F. Kim, B. Kwon, Y. Eom, J.E. Lee, S. Park, S. Jo, et al., 3D printing of shape-conformable thermoelectric materials using all-inorganic Bi2Te3-based inks, Nat. Energy 3 (4) (2018) 301–309.
[167] C. Oztan, S. Ballikaya, U. Ozgun, R. Karkkainen, E. Celik, Additive manufacturing of thermoelectric materials via fused filament fabrication, Appl. Mater. Today 15 (2019) 77–82.
[168] T.M. Tritt, Thermoelectric phenomena, materials, and applications, Annu Rev. Mater. Res 41 (1) (2011) 433–448.
[169] J.R. Sootsman, D.Y. Chung, M.G. Kanatzidis, New and old concepts in thermoelectric materials, Angew. Chem. Int Ed. Engl. 48 (46) (2009) 8616–8639.
[170] Crane D. , Gentherm . Thermoelectric waste heat recovery program for passenger vehicles. In: US Department of Energy Annual Merit Review. U.S. Department of Energy; 2013.
[171] A. Schmitz, C. Stiewe, E. Müller, Preparation of ring-shaped thermoelectric legs from pbte powders for tubular thermoelectric modules, J. Electron Mater. 42 (7) (2013) 1702–1706.
[172] A.Z. Sahin, B.S. Yilbas, The thermoelement as thermoelectric power generator: effect of leg geometry on the efficiency and power generation, Energy Convers. Manag 65 (2013) 26–32.
[173] Y. Thimont, S. Leblanc, The impact of thermoelectric leg geometries on thermal resistance and power output, J. Appl. Phys. 126 (9) (2019).
[174] B. Şişik, S. LeBlanc, The influence of leg shape on thermoelectric performance under constant temperature and heat flux boundary conditions, Front Mater. 7 (2020) 389.
[175] J.H. Bahk, H. Fang, K. Yazawa, A. Shakouri, Flexible thermoelectric materials and device optimization for wearable energy harvesting, J. Mater. Chem. C. R. Soc. Chem. 3 (2015) 10362–10374.
[176] Y. Du, J. Xu, B. Paul, P. Eklund, Flexible thermoelectric materials and devices, Appl. Mater. Today (2018) 366–388.
[177] M. Orrill, S. LeBlanc, Printed thermoelectric materials and devices: fabrication techniques, advantages, and challenges, J. Appl. Polym. Sci. 134 (3) (2017).
[178] A. El-Desouky, M. Carter, A. MAMA, B. PMPM, S. LeBlanc, Rapid processing and assembly of semiconductor thermoelectric materials for energy conversion devices, Mater. Lett. (2016) 185.
[179] M. He, Y. Zhao, B. Wang, Q. Xi, J. Zhou, Z. Liang, 3D printing fabrication of amorphous thermoelectric materials with ultralow thermal conductivity, Small 11 (44) (2015) 5889–5894.
[180] J. Qiu, Y. Yan, T. Luo, K. Tang, L. Yao, J. Zhang, et al., 3D Printing of highly textured bulk thermoelectric materials: Mechanically robust BiSbTe alloys with superior performance, Energy Environ. Sci. 12 (10) (2019) 3106–3117.
[181] K. Wu, Y. Yan, J. Zhang, Y. Mao, H. Xie, J. Yang, et al., Preparation of n-type Bi_2Te_3 thermoelectric materials by non-contact dispenser printing combined with selective laser melting, Phys. Status Solidi Rapid Res. Lett. 11 (6) (2017), 1700067.
[182] A. El-Desouky, M. Carter, M. Mahmoudi, A. Elwany, S. LeBlanc, Influences of energy density on microstructure and consolidation of selective laser melted bismuth telluride thermoelectric powder, J. Manuf. Process 25 (2017) 411–417.
[183] M.J. Carter, A. El-Desouky, M.A. Andre, P. Bardet, S. LeBlanc, Pulsed laser melting of bismuth telluride thermoelectric materials, J. Manuf. Process (2019) 43.
[184] H. Zhang, D. Hobbis, G.S. Nolas, S. LeBlanc, Laser additive manufacturing of powdered bismuth telluride, J. Mater. Res 33 (23) (2018) 4031–4039.
[185] Y. Yan, H. Ke, J. Yang, C. Uher, X. Tang, Fabrication and thermoelectric properties of n-Type $CoSb_{2.85}$ $Te_{0.15}$ using selective laser melting, ACS Appl. Mater. Interfaces 10 (16) (2018) 13669–13674.
[186] Y. Yan, W. Geng, J. Qiu, H. Ke, C. Luo, J. Yang, et al., Thermoelectric properties of n-type ZrNiSn prepared by rapid non-equilibrium laser processing, RSC Adv. 8 (28) (2018) 15796–15803.
[187] Y. Thimont, L. Presmanes, V. Baylac, P. Tailhades, D. Berthebaud, F. Gascoin, Thermoelectric higher manganese silicide: synthetized, sintered and shaped simultaneously by selective laser sintering/Melting additive manufacturing technique, Mater. Lett. 214 (2018) 236–239.
[188] J.M. Houston, Theoretical efficiency of the thermionic energy converter (Available from), J. Appl. Phys. 30 (4) (2021) 481–487, https://doi.org/10.1063/1.1702392.
[189] M.F. Campbell, T.J. Celenza, F. Schmitt, J.W. Schwede, I. Bargatin, Progress toward high power output in thermionic energy converters, Adv. Sci. (2021), https://doi.org/10.1002/advs.202003812.
[190] J.E. Beggs, Vacuum thermionic energy converter, Adv. Energy Convers. 3 (2) (1963) 447–453.
[191] G.N. Hatsopoulos , E.P. Gyftopoulos . Thermionic EnergyConversion: Processes and Devices. Cambridge; 1973.
[192] T.E. Humphrey, M.F. O'Dwyer, H. Linke, Power optimization in thermionic devices, J. Phys. D. Appl. Phys. [Internet]. 2005 Jun. 21 [cited 38 (12) (2021 29) 2051–2054 (Available from), ⟨https://iopscience.iop.org/article/10.1088/0022-3727/38/12/029⟩.
[193] K.A.A. Khalid, T.J. Leong, K. Mohamed, Review on thermionic energy converters, IEEE Trans. Electron Devices 63 (6) (2016) 2231–2241.
[194] J.H. Chung, J.H. Ryu, J.W. Eun, B.G. Choi, K.B. Shim, One-step synthesis of a 12CaO·7Al 2O 3 electride via the spark plasma sintering (SPS) method,

Electrochem Solid-State Lett. 14 (12) (2021), E41 (Available from), ⟨https://iopscience.iop.org/article/10.1149/2.021112esl⟩.
[195] X. Tang, A.E. Kuehster, B.A. DeBoer, A.D. Preston, K. Ma, Enhanced thermionic emission of mayenite electride composites in an Ar glow discharge plasma, Ceram. Int 47 (12) (2021) 16614–16631.
[196] W.B. Nottingham, Thermionic emission from tungsten and thoriated tungsten filaments, Phys. Rev. 49 (1) (2021) 78–97 (Available from), ⟨https://journals.aps.org/pr/abstract/10.1103/PhysRev.49.78⟩.
[197] D.B. King , The microminiature thermionic converter AIP Conference Proceedings [Internet] 2003 AIP Publishing, 1152 1157 doi: 10.1063/1.1358065.
[198] D.M. Kirkwood, S.J. Gross, T.J. Balk, M.J. Beck, J. Booske, D. Busbaher, et al., Frontiers in thermionic cathode research, IEEE Trans. Electron Devices 65 (6) (2018) 2061–2071.
[199] R.Y. Belbachir, Z. An, T. Ono, Thermal investigation of a micro-gap thermionic power generator, J. Micromech. Microeng. 24 (8) (2021), 085009 (Available from), ⟨https://iopscience.iop.org/article/10.1088/0960-1317/24/8/085009⟩.
[200] J.H. Lee , I. Bargatin , J. Provine ,F. Liu , M.K. Seo , R. Maboudian , et al. , Effect of illlumination on thermionic emission from microfabricated silicon carbide structures. In: 2011 16th International Solid-State Sensors, Actuators and Microsystems Conference, TRANSDUCERS'11. 2011. p. 2658–61.
[201] C.L. Cramer , H. Armstrong , A. Flores-Betancourt , L. Han , A.M. Elliott , E. Lara-Curzio , et al. , Processing and properties of SiC composites made via binder jet 3D printing and infiltration and pyrolysis of preceramic polymer. Int J Ceram Eng Sci [Internet]. 2020 Nov 27 [cited 2021 Feb 4];2(6):320–31. Available from: ⟨https://onlinelibrary.wiley.com/doi/10.1002/ces2.10070⟩.
[202] K. Terrani , B. Jolly , M. Trammell , 3D printing of high-purity silicon carbide. J Am Ceram Soc [Internet]. 2020 Mar 19 [cited 2020 Apr 3];103(3):1575–81. Available from: ⟨https://onlinelibrary.wiley.com/doi/abs/10.1111/jace.16888⟩.
[203] C.L. Cramer , A.M. Elliott , E. Lara-Curzio , A. Flores-Betancourt , M.J. Lance , L. Han , et al. , Properties of SiC-Si made via binder jet 3D printing of SiC powder, carbon addition, and silicon melt infiltration. J Am Ceram Soc. 2021;.
[204] E. Rephaeli ,S. Fan , Absorber and emitter for solar thermo-photovoltaic systems to achieve efficiency exceeding the Shockley-Queisser limit. Opt Express [Internet]. 2009 Aug 17 [cited 2021 Jun 29];17(17):15145. Available from: ⟨https://www.osapublishing.org/viewmedia.cfm?uri=oe-17-17-15145&seq=0&html=true⟩.
[205] M.D. Campanell , G.R. Johnson , Thermionic Cooling of the Target Plasma to a Sub-eV Temperature. Phys Rev Lett [Internet]. 2019 Jan 10 [cited 2021 Jun 29];122(1):015003. Available from: ⟨https://journals.aps.org/prl/abstract/10.1103/PhysRevLett.122.015003⟩.
[206] L.A. Uribarri , E.H. Allen , Electron transpiration cooling for hot aerospace surfaces. In: 20th AIAA International Space Planes and Hypersonic Systems and Technologies Conference, 2015 [Internet]. AIAA American Institute of Aeronautics and Astronautics; 2015 [cited 2021 Jun 29]. Available from: ⟨https://arc.aiaa.org/doi/abs/10.2514/6.2015–3674⟩.
[207] Emission Standards: USA: Cars and Light-Duty Trucks—Tier 1.
[208] R.M. Heck , R. J. Farrauto , S.T. Gulati , Catalytic Air Pollution Control: Commercial Technology: Third Edition. Catal Air Pollut Control Commer Technol Third Ed. 2012 Apr 11;.
[209] M. Masoudi, N.C. Felix, A Novel honeycomb for both downsizing and significant PGM Saving, Platin. Met. Rev. 6th Int. Conf. Environ. Catal. (2011) 170–174.
[210] R.D. Bagley, Honeycombed structures having open-ended cells formed by interconnected walls with longitudinally extending discontinuities, Google Patents US Pat. 3 (983) (1976) 283.
[211] Mansour Masoudi, Catalytic converters having non-linear flow channels, US Pat. (2016), 10815856B2.
[212] W. Chaikittisilp, H.-J. Kim, C.W. Jones, Mesoporous alumina-supported amines as potential steam-stable adsorbents for capturing CO_2 from simulated flue gas and ambient air, Energy Fuels 25 (11) (2011 17) 5528–5537.
[213] National Academy of Science E and M Negative emissions technologies and reliable sequestration: A research agenda. 2019.
[214] M.J. Regufe, A.F.P. Ferreira, J.M. Loureiro, A. Rodrigues, A.M. Ribeiro, Electrical conductive 3D-printed monolith adsorbent for CO_2 capture, Microporous Mesoporous Mater. 278 (2019) 403–413.
[215] S. Couck, J. Lefevere, S. Mullens, L. Protasova, V. Meynen, G. Desmet, et al., CO_2, CH4 and N2 separation with a 3DFD-printed ZSM-5 monolith, Chem. Eng. J. 308 (2017) 719–726.
[216] H. Thakkar, S. Lawson, A.A. Rownaghi, F. Rezaei, Development of 3D-printed polymer-zeolite composite monoliths for gas separation, Chem. Eng. J. 348 (2018) 109–116.
[217] J.H.L. Voncken, Recovery of Ce and La from spent automotive catalytic converters. Critical and Rare Earth Elements, CRC Press, 2019.
[218] M. Masoudi, E.Novel Tegeler, Smaller contactor for markedly reducing the total cost of the direct air capture of CO2, Mater. Res. Soc. Fall Meet. (2021).
[219] M. Moran, Fundamentals of engineering thermodynamics, fourth ed., Wiley, New York, 2000.
[220] BG. Miller , Clean Coal Engineering Technology [Internet]. 2017 [cited 2020 Oct 20]. 261–308 p. Available from: www.elsevier.com/permissions.
[221] B.M. Kumfer , S.A. Skeen , R. Chen , R.L. Axelbaum , Measurement and analysis of soot inception limits of oxygen-enriched coflow flames. Combust Flame [Internet]. 2006 [cited 2020 Oct 20];147:233–42. Available from: ⟨http://www.elsevier.com/locate/permissionusematerialwww.elsevier.com/locate/combustflame⟩.
[222] Science PS-T. , 2020 undefined. Scientific activity of Prof. Naim Afgan at Laboratory for Thermal Engineering and Energy, Institute for Nuclear Sciences-Vinča [Internet]. doiserbia.nb.rs. [cited 2020 Oct 20]. Available from: ⟨http://www.doiserbia.nb.rs/ft.aspx?id=0354–983620002655S⟩.
[223] L.M. Crosbie , D. Chapin Hydrogen Production by Nuclear Heat.
[224] L. Magistri , A. Traverso , A.F. Massardo , R.K. Shah , Heat exchangers for fuel cell and hybrid system applications. In: Proceedings of the 3rd International Conference on Fuel Cell Science, Engineering, and Technology, 2005. American Society of Mechanical Engineers; 2005. p. 359–66.
[225] GO Musgrove , J. Nash , R. Le Pierres , C. Pittaway , D. Shiferaw , S. Sullivan , et al. , Heat Exchangers for Supercritical CO2 Power Cycle Applications Tutorial: Slides and material composed by [Internet]. sco2symposium.com. 2014 [cited 2020 Oct 20]. Available from: ⟨http://sco2symposium.com/papers2014/tutorials/musgrove.pdf⟩.
[226] H. Xu , S. Gong , L. Deng Preparation of thermal barrier coatings for gas turbine blades by EB-PVD. Thin Solid Films [Internet]. 1998 Dec 4 [cited 2019 Jan 26];334(1–2):98–102. Available from: ⟨https://www.sciencedirect.com/science/article/pii/S0040609098011249⟩.
[227] Padture NP , Gell M. , Jordan EH. Thermal barrier coatings for gas-turbine engine applications. Science [Internet]. 2002 Apr 12 [cited 2019 May 29];296(5566):280–4. Available from: ⟨http://www.ncbi.nlm.nih.gov/pubmed/11951028⟩.
[228] U. Scheithauer, E. Schwarzer, T. Moritz, A. Michaelis, Additive manufacturing of ceramic heat exchanger: opportunities and limits of the lithography-based ceramic manufacturing (LCM), J. Mater. Eng. Perform. 27 (1) (2018 1) 14–20.
[229] H. Shulman , N. Ross , Additive manufacturing for cost efficient production of compact ceramic heat exchangers and recuperators. 2015 [cited 2020 Jul 14]; Available from: ⟨https://www.osti.gov/biblio/1234436⟩.
[230] W. Sixel , M. Liu , G. Nellis , B. Sarlioglu , Ceramic 3D printed direct winding heat exchangers for improving electric machine thermal management 2019 IEEE Energy Convers. Congr. Expo., ECCE 2019. Inst. Electr. Electron. Eng. Inc. 2019 769 776.
[231] D. Singh, W. Yu, D.M. France, T.P. Allred, I.H. Liu, W. Du, et al., One piece ceramic heat exchanger for concentrating solar power electric plants, Renew. Energy 160 (2020) 1308–1315.
[232] M. Pelanconi, M. Barbato, S. Zavattoni, G.L. Vignoles, A. Ortona, Thermal design, optimization and additive manufacturing of ceramic regular structures to maximize the radiative heat transfer, Mater. Des. 163 (2019), 107539.
[233] M. Pelanconi , S. Zavattoni , L. Cornolti , R. Puragliesi , E. Arrivabeni , L. Ferrari , et al. Application of Ceramic Lattice Structures to Design Compact, High Temperature Heat Exchangers: Material and Architecture Selection. Materials (Basel) [Internet]. 2021 Jun 11 [cited 2021 Jun 23];14(12):3225. Available from: ⟨https://www.mdpi.com/1996–1944/14/12/3225⟩.
[234] S.J. Zinkle, G.S. Was, Materials challenges in nuclear energy, Acta Mater. 61 (3) (2013) 735–758.
[235] B.J. Ade, B.R. Betzler, A.J. Wysocki, M.S. Greenwood, P.C. Chesser, K.A. Terrani, et al., Candidate Core Designs for the Transformational Challenge Reactor (Available from), J. Nucl. Eng. 2 (1) (2021) 74–85, https://doi.org/10.3390/jne2010008.
[236] J. Arborelius, K. Backman, L. Hallstadius, M. Limbäck, J. Nilsson, B. Rebensdorff, et al., Advanced doped UO2 pellets in LWR applications, J. Nucl. Sci. Technol. 43 (9) (2021) 967–976 (Available from), ⟨https://www.tandfonline.com/action/journalInformation?journalCode=tnst20⟩.
[237] S.S. Mustafa, E.A. Amin, The effect of soluble boron and gadolinium distribution on neutronic parameters of small modular reactor assembly, Radiat. Phys. Chem. 171 (2020), 108724.
[238] G. Gündüz, I. Uslu, H.H. Durmazuçar, Boron-nitride-coated nuclear fuels (Available from), Nucl. Technol. 116 (1) (2021 22) 78–90, https://doi.org/10.13182/NT96-A35313.
[239] A.T. Nelson, P. Demkowicz, Other power reactor fuels. Advances in Nuclear Fuel Chemistry, Elsevier,, 2020, pp. 215–247.
[240] P.A. Demkowicz, B. Liu, J.D. Hunn, Coated particle fuel: historical perspectives and current progress, J. Nuclear Mater. (2019) 434–450.
[241] K.A. Terrani, L.L. Snead, J.C. Gehin, Microencapsulated fuel technology for commercial light water and advanced reactor application, J. Nucl. Mater. 427 (1–3) (2012) 209–224.
[242] K.A. Terrani, J.O. Kiggans, Y. Katoh, K. Shimoda, F.C. Montgomery, B. L. Armstrong, et al., Fabrication and characterization of fully ceramic microencapsulated fuels, J. Nucl. Mater. 426 (1–3) (2012) 268–276.
[243] K.A. Terrani, J.O. Kiggans, C.M. Silva, C. Shih, Y. Katoh, L.L. Snead, Progress on matrix SiC processing and properties for fully ceramic microencapsulated fuel form, J. Nucl. Mater. 457 (2015) 9–17.
[244] P.J. Pappano, T.D. Burchell, J.D. Hunn, M.P. Trammell, A novel approach to fabricating fuel compacts for the next generation nuclear plant (NGNP), J. Nucl. Mater. 381 (1–2) (2008) 25–38.
[245] R.N. Morris, P.J. Pappano, Estimation of maximum coated particle fuel compact packing fraction, J. Nucl. Mater. 361 (1) (2007) 18–29.
[246] S.J. Zinkle, K.A. Terrani, J.C. Gehin, L.J. Ott, L.L. Snead, Accident tolerant fuels for LWRs: a perspective, J. Nucl. Mater. 448 (1–3) (2014) 374–379.
[247] K.A. Terrani, Accident tolerant fuel cladding development: Promise, status, and challenges, J. Nuclear Mater. (2018) 13–30.
[248] E.J. Opila , R.E. Hann , Paralinear oxidation of CVD SiC in water vapor. J Am Ceram Soc [Internet]. 1997 Jan 1 [cited 2021 Jun 23];80(1):197–205. Available from: ⟨https://ceramics.onlinelibrary.wiley.com/doi/full/10.1111/j.1151–2916.1997.tb02810.x⟩.
[249] K. Shimoda, T. Hinoki, H. Kishimoto, A. Kohyama, Enchanced high-temperature performances of SiC/SiC composites by high densification and crystalline structure, Compos Sci. Technol. 71 (3) (2011) 326–332.

[250] W.J. Kim, D. Kim, J.Y. Park, Fabrication and material issues for the application of SiC composites to LWR fuel cladding, Nucl. Eng. Technol. 45 (4) (2013) 565–572.
[251] Y. Katoh , KA. Terrani , Systematic Technology Evaluation Program for SiC/SiC Composite-based Accident-Tolerant LWR Fuel Cladding and Core Structures: Revision 2015 [Internet]. info.ornl.gov. 2015 [cited 2021 Jun 23]. Available from: ⟨http://www.osti.gov/scitech/⟩.
[252] K. Yueh, K.A. Terrani, Silicon carbide composite for light water reactor fuel assembly applications, J. Nucl. Mater. 448 (1–3) (2014) 380–388.
[253] D.C. Crawford, D.L. Porter, S.L. Hayes, M.K. Meyer, D.A. Petti, K. Pasamehmetoglu, An approach to fuel development and qualification, J. Nucl. Mater. 371 (1–3) (2007) 232–242.
[254] C. Hensley, K. Sisco, S. Beauchamp, A. Godfrey, H. Rezayat, T. McFalls, et al., Qualification pathways for additively manufactured components for nuclear applications, J. Nucl. Mater. 548 (2021), 152846.
[255] K.A. Terrani, N.A. Capps, M.J. Kerr, C.A. Back, A.T. Nelson, B.D. Wirth, et al., Accelerating nuclear fuel development and qualification: Modeling and simulation integrated with separate-effects testing, J. Nucl. Mater. 539 (2020), 152267.
[256] A. Nelson , Features that further performance limits of nuclear fuel fabrication: opportunities for additive manufacturing of nuclear fuels. 2019 [cited 2021 Jun 23]; Available from: ⟨https://www.osti.gov/servlets/purl/1669784⟩.
[257] J.P. Gorton, D. Schappel, A.T. Nelson, N.R. Brown, Impact of uranium oxide (UO2) fuel with molybdenum (Mo) inserts on pressurized water reactor performance and safety, J. Nucl. Mater. 542 (2020), 152492.
[258] T. Koyanagi, K. Terrani, S. Harrison, J. Liu, Y. Katoh, Additive manufacturing of silicon carbide for nuclear applications, J. Nucl. Mater. 543 (2021), 152577.
[259] K.A. Terrani, B.C. Jolly, M.P. Trammell, G. Vasadevamurthy, D. Schappel, B. Ade, et al., Architecture and properties of TCR fuel form, J. Nucl. Mater. 547 (2021), 152781.
[260] C.M. Petrie, A.M. Schrell, D.N. Leonard, Y. Yang, B.C. Jolly, K.A. Terrani, Embedded sensors in additively manufactured silicon carbide, J. Nucl. Mater. 552 (2021), 153012.
[261] K.A. Terrani, T. Lach, H. Wang, Coq A Le, K. Linton, C. Petrie, Irradiation stability and thermomechanical properties of 3D-printed SiC, J. Nucl. Mater. 551 (2021 1), 152980.
[262] M.K. Meyer, R. Fielding, J. Gan, Fuel development for gas-cooled fast reactors, J. Nucl. Mater. 371 (1–3) (2007&;;) 281–287.
[263] Y. Long, A. Javed, J. Chen, Z.K. Chen, X. Xiong, Phase composition, microstructure and mechanical properties of ZrC coatings produced by chemical vapor deposition, Ceram. Int 40 (1 Part A) (2014) 707–713.
[264] T. Carter, A. Gleason, R. Maingi, E. Trask, S. Baalrud, C. Holland, et al. Powering the Future: Fusion & Plasmas.
[265] S.J. Zinkle, J.P. Blanchard, R.W. Callis, C.E. Kessel, R.J. Kurtz, P.J. Lee, et al., Fusion materials science and technology research opportunities now and during the ITER era, Fusion Eng. Des. 89 (7–8) (2014) 1579–1585.
[266] M.S. Tillack , S. Malang , High performance PbLi blanket Proceedings - Symposium on Fusion Engineering 1998 IEEE, 1000 1004.
[267] R.W. Conn, G.L. Kulcinski, C.W. Maynard, The UWMAK-II study: A conceptual design of a helium cooled, solid breeder, Tokamak fusion reactor system, Nucl. Eng. Des. 39 (1) (1976) 5–44.
[268] A.R. Raffray, L. El-Guebaly, S. Gordeev, S. Malang, E. Mogahed, F. Najmabadi, et al., High performance blanket for ARIES-AT power plant, Fusion Eng. Des. 58–59 (2001) 549–553.
[269] P. Norajitra, L. Bühler, U. Fischer, S. Malang, G. Reimann, H. Schnauder, The EU advanced dual coolant blanket concept, Fusion Eng. Des. 61–62 (2002 1) 449–453.
[270] X.R. Wang , M.S. Tillack , C. Koehly , S Malang. , H.H. Toudeshki , F. Najmabadi , ARIES-ACT1 system configuration, assembly, and maintenance. Fusion Sci Technol [Internet]. 2015 Jan 1 [cited 2021 Jun 24];67(1):22–48. Available from: ⟨https://www.tandfonline.com/action/journalInformation?journalCode=ufst20http://dx.doi.org/10.13182/FST14–797⟩.
[271] N.B. Morley, Y. Katoh, S. Malang, B.A. Pint, A.R. Raffray, S. Sharafat, et al., Recent research and development for the dual-coolant blanket concept in the US, Fusion Eng. Des. 83 (7–9) (2008) 920–927.
[272] S. Nishio, S. Ueda, I. Aoki, R. Kurihara, T. Kuroda, H. Miura, et al., Improved tokamak concept focusing on easy maintenance, Fusion Eng. Des. 41 (1–4) (1998) 357–364.
[273] D. Maisonnier, I. Cook, S. Pierre, B. Lorenzo, B. Edgar, B. Karin, et al., The European power plant conceptual study, Fusion Eng. Des. 75–79 (Suppl) (2005) 1173–1179.
[274] G. Casini, Thermal and structural design issues of breeding blankets for testing in the Next European Torus (NET), Fusion Eng. Des. 6 (C) (1988) 95–107.
[275] G. Zhou, F. Hernández, L.V. Boccaccini, H. Chen, M. Ye, Design study on the new EU DEMO HCPB breeding blanket: Thermal analysis, Prog. Nucl. Energy 98 (2017) 167–176.
[276] Y. Katoh , L.L Snead , I. Szlufarska , W.J. Weber , Radiation effects in SiC for nuclear structural applications. Curr Opin Solid State Mater Sci [Internet]. 2012 Jun 1 [cited 2018 May 21];16(3):143–52. Available from: ⟨https://orproxy.lib.utk.edu:2054/science/article/pii/S1359028612000095⟩.
[277] B.A. Pint , J.R. DiStefano , P.F. Tortorelli , High temperature compatibility issues for fusion reactor structural materials. Fusion Sci Technol [Internet]. 2003 [cited 2021 Jun 24];44(2):433–40. Available from: ⟨https://www.tandfonline.com/action/journalInformation?journalCode=ufst20⟩.
[278] Y. Katoh, K. Ozawa, C. Shih, T. Nozawa, R.J. Shinavski, A. Hasegawa, et al., Continuous SiC fiber, CVI SiC matrix composites for nuclear applications: properties and irradiation effects, J. Nucl. Mater. 448 (1–3) (2014) 448–476.
[279] S. Sharafat , A. Aoyama , N. Morley , S. Smolentsev , Y. Katoh , B. Williams , et al. , Development status of a sic-foam based flow channel insert for a U.S.-ITER DCLL tbm. In: Fusion Science and Technology [Internet]. American Nuclear Society; 2009 [cited 2021 Jun 24]. p. 883–91. Available from: ⟨https://www.tandfonline.com/action/journalInformation?journalCode=ufst20⟩.
[280] P. Norajitra , W.W. Basuki, M. Gonzalez, D. Rapisard , M. Rohde , L. Spatafora , Development of sandwich flow channel inserts for an EU demo dual coolant blanket concept. In: Fusion Science and Technology [Internet]. American Nuclear Society; 2015 [cited 2021 Jun 24]. p. 501–6. Available from: ⟨https://www.tandfonline.com/action/journalInformation?journalCode=ufst20⟩.
[281] R. Knitter, P. Chaudhuri, Y.J. Feng, T. Hoshino, I.K. Yu, Recent developments of solid breeder fabrication, J. Nucl. Mater. 442 (1–3) (2013) S420–S424.
[282] R. Naslain, Design, preparation and properties of non-oxide CMCs for application in engines and nuclear reactors: An overview, Compos Sci. Technol. 64 (2) (2004) 155–170.
[283] S. Smolentsev, C. Courtessole, M. Abdou, S. Sharafat, S. Sahu, T. Sketchley, Numerical modeling of first experiments on PbLi MHD flows in a rectangular duct with foam-based SiC flow channel insert, Fusion Eng. Des. 108 (2016 1) 7–20.
[284] O. Karakoc , K. Mao , J. Xi , T. Koyanagi , I. Szlufarska , Y. Katoh . Single-step additive manufacturing of silicon carbide through laser-induced phase separation. Prep.
[285] M. Singh , C. Michael Halbig , Joseph E. Grady , Additive Manufacturing of Light Weight Ceramic Matrix Composites For Gas Turbine Engine Applications. Ceram Eng Sci Proc [Internet]. 2015 Dec 25 [cited 2019 May 31];36(6):145–50. Available from: ⟨http://doi.wiley.com/10.1002/9781119211662.ch16⟩.
[286] S. Sharafat, B. Williams, N. Ghoniem, A. Ghoniem, M. Shimada, A. Ying, Development of a new cellular solid breeder for enhanced tritium production, Fusion Eng. Des. 109–111 (2016) 119–127.
[287] Y. Liu, Z. Chen, J. Li, B. Gong, L. Wang, C. Lao, et al., 3D printing of ceramic cellular structures for potential nuclear fusion application, Addit. Manuf. 35 (2020), 101348.
[288] JR. Nicholls , Advances in Coating Design for High-Performance Gas Turbines. MRS Bull [Internet]. 2003 [cited 2021 Aug 1];28(9):659–70. Available from: ⟨https://www.cambridge.org/core/journals/mrs-bulletin/article/abs/advances-in-coating-design-for-highperformance-gas-turbines/1814539F4759FAA5259F3981B4E9DFAF⟩.
[289] Superalloy GS-7th international symposium on, 2010 undefined. Casting superalloys for structural applications. tms.org [Internet]. [cited 2021 Aug 1]; Available from: ⟨https://www.tms.org/superalloys/10.7449/2010/Superalloys_2010_117_130.pdf⟩.
[290] Nader El-Bagoury , "Ni based superalloy: casting. - Google Scholar. El-Bagoury, Nader "Ni based superalloy Cast Technol metInternational J Eng Sci Res Technol 5, no 2 108–152 [Internet]. [cited 2021 Aug 1]; Available from: ⟨https://scholar.google.com/scholar?hl=en&as_sdt=0%2C43&q=El-Bagoury%2C+Nader.+%22Ni+based+superalloy%3A+casting+technology%2C+metallurgy%2C+development%2C+properties+and+applications.%22+International+Journal+of+Engineering+Sciences+%26+Research+Technology+5%2C+no.+2+%282016%29%3A+108–152.&btnG=⟩.
[291] R. Schafrik , R. Sprague , Superalloy Technology - A Perspective on Critical Innovations for Turbine Engines. Key Eng Mater [Internet]. 2008 Mar [cited 2021 Aug 1];380:113–34. Available from: ⟨https://www.scientific.net/KEM.380.113⟩.
[292] J.E. Kanyo, S. Schafföner, R.S. Uwanyuze, K.S. Leary, An overview of ceramic molds for investment casting of nickel superalloys, J. Eur. Ceram. Soc. 40 (15) (2020) 4955–4973.
[293] P.K. Wright, A.G. Evans, Mechanisms governing the performance of thermal barrier coatings, Curr. Opin. Solid State Mater. Sci. 4 (3) (1999 1) 255–265.
[294] M. Gromada , A. Wieca , M. Kostecki , A. Olszyna , R. Cygan , Ceramic cores for turbine blades via injection moulding. J Mater Process Technol. 2015 Jun 1;220:107–112.
[295] N.M. Angel , A. Basak , On the Fabrication of Metallic Single Crystal Turbine Blades with a Commentary on Repair via Additive Manufacturing. J Manuf Mater Process 2020, Vol 4, Page 101 [Internet]. 2020 Oct 26 [cited 2021 Aug 5];4(4):101. Available from: ⟨https://www.mdpi.com/2504–4494/4/4/101/htm⟩.
[296] C.J. Bae, D. Kim, J.W. Halloran, Mechanical and kinetic studies on the refractory fused silica of integrally cored ceramic mold fabricated by additive manufacturing, J. Eur. Ceram. Soc. 39 (2–3) (2019 1) 618–623.
[297] L.Y. Wang, M.H. Hon, The effect of cristobalite seed on the crystallization of fused silica based ceramic core — a kinetic study, Ceram. Int. 21 (3) (1995 1) 187–193.
[298] L.-Y. Wang, M.-H. Hon, The effects of zircon addition on the crystallization of fused silica a kinetic study, J. Ceram. Soc. Jpn. 102 (1186) (1994 1) 517–521.
[299] C.J. Bae , J.W. Halloran , Integrally Cored Ceramic Mold Fabricated by Ceramic Stereolithography. Int J Appl Ceram Technol [Internet]. 2011 Nov 1 [cited 2021 Aug 5];8(6):1255–62. Available from: ⟨https://ceramics.onlinelibrary.wiley.com/doi/full/10.1111/j.1744–7402.2010.02568.x⟩.
[300] P.J. Coty, A.D. Lane, J.B. Lee, L.J. Meyer, A Design Review of Ceramic Components for Turbine Engines, J. Eng. Power 102 (2) (1980 1) 437–447.
[301] H.T. Lin , M.K. Ferber, P.F. Becher , J.R. Price, M.Van Roode , J.B. Kimmel , et al. , Characterization of First-Stage Silicon Nitride Components After Exposure to an Industrial Gas Turbine. J Am Ceram Soc [Internet]. 2006 Jan 1 [cited 2021 Aug 5];89(1):258–65. Available from: ⟨https://ceramics.onlinelibrary.wiley.com/doi/full/10.1111/j.1551–2916.2005.00678.x⟩.
[302] M. Halbig , J. Grady , M. Singh , J. Ramsey , C. Patterson , A Fully Nonmetallic Gas Turbine Engine Enabled by Additive Manufacturing of Ceramic Composites. Part III; Additive Manufacturing and Characterization of Ceramic. 2015 [cited 2021 Aug 5]; Available from: ⟨https://ntrs.nasa.gov/search.jsp?R=20150023455⟩.

[303] J.E. Grady , W.J. Haller , P.E .Poinsatte , M.C. Halbig , S.L. Schnulo , M. Singh , et al. , A Fully Non-Metallic Gas Turbine Engine Enabled by Additive Manufacturing Part I: System Analysis, Component Identification, Additive Manufacturing, and Testing of Polymer Composites [Internet]. 2015 [cited 2021 Aug 5]. Available from: ⟨http://www.sti.nasa.gov⟩.
[304] T. Rosfjord , W. Tredway , A. Chen, J. Mulugeta, T. Bhatia , Advanced Microturbine Systems. 2008 Dec 31 [cited 2021 Aug 5]; Available from: ⟨http://www.osti.gov/servlets/purl/924484/⟩.
[305] Systems IE. DoE Advanced Ceramic Microturbine. 2004 May 31 [cited 2021 Aug 5]; Available from: ⟨https://digital.library.unt.edu/ark:/67531/metadc902171/⟩.
[306] M.K. Tran , A. Bhatti, R. Vrolyk , D. Wong, S. Panchal , M. Fowler, et al. , A Review of Range Extenders in Battery Electric Vehicles: Current Progress and Future Perspectives. World Electr Veh J 2021, Vol 12, Page 54 [Internet]. 2021 Apr 1 [cited 2021 Aug 5];12(2):54. Available from: ⟨https://www.mdpi.com/2032–6653/12/2/54/htm⟩.
[307] V. Sethi , MK El-hossani , EC Barbu , R. Petcu , V. Vilag , V. , SilivestruProgress in Gas Turbine Performance. 2013.
[308] E. Konečná , Engineering VM-C. , 2019. Review of Gas Microturbine Application in Industry. researchgate.net [Internet]. [cited 2021 Aug 5]; Available from: ⟨https://www.researchgate.net/profile/Eva-Konecna/publication/337631866_Review_of_Gas_Microturbine_Application_in_Industry/links/5e0db737299bf10bc389cf79/Review-of-Gas-Microturbine-Application-in-Industry.pdf⟩.
[309] N. Kochrad, N. Courtois , M. Charette ,B. Picard, A. Landry-Blais , D. Rancourt , et al. , System-Level Performance of Microturbines With an Inside-Out Ceramic Turbine. J Eng Gas Turbines Power [Internet]. 2017 Feb 1 [cited 2018 May 29];139(6):062702. Available from: ⟨http://gasturbinespower.asmedigitalcollection.asme.org/article.aspx?doi=10.1115/1.4035648⟩.
[310] GC DeBell , JR Secord , Development and Testing of a Ceramic Turbocharger Rotor. Proc ASME Turbo Expo [Internet]. 2015 Apr 15 [cited 2021 Aug 5];4. Available from: ⟨http://asmedigitalcollection.asme.org/GT/proceedings-pdf/GT1981/79641/V004T12A004/2393680/v004t12a004–81-gt-195.pdf⟩.
[311] T. Shimizu , K. Takama , H. Enokishima , K. Mikame , S. Tsuji, N. , Kamiya Silicon Nitride Turbocharger Rotor for High Performance Automotive Engines. SAE Tech Pap [Internet]. 1990 Feb 1 [cited 2021 Aug 5]; Available from: ⟨https://www.sae.org/publications/technical-papers/content/900656/⟩.
[312] K. Watanabe, T. Takahashi, T. Nagae, H. Tsuji, Precision forming and machining technologies for ceramic-based components, Int J. Autom. Technol. 12 (5) (2018) 739–749.
[313] T. Fukudome , S. Tsuruzono , T. Tatsumi , Y. Ichikawa , T. Hisamatsu , I. Yuri , Development of Silicon Nitride Components for Gas Turbine. Key Eng Mater [Internet]. 2005 Jun [cited 2021 Aug 5];287:10–5. Available from: ⟨https://www.scientific.net/KEM.287.10⟩.
[314] H. Kawase, K. Kato, T. Matsuhisa, T. Mizuno, Development of Ceramic Turbocharger Rotors for High-Temperature Use, J. Eng. Gas. Turbines Power 115 (1) (1993) 23–29.
[315] BJ , Busovne,JP Pollinger , Development of Silicon Nitride Rotors for the ATTAP Program at Garrett Ceramic Components. Proc ASME Turbo Expo [Internet]. 2015 Mar 10 [cited 2021 Aug 5];5. Available from: ⟨http://asmedigitalcollection.asme.org/GT/proceedings-pdf/GT1991/79023/V005T13A010/2401319/v005t13a010–91-gt-154.pdf⟩.
[316] M. Yoshida , S. Tsuruzono , T. Ono , H. Gejima , Development of Silicon Nitride Rotors for Gas Turbine Applications. Proc ASME Turbo Expo [Internet]. 2015 Feb 18 [cited 2021 Aug 5];2. Available from: ⟨http://asmedigitalcollection.asme.org/GT/proceedings-pdf/GT1994/78842/V002T04A018/2404161/v002t04a018–94-gt-332.pdf⟩.
[317] J. Nick, D. Newson, R. Masseth, S. Monette, O. Omatete, Gelcasting Automation for High-Volume Production of Silicon Nitride Turbine Wheels, Ceramic Eng. Sci. Proc. 20 (3) (1999) 225–232 (23rd Annual Conference on Composites, Advanced Ceramics, Materials, and Structures: A).
[318] H.-H. Tang, H.-C. Yen, Ceramic parts fabricated by ceramic laser fusion, Mater. Trans. 45 (8) (2004) 2744–2751.
[319] M. Huang, D.Q. Zhang, Z.H. Liu, J. Yang, F. Duan, C.K. Chua, et al., Comparison study of fabrication of ceramic rotor using various manufacturing methods, Ceram. Int 40 (8) (2014) 12493–12502.
[320] M. Ahlhelm, H.-J. Richter, K. Haderk. Selective Laser Sintering as an Additive Manufacturing method for manufacturing ceramic components. J Ceram Sci Tech [Internet]. 2013 [cited 2021 Aug 5];4(1):33–40. Available from: ⟨https://scholar.google.com/scholar?hl=en&as_sdt=0%2C43&q=2013+Selective+Laser+Sintering+as+an+Additive+Manufacturing+Method+for+Manufacturing+Ceramic+Components&btnG=⟩.
[321] A.A. Altun , T. Prochaska , T. Konegger , Schwentenwein M. Dense , Strong, and Precise Silicon Nitride-Based Ceramic Parts by Lithography-Based Ceramic Manufacturing. Appl Sci 2020, Vol 10, Page 996 [Internet]. 2020 Feb 3 [cited 2021 Aug 5];10(3):996. Available from: ⟨https://www.mdpi.com/2076–3417/10/3/996/htm⟩.
[322] S. Smolentsev, N.B. Morley, M.A. Abdou, S. Malang, Dual-coolant lead-lithium (DCLL) blanket status and R&D needs, Fusion Eng. Des. 100 (2015) 44–54, https://doi.org/10.1016/j.fusengdes.2014.12.031.
[323] X.R. Wang, M.S. Tillack, C. Koehly, S. Malang, H.H. Toudeshki, F. Najmabadi, ARIES-ACT2 DCLL power core design and engineering, Fusion Sci. Technol. 67 (1) (2015) 193–219, https://doi.org/10.13182/FST14-798.
[324] K. Terrani, B. Jolly, M. Trammell, 3D printing of high-purity silicon carbide, J. Am. Ceram. Soc. 103 (2020) 1575–1581, https://doi.org/10.1111/jace.16888.
[325] P.J. French, A.G.R. Evans, Piezoresistance in polysilicon and its applications to strain gauges, Solid-State Electron. 32 (1) (1989) 1–10, https://doi.org/10.1016/0038-1101(89)90041-5. ISSN 0038-1101.
[326] J. Richter, O. Hansen, A. Nylandsted Larsen, J. Lundsgaard Hansen, G.F. Eriksen, E.V. Thomsen, Piezoresistance of silicon and strained $Si_{0.9}Ge_{0.1}$, Sens. Actuator A Phys. 123–124 (2005) 388–396, https://doi.org/10.1016/j.sna.2005.02.038. ISSN 0924-4247, https://www.sciencedirect.com/science/article/pii/S0924424705001287.
[327] E. Ricohermoso III, F. Klug, H.F. Schlaak, R. Riedel, I. Ionescu, Microstrain-range giant piezoresistivity of silicon oxycarbide thin films under mechanical cycling loads, Mater. Des. 213 (2022), 110323.

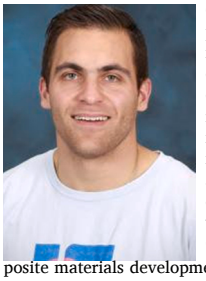

Cramer has been performing research and development in processing, characterization, and testing of high temperature materials, including ceramics, cermets, and ceramic matrix composites. He is a staff scientist at Oak Ridge National Laboratory (ORNL) and has led projects on reaction-bonded ceramics, metal-matrix composites, cermets, binder jet additive manufacturing, and ceramic stereolithography printing for next generation of ceramic composites and hybrids for use in aerospace, aero-engine, nuclear and advanced energy applications. He also has interest in robocasting ceramic printing as well as hot pressing and field-assisted sintering techniques. Dr. Cramer's current areas of research include ceramic and composite materials development for additive manufacturing, development of new ceramic-matrix composites, processing of ceramics, and novel processing and printing of continuous fiber ceramic matrix composites. He is a member of ACERS. Dr. Cramer is a staff scientist at Oak Ridge National Laboratory (ORNL) leading projects in ceramic processing and additive manufacturing methods such as binder jet, stereolithography, and slurry extrusion for next generation of ceramic composites and hybrids for use in aerospace, aero-engine, nuclear and advanced energy applications. His current areas of research include hot pressing, field-assisted sintering, composite materials development for additive manufacturing, development of new ceramic-matrix composites, and novel processing and printing of continuous fiber ceramic matrix composites.

Emanuel Ionescu has been the Head of the Department „Digitalization of Resources" at the Fraunhofer Research Institution for Materials Recycling and Resource Strategies (IWKS) in Alzenau, Germany. He has also been affiliated as Research Fellow and Docent to the Institute for Materials Science at Technical University Darmstadt. His scientific background and interests relate in general to materials synthesis and processing and in particular to the development of advanced ceramics for energy-related, environmental and biomedical applications. Additionally, he has been working on aspects concerning circular economy and digitalization of added value chains as well as on advanced data-driven materials recycling and upcycling concepts. He has been serving since 2019 as an Editor of the Journal of the European Ceramic Society.

Magdalena Graczyk-Zajac is a project leader in the Research and Development Department of the EnBW Energie Baden-Württemberg AG, a publicly traded energy company headquartered in Karlsruhe, Germany. Optimization and efficient operation of stationary storage installations including testing and evaluation of innovative storage solutions are in the focus of her interests. She is also involved in the activities of EnBW related to lithium recovery from geothermal sources. In parallel she is acquiring the qualification for lecturing in higher education ("Habilitation") at TU Darmstadt and is a deputy coordinator of the Horizon 2020 granted project SIMBA (Sodium Ion and Sodium Metal Batteries, Grant Agreement no. 883753). Her research interests include innovative processing routes to obtain well-performing materials for Lithium and beyond Lithium technologies, as well as advances in recycling routes of Li-ion batteries. Magdalena received her PhD in Physical Chemistry at Burgundy University (Dijon, France) in 2007 and then moved to CEA Grenoble as a research engineer. Later, she moved back to academia and continued her research on polymer-derived ceramics for energy-related applications as a Postdoc and later Junior Group Leader in Material Science Department of TU Darmstadt, Germany.

Andrew T. Nelson received his Ph.D. in Nuclear Engineering from the University of Wisconsin-Madison. He is a distinguished staff scientist and section head of the Fuel Development Section at Oak Ridge National Laboratory. Prior to joining ORNL in 2018, Dr. Nelson served as the team leader for Ceramic Nuclear Fuels in the Materials Science and Technology Division at Los Alamos National Laboratory. Dr. Nelson's research interests are focused on the development and assessment of novel nuclear fuel forms, with an emphasis on advanced fuel systems for light water reactors. He is also active in development of high-density dispersion and particle fuel concepts for nonproliferation applications. Dr. Nelson has authored or co-authored over one hundred peer-reviewed publications in the areas of nuclear fuel and cladding materials, ceramics, and high temperature materials.

Yutai Katoh (a.k.a. Kato) is a Corporate Fellow and Section Head for Materials in Extremes in the Materials Science and Technology Division of Oak Ridge National Laboratory. He received a Ph.D. in Materials Science from the University of Tokyo, Tokyo, Japan. Before arriving ORNL, he was serving as an Assistant Professor for the National Institute for Fusion Science then as a tenured Associate Professor for Kyoto University. His research interests range from the fundamental physics of defects in solids to processing and application of advanced materials to qualification of new materials for nuclear fusion and fission applications. He has published more than 300 peer-reviewed journal articles in materials science and engineering with more than 15,000 citations. He is a Fellow of the American Ceramic Society and the American Nuclear Society.

Jeffery J. Haslam holds a Ph.D. in Materials Science from the University of California at Santa Barbara, an M.S. in Engineering from Stanford University, and a B.S. in Engineering, with Highest Distinction, from the University of Kansas. Dr. Haslam's background includes innovative work in the ceramic processing and mechanical properties of porous oxide matrix and oxide fiber composites. He has worked in a variety of programs at Lawrence Livermore National Laboratory including: solid oxide fuel cells, amorphous metal, corrosion-resistant thermal spray coatings, functional graded density materials, ceramic nanofibers production via electrospinning, and high temperature filters. He has also worked on the application of additive manufacturing for ceramic molten salt-resistant heat exchangers and additive manufacturing of ceramics for metal casting cores and molds. Dr. Haslam is currently the Group Leader for the Ceramics and Polymers Group in the Materials Engineering Division at Lawrence Livermore National Laboratory.

Lothar Wondraczek is Professor of Glass Chemistry and Director of the Otto Schott Institute of Materials Research at the Friedrich Schiller University Jena. Previously, he was a Professor of Materials Science at the University of Erlangen-Nuremberg (2008–2012), and a Senior Research Scientist at Corning's European Technology Center (2005–2008). He holds a Dr.-Ing. from Clausthal University of Technology. His research interests involve glasses and other types of disordered materials, from chemical formulation to post-processing and the design of prototype devices; his work was recognized by various awards and recognitions, including the Weyl, Dietzel, Gottardi and Zachariasen awards for excellence in glass science, and ERC consolidator and proof-of-concept grants. In the 2022 International Year of Glass, he is organizing the program of the Opening Ceremony, and also serves as the program chair of the International Congress on Glass in Berlin, Germany.

Trevor Aguirre joined Oak Ridge National Laboratory in October 2020 as an Alvin M. Weinberg Distinguished Staff Fellow in the Extreme Environment Materials Processing Group at the Manufacturing Demonstration Facility. His research centers around processing and properties of additively manufactured ceramics, ceramic-metallic composites, and ceramic matrix composites. His research goals are to help develop the next generation of ultra-high temperature, harsh environment ceramics, composites, and hybrid materials for use in aerospace, nuclear, and advanced heat exchange applications. He received his Ph.D. in Mechanical Engineering from Colorado State University in 2020, where his dissertation focused on development of bioinspired structures for light-weighting and impact attenuation applications. He has published literature in processing ceramics, additive manufacturing, and bioinspired design.

Saniya LeBlanc is an Associate Professor in the Department of Mechanical & Aerospace Engineering and Director of the Energy Innovation Initiative at the George Washington University. Her research goals are to create next-generation energy solutions leveraging advanced materials and manufacturing techniques. Previously, she was a scientist at a startup company where she evaluated new power generation materials and created research, development, and manufacturing solutions for waste heat recovery applications. Dr. LeBlanc obtained a PhD and MS in mechanical engineering with a minor in materials science and engineering at Stanford University. She was a Churchill Scholar at University of Cambridge where she received an MPhil in engineering, and she has a BS in mechanical engineering from Georgia Institute of Technology.

Hsin Wang, received his BS degree of Solid-State Physics from Tsinghua University in 1989 and his MS and Ph.D. in Ceramic Science from the New York State College of Ceramics at Alfred University in 1991 and 1994. He joined Oak Ridge National Laboratory in 1995 and is currently a distinguished scientist at the Materials Science and Technology Division. His research focuses are on transport properties of materials, advanced thermal imaging, thermal management and reliability of energy storage systems, and effect of neutron irradiation on material properties. He was the president of the International Thermal Conductivity Conference (ITCC) and is a current member of ITCC board of directors. He was the host of the International Thermoelectric Conference (ICT) in 2014 and a board member of ICT from 2012 to 2019. He was the Thermoelectric Materials Annex leader of the International Energy Agency (IEA) from 2010 to 2020. He is current a member of the NASA NextGen team and ORNL task leader on SiGe development.

Mansour Masoudi has been involved in research, development, and application of refractory ceramics for more than two decades. Such varied applications have included automotive emission control and carbon capture. He received his PhD in Mechanical and Aerospace Engineering from the University of California (1998) and is the founder and editor-in-chief of the international journal Emission Control Science and Technology, published by Springer Nature™. Note: This author did not provide any photo, as he did not have any photo available.

Edward Tegeler holds a B.Sc. in Chemical Engineering from the University of Washington. Following several years of work in thermal wastewater treatment at GE Water and Process Technologies, Ed has spent nearly 6 years with the Emissol R&D team, where his work focuses on the modeling, simulation, design, manufacture, and testing of novel catalyst and sorbent substrates for use in automotive emission aftertreatment and direct air capture (DAC) of CO2.

Riedel got a PhD degree in Inorganic Chemistry in 1986 at the University of Stuttgart. After a PostDoc period at the Max-Planck Institute for Metals Research in Stuttgart, he became Full Professor at the Institute of Materials Science at the Technical University of Darmstadt in 1993. He is an elected member of the World Academy of Ceramics, Fellow of the American Ceramic Society, the European Ceramic Society as well as Fellow of the School of Engineering at The University of Tokyo in Japan. Prof. Riedel was awarded with the Gold Medal for Merits in Natural Sciences and with a honory doctorate of the Slovak Academy of Science as well as with the Gustav Tammann Prize of the German Society of Materials Science (DGM). In 2009, he received a honorary Professorship at the Tianjin University in Tianjin, China. He was Guest Professor at the Jiangsu University in Zhenjiang and at the Xiamen University in China. Recently, Prof. Riedel received the Innovation Talents Award of Shaanxi Province, China at the Northwestern Polytechnical University in Xi'an. He is Guest Professor at the University of Tokyo in the group of Prof. Ikuhara, Japan and was awarded with the International Ceramics Prize 2020 for "Basic Science" of the World Academy of Ceramics. He is Editor in Chief of the Journal of The American Ceramic Society and of Ceramics International. His current research interest is focused on two research areas, namely i) molecular synthesis of advanced structural and functional ceramics for ultra-high temperature and energy-related applications as well as ii) ultra high pressure materials synthesis.

Paolo Colombo is currently professor of Materials Science and Technology at the Department of Industrial Engineering, University of Padova, Italy. He graduated from the University of Padova with a degree in chemical engineering in 1985 and a diploma in glass engineering in 1988. He was assistant professor at the University of Padova from 1990 to 1998 and then associate professor at the University of Bologna, until 2005. He is also adjunct professor of Materials Science and Engineering at the Pennsylvania State University, visiting professor in the Department of Mechanical Engineering of University College London, UK, and member of the World Academy of Ceramics and of the European Academy of Sciences. He was Foreign Scientist at INSA, Lyon, France in 2015, and DFG Mercator Professor at the Technical University Bergakademie Freiberg, Germany in 2016. He is also fellow of the American Ceramic Society, fellow of the Institute of Materials, Minerals and Mining and fellow of the European Ceramic Society. He has received several awards and is president-elect of the International Ceramic Federation (ICF). He was chair of the XVI conference of the European Ceramic Society in 2019. He published more than 290 papers, 9 book chapters and two books, and holds 11 international patents. He is Editor-in-Chief of Open Ceramics, and is in the editorial board of 8 other international scientific journals. Paolo Colombo's research interests include novel processing routes to porous glasses and ceramics (currently focusing mainly on Additive Manufacturing, using different technologies), the development of ceramic components from preceramic polymers and geopolymers, and the upcycling of hazardous industrial and natural waste.

Majid Minary Jolandan is currently an Associate Professor of Mechanical and Aerospace Engineering at the School for Engineering of Matter, Transport and Energy of the Ira A. Fulton School of Engineering at Arizona State University (ASU). From 2012–2021 he was a Eugene McDermott Associate Professor and previously an Assistant Professor in the Department of Mechanical Engineering at the University of Texas at Dallas (UT Dallas). He received his PhD from University of Illinois at Urbana-Champaign (UIUC), followed by a Postdoctoral training at Northwestern University. His group is interested in Additive and Advanced Manufacturing of multifunctional materials. Minary is the recipient of two Young Investigator awards from the Department of Defense (ONR-YIP and AFOSR-YIP), and a recipient of School of Engineering Junior Faculty Research Award from UT Dallas.